The SEA-CALIPSO volcano imaging experiment at Montserrat: plans, campaigns at sea and on land, scientific results, and lessons learned

Voight, B.[1], Sparks, R.S.J.[2], Shalev, E.[3,4], Minshull, T.[5], Paulatto, M.[5], Annen, C., Kenedi, C.[3,4], Hammond, J.[2], T.J. Henstock5, Brown, L.[6], E. Kiddle2, Malin, P.[3,4], Mattioli, G.[7], Ammon, C.[1], Arias-Dotson, E. 8, Belousov, A.[1], Carothers, L.[8], Clarke, A.[9], Dean, S.[5], Ellett, L.[10], Elsworth, D.[1], Hidayat, D.[1], Herd, R.[11], Johnson, M.[8], Lee, A.[3], Miller, V.[1], Murphy, B.[10], Peirce, C.[12], Ryan, G.,[13], Saldana, S.[14], Snelson, C.[14], Stewart, R.[13], Syers, R.[13], Widiwijayanti, C.[1], Young, S.R.[1], Zamora, W.[8]

1. College of Earth and Mineral Sciences, Penn State University, University Park, PA 16802, USA.
2. Department of Earth Sciences, , University of Bristol, Bristol BS8 1RJ, UK
3. Earth & Ocean Sciences, Duke University, Durham, NC 27708-0227
4. Institute Earth Science & Engineering, University of Auckland, Private Bag 92019, New Zealand.
5. National Oceanography Centre, Univ. Southampton, SO14 3ZH, UK
6. Department of Geosciences, Cornell University, Ithaca, New York, USA
7. Department of Geosciences, University of Arkansas, Fayetteville, AR 72701
8. PASSCAL Instrument Center, East Road Industrial Park, Socorro, NM 87801
9. Dept. Geological Sciences, Arizona State University, Tempe, Arizona, USA
10. Scripps Institution of Oceanography, San Diego, CA, USA
11. School Environmental Science, University East Anglia, Norwich, NR4 7TJ, UK
12. Dept. Geological Sciences, University of Durham, Durham DH1 3LE, UK
13. Montserrat Volcano Observatory, Flemming, Montserrat, W.I.
14. Department Earth Environ. Sci., New Mexico Institute of Mining and Technology, Socorro, New Mexico 87801

Abstract

Since 1995 the eruption of the andesitic Soufrière Hills volcano (SHV),

Montserrat, has been studied in substantial detail. As an important contribution to this effort, the SEA-CALIPSO experiment was devised to image the arc crust underlying Montserrat and, if possible, the magma system at SHV using tomography and reflection seismology. Field operations was carried out in October-December 2007, with deployment of over 200 seismometers on land supplementing 9 volcano observatory stations, and with an array of 10 ocean bottom seismometers deployed offshore. The RRS James Cook on NERC cruise JC19 towed a tuned airgun array plus a digital 48-channel streamer on encircling and radial tracks for 77 h about Montserrat during December 2007, firing 4414 airgun shots yielding about 47 Gb of data. The main objecctives of the experiment were achieved. Preliminary analyses of these data published in 2010 generated images of heterogeneous high-velocity bodies representing the cores of volcanoes and subjacent intrusions, and shallow areas of low velocity on the flanks of the island that reflect volcaniclastic deposits and hydrothermal alteration. The resolution of this preliminary study did not extend beyond five km depth. An improved three-dimensional seismic velocity model was then obtained by inversion of 181,665 first arrival travel-times from a more-complete sampling of the dataset, yielding clear images to 7.5 km depth of a low-velocity volume that was interpreted as the magma chamber that feeds the current eruption, with an estimated volume 13 km^3. Coupled thermal and seismic modeling revealed properties of the partly crystallised magma. Seismic reflection analyses aimed at imaging structures under southern Montserrat had limited success and suggest subhorizontal layering interpreted as sills between 6 and 19 km depth. Seismic reflection profiles collected offshore reveal deep fans of volcaniclastic debris and fault offsets, leading to new tectonic interpretations. This paper presents the project goals and planning concepts, describes in detail the campaigns at sea and on land, summarises the major results, and identifies the key lessons learned.

KEYWORDS: Montserrat, Soufrière Hills volcano, SEA-CALIPSO, seismic imaging experiment, tomography, seismic reflection profiles, magma chamber

Introduction

The ongoing eruption of the andesitic Soufrière Hills volcano (SHV), Montserrat, has been studied in detail since 1995, and the volcano has become an important natural laboratory for investigations of volcanic processes (Druitt & Kokelaar 2002; Voight & Sparks 2010). About one cubic kilometer of lava has been erupted (Wadge *et al*. 2010). Deep processes exert important controls on this eruption, but the structure of the crust, upper mantle and the magmatic system has been inadequately defined. Thus we designed the SEA-CALIPSO experiment to investigate the physical structure of the arc crust under Montserrat through active source seismic tomography and reflection seismology (Voight *et al.* 2010a). The SEA-CALIPSO experiment (*Seismic Experiment with Airgun-source*) was conducted under the umbrella of the CALIPSO consortium project (*Caribbean Andesitic Lava Island Precision Seismo-geodetic Observatory*) (Mattioli *et al*. 2004). SEA-CALIPSO complements a number of ancillary CALIPSO project studies, involving analyses of GPS and strainmeter data (Mattioli *et al*. 2010; Linde *et al*. 2010; Chardot *et al.,* 2010; Voight *et al.* 2010b,c; Elsworth *et al.* 2008; Foroozan *et al.* 2010, 2011), receiver function investigations (Sevilla *et al.* 2010), and petrologic studies (Kiddl*e et al*. 2010)

The outcomes of this project contribute to an improved understanding of volcanic processes, island arc volcanism and tectonics, arc crust evolution and magma genesis. The experiment successfully imaged the subsurface under Montserrat and the surrounding offshore region, and detected and characterised the shallow magma chamber.

This paper provides background on the tectonic and magmatic setting, describes the SEA-CALIPSO aims, plans, support and funding, outlines details of the active seismic source, the seismometer arrays and other equipment, delineates the land and ship-borne operations, and summarises important research outcomes. The paper concludes with a discussion of critical issues affecting the success of the venture, and offers some key lessons learned that could be of value to researchers involved in future volcano imaging projects.

Background

The island of Montserrat in the volcanic arc of the Lesser Antilles was clearly an ideal target for a seismic tomography experiment, partly because of its small size and relatively simple volcanic history, and especially because of the need to better understand the current dangerous eruption (Voight *et al*. 2010a). The tectonic setting and bathymetry about Montserrat is shown in Figure 1. Montserrat is composed of the lava domes and associated pyroclastic deposits of three andesite volcanoes, Silver Hills (2600–1200 ka), Centre Hills (ca 950–550 ka) and the Soufrì`ere Hills Volcano (170 ka – present) (Fig. 1, inset figure). The three volcanoes have very similar petrology and a clear age progression from north to south

(Harford *et al*. 2002), making comparisons between the centres straightforward and valuable. Volcanic activity at SHV started in 1995 after over three centuries of quiescence and was preceded by a series of periods of increased seismic activity spaced approximately at three-decade intervals (Powell 1939; Perret 1939; Shepherd *et al*. 1971; Aspinall *et al*. 1998). The activity is characterised by the growth of an andesite lava dome and associated dome collapses, explosions and pyroclastic flows. The eruption is still ongoing in 2012 and has so far consisted of five eruptive phases of continuous lava extrusion interrupted by periods of quiescence (Wadge *et al*. 2010).

The magmatic system of SHV is thought to be composed of four main elements: a primary source of mafic magma in the mantle wedge with storage in the deep crust at about 30 km depth (Zellmer *et al*. 2003a,b; Sevilla *et al*. 2010), a mid-crustal magma storage region where andesite is generated by fractionation of basalt (Sparks & Young 2002; Elsworth *et al*. 2008), a shallow magma reservoir, where andesite resides prior to eruption and undergoes further transformation (Murphy *et al*. 2000), and a stratovolcano, consisting of a core of lava domes and a soft apron of volcaniclastic deposits (Harford *et al*. 2002; Paulatto *et al*. 2010a,b; Shalev *et al*. 2010). Some characteristics of the shallow magma reservoir have been constrained with petrological and geodetic data. Analysis of SHV andesites and modeling of ground deformation and magma efflux suggest that the shallow magma chamber lies below approximately 5 km depth, but details on its geometry are debated (Murphy *et al*. 2000; Voight *et al*. 2006, 2010b; Elsworth *et al*. 2008; Mattioli *et al*. 2010; Foroozan *et al*. 2010; Hautmann *et al*., 2009, 2010). The dynamics of magma flow are influenced by geometric considerations (Voight *et al*. 1999, 2006, 2010b; Costa *et al*. 2007; Foroozan *et al*. 2011; Melniik & Sparks 2002, 2005; Melnik & Costa this volume; Widiwijayanti *et al*. 2005). Geothermometry indicates that the magma is relatively cool (~850◦C) and highly crystalline (60–65 vol%) (Murphy *et al*. 2000; Rutherford & Devine 2003). Several independent observations support the hypothesis of continued input of mafic magma at depth during the course of the SHV eruption (Barclay *et al*. 2010; Christopher *et al*. 2010; Edmonds *et al*. 2011; Humphreys *et al*. 2009; Voight *et al*. 2010b).

Our tomographic studies were aimed to improve understanding of the magmatic system (e.g. Lees 2007). Analyses of our data proceeded in several steps. Our preliminary results generated useful images of the subsurface at Montserrat (Paulatto *et al*. 2010a; Shalev *et al*. 2010; Kenedi *et al*. 2010), but lacked the resolution beyond 5 km depth to constrain the shallow crustal magma chamber. An improved three-dimensional seismic velocity model for Montserrat was then obtained by regularized inversion of first arrival travel-times from a more complete subset of wide-angle seismic data recorded on our array of land and ocean-bottom seismometers (Paulatto *et al*. 2012). Some key results from these various researches are summarized below, following discussion of the planning and execution of the experiment.

Planning and funding

Plans and preparations

Our project plans evolved between 2004 and 2007. Our initial concept was to record signals from a three-day active source experiment using an airgun array towed by a research vessel around Montserrat, taking opportunistic advantage of the NERC RRS James Clark Ross operation scheduled for May 2005. In this original plan we expected about 10 Gb of data to be collected from ~100 seismometers on land, and after stacking, about 1000 shot points and up to 100,000 separate raypaths. The loan of seismeters was approved by IRIS-PASSCAL. However due to cruise schedule delays, our cruise availability was withdrawn for 2005, and was rescheduled to 2007. Although not welcomed at the time, this delay proved useful in providing opportunities for development of more thorough planning, more ship time, the addition of important equipment, and augmented financial support, all factors that facilitated a vastly improved experiment. In retrospect we were quite fortunate that the delay occurred, because the full success of the experiment hinged critically on a several of these factors.

Once funds were largely in place and following a planning workshop in Washington D.C. in November 2006, final-stage logistical plans were worked out in May 2007 with a meeting involving the participating institutions. A cruise planning meeting was held at Southampton on 5 May 2007, with formal minutes circulated by Colin Day (UKORS) to note recent pertinent developments, and to highlight points that needed to be circulated to participants of the project and required some action. It was noted for instance that B. Voight was looking into streamer acquisition and support, and that the PI of the previous JC18 cruise agreed to allow Geopro staff and airgun kit to be loaded onto the vessel at the beginning of his cruise, after re-assurance that the kit and activity would not affect his JC18 work. The RRS James Cook was scheduled to be in Antigua port call between 30 November and 3 December. The mobilisation logistics were planned, with loading and stowing of Geopro airgun equipment to be done on 5 November, with Geopro to mobilise kit at Antigua port call. Two Geopro technicians would board the JC18 cruise to test equipment, and it was noted that if a streamer is deployed then this must be loaded on the James Cook in this same period.

Our Duke University colleagues (subsequently associated with University of Auckland) led the land seismometer operations and sent teams to Montserrat for scouting and deployment in August, October, November, and December 2007. These trips included participants from Penn State University, a representative from the Seismic Research Centre of the University of West Indies, and several from IRIS PASSCAL (*Incorporated Research Institutions for Seismology* (IRIS) *Program for Array Seismic Studies of the Continental Lithosphere* (PASSCAL)). The final deployment in December 2007 required numerous personnel and involved assistance from the main collaborating institutions, as well as University of East Anglia, UK, New Mexico Institute of Mining and Technology, and University of Auckland, together with local cooperation and assistance, especially from the Montserrat Volcano Observatory (MVO). Sea operations were led by colleagues from University of Bristol and University of Southampton, and mainly involved use of the RRS James Cook (NERC).

The active-source imaging experiment had two components: a seismic reflection component, aimed at imaging the top of the magma body using wide-angle seismic reflections, and a seismic tomographic component, in which any velocity anomaly associated with the magma body, as well as the larger-scale crustal structure, could be determined. The planned experiment geometry was based on principles set out by Okaya *et al*. (2002) and on previous experience at volcanic ocean islands (Evangelidis *et al*. 2004; Minshull *et al*. 2005; cf. Zandomeneghi *et al*. 2009).

Ray-trace modelling to assist planning used an estimated velocity structure based on models used at MVO, derived by trial-and-error modification of a seismic model previously developed at Guadaloupe, the volcanic island immediately to the south of Montserrat (Power *et al.* 1998). This modelling showed that for a geometry involving onshore receivers only, the refracted rays might not reach a magma body at ~ 5 km, the position that had been inferred from earlier petrologic and seismic arguments (Barclay *et al*. 1998; Aspinall *et al*. 1998). Thus we aimed to improve ray penetration by deploying Ocean Bottom Seismometers (OBS) up to 20 km from the Montserrat coast, expanding the source-receiver offsets.

The planned shooting tracks comprised a series of sub-circular tracks at 2 to 10 km from the coast, supplemented by radial tracks extending up to 30 km from the coast to determine deeper velocity structure (Fig. 2). A streamer was added to our plans in order to map the sediment thickness, and thus to account for corresponding travel-time delays in signals from the airgun shots.

Funding and support

A proposal was submitted to NERC for the survey and associated science in July 2005 and received an alpha 3 grade, making the project eligible for free access to NERC ships. NERC permitted our use of the ship on the condition that external financial support could be secured for add-on ship costs such as airguns, and we managed to cobble together the necessary funds from several sources. Funding overall was provided by the NSF, NERC, Discovery Channel TV, the British Geological Survey (BGS) and the Foreign and theCommonwealth Office (FCO) of the UK. In several grants the NSF covered the IRIS-PASSCAL operations, streamer costs, and field costs and analyses by US-based university research groups. The NSF had approved funding in 2004 for the originally-planned 2005 deployment, and generously allowed us to carry-over these funds for the re-scheduled cruise. Likewise PASSCAL arranged to re-schedule provision of seismic equipment for 2007, and increased the number of loaned instruments. Funding for UK university research was provided by NERC. Funding from Discovery Channel TV proved essential in supporting costs for an augmented airgun array and technical support, and BGS supported the important OBS operations. The FCO supported costs for required environmental impact reporting.

Seismic source

The seismic source, provided on commercial contract by GeoPro, consisted of eight Bolt 'Long Life' units assembled on two rigid frames connected to the ship by electric cables and high-pressure tubes, towed side by side with a separation of 9 m (e.g., Bailey & Garces 1988). The total volume of the array was 2600 cu. in. (42.61 L), subdivided into 1430 cu. in. on the port-side frame and 970 on starboard-side frame (Fig. 3). The airgun source comprised 2 x 500, 1 x 340, 3 x 290 and 2 x 195 cu. in. (2 x 8.2, 1 x 5.6, 3 x 4.8 and 2 x 3.2 L) guns in clustered pairs. The source design was a compromise that maximized low-frequency energy and tuning to attenuate the bubble pulse, and had modeled 6 dB points of ~5 Hz and 50 Hz, and a primary-to-bubble ratio of about 3.5 to 1 (Strandenes *et al*. 1991).

Synchronization of the guns was obtained by GPS using a 'Long-Shot' gun controller and time-triggering was given by a quartz clock driven by GPS timing. The source fired at a constant shot interval of 60 s at a pressure of 2000 p.s.i. (1.382×10^7 Pa). This shot interval was used in order to avoid contamination of records by previous-shot noise. The array was towed at a depth of 10 m and at an average speed of 4.5 knots (2.3 m s^{-1}), giving a mean shot spacing of 139 m. Shot coordinates were calculated by interpolating the ship's navigation using a gun setback of 91 m (Fig. 4, 11). 4414 shots were fired over a period of 77 hours, with a few interruptions due to gun maintenance or the presence of marine mammals or other vessels in proximity of the guns.

Seismometers and other equipment

Ocean Bottom Seismometers

The OBSs were supplied by OBIC, the Ocean Bottom Instrument Consortium (Minshull *et al*. 2005), comprising the University of Southampton, Durham University and Imperial College. The Instruments deployed were three LC2000 two-component OBSs and seven LC2000 four-component OBSs designed by Scripps Institution of Oceanography (Fig. 5, 6). The four-channel OBSs were equipped with a hydrophone and a three-component 4.5 Hz geophone package, and the two-channel OBSs were equipped with a hydrophone and a 2 Hz vertical geophone. The sample rate for the experiment was set at 250 Hz.

OBS sites were chosen to avoid potentially hazardous areas such as submarine canyons, steep slopes, areas covered by recent debris flows, and to be outside the Maritime Exclusion Zone set for volcanic hazards around the south of Montserrat. Sites to the west, on the lee of the island with respect to the predominant trade winds, were preferred to facilitate deployment and recovery of the instruments.

OBS coordinates were determined after the cruise by minimizing residuals between observed and calculated first arrivals of seismic waves through the water from GPS located shots near each OBS, leading to OBS position uncertainties of 20-50 m, from shot location uncertainties of 5-20 m (Paulatto *et al*. 2012). The JC19 Cruise Report (NOC 2008) lists the distances between deployment position and relocated position, the direction of drift from the north, and serial number and number of channels for all instruments, plus instrument deployment and recovery times, sync time, end of record periods, and time drift of instrument clock during recording period.

All instruments deployed were recovered, after recording continuously the 4414 shots fired from the RRS James Cook. Most instruments recorded successfully on all channels. The only exceptions were the instruments on sites O09 and O14 (Figs. 2, 28). The instrument on site O09, 15 km SSE of the Montserrat coast, was a four- component OBS but recorded only on two channels, the hydrophone and the vertical geophone, because of a weak connection in the data logger. The instrument on site O14, 19 km south of the coast, was a four- component type, but the geophone mounted in the vertical position was a horizontal type phone and this resulted in unusable data on the vertical component.

Land array

Two types of land-based seismographs were provided by IRIS-PASSCAL, the RefTek RT130 recorder with 3-component Mark Products L22 2.0 Hz geophones (hereafter called the RefTek), and the RefTek RT125A, a single vertical component Mark Products L40 (or L28) 4.5 Hz sensor and recorder (hereafter referred to as the Texan) (see Fig. 7, 8). The 29 RefTeks were deployed from October through December, powered by deep cycle batteries with solar panel recharging (Fig. 9). PASSCAL technicians accompanied the two deployment trips to maintain the instruments and instruct other participants on installation. The Texans were deployed only for the December experiment.

RefTeks were intended primarily for 3D tomography analysis, while the Texans were intended for two purposes, for reflection seismology, and to fill-in the tomographic grid. The design for the 3D tomography required that the 3-component RefTeks be arrayed as closely as possible in an even-spaced regular grid (Fig. 10). In the planned tomographic analysis, the subsurface is described by velocity nodes at X, Y, Z coordinates (Shalev *et al*. 2010), with node density adjusted based on the number of rays passing in the vicinity of the node. A higher node density and higher resolution is possible where there are more data, and this is influenced by station density. The number of RefTek stations was limited by availability from IRIS-PASSCAL. Sites were primary chosen to be easily accessible by car, but many instruments had to be deployed on foot or with access by boat from the sea, especially in the south of the island. The final RefTek grid developed did not include the higher parts of the Centre Hills and Soufrière

Hills, due to forbidding terrain and difficulty or hazards of installation. The final array consisted of stations about every 1 to 2 km and produced a final resolution of approximately 500 m (Fig. 10; Shalev *et al*. 2010). Limited access within the exclusion zone resulted in poorer coverage in the south than in the north.

The permanent Montserrat Volcano Observatory (MVO) seismic network, then comprising nine broadband seismographs (Guralp CMG-40T) and two short-period vertical-component seismographs (Mark Products L4) more or less evenly spaced around Soufri´ere Hills (Fig. 10), also recorded the shots.

The design for the reflection survey included three quasi-linear Texan arrays on the island, integrated with the ship track. Two of these arrays radiated outwards from SHV, and the ship track followed the continuation of the alignment offshore on the opposite side of the volcano (cf. Figs. 2a, 2b, 10). The radial lines were designed to "undershoot" SHV, and with increasing distance between shots and receivers, the seismic waves could in principle reach deeper reflectors under the volcano.

Another array was designed to receive reflections for detailed, horizontal 'fan' style recording of the marine source as it traversed an offshore arc about the volcano. The array approximated an arc of the SHV circumference, located about 6 km north and northwest of the SHV summit (Fig. 10), that mirrored an offshore arc, about 6 km south and southeast of the SHV (Fig. 2b). To record the greatest number of rays through the volcano subsurface, the circumferential array was designed to cover the longest feasible northeast-southwest path across Montserrat. While the ship made rings at increased radius from the volcano, Montserrat's narrowing northern tip and increasing number of deep, incised valleys in the north discouraged deployment of a second arc of instruments.

While in advanced stages of planning in July 2007 we received disturbing news from B. Beaudoin at PASSCAL:

"*I regret to inform you that our entire Texan pool was in a serious truck accident in China…it appears that many, if not most, of the Texan's oscillators have been damaged. We will be receiving half of the equipment at PASSCAL by mid-August and will begin testing dataloggers. The remaining equipment will return to PASSCAL early-September and will also need testing. Depending on the severity and magnitude of damage the dataloggers may need to be returned to RefTek…At this time we are unable to guarantee that we will have Texans available for shipping to SEA-CALIPSO. I am sorry that we cannot promise Texans at this time, however we will do everything possible to meet our commitment.*"

This circumstance caused us to promptly seek Texans from other sources in contingency, and we had limited success in securing a promise from New Mexico Institute of Mining and Technology of about 35 instruments, as a fall-back solution. Fortunately by mid-September PASSCAL had done sufficient testing of the equipment involved in the accident to firmly commit 140 256 MB Texans for SEA-CALIPSO, and by December we had obtained the full number originally planned.

Figure 2c and 28 display the distribution of installed seismic stations and the ship tracks, which broadly match the original plans with the exception of some OBS sites (Fig. 2b). Some modifications are apparent due to logistic issues, especially at sea and as described below.

Seismic lines, sonobuoys and XBT probes

A 600-m 48-channel streamer provided by Scripps Oceanographic Institution and operated by their technical staff recorded 26 seismic lines during shooting. The geometry of the steamer is shown in Fig. 11. The sample frequency used was 500 Hz. The streamer was used to map the sediment thickness, in order to account for travel-time delays in signals from the airgun shots, and to provide reflection profiles indicating sediment type and structure.

Deployment of 48 sonobuoys donated by Lamont-Doherty Oceanographic Institution was accomplished during the cruise, with the intent of providing better ray coverage offshore. The sonobuoys were stripped from the parachute and deployed by hand from the stern of the ship (NOC 2008). A shipboard radio receiver was set up to record the signals transmitted by the sonobuoys. The sonobuoy data was then digitised and recorded on two additional channels on the MCS data logger. However, due to the bad state of preservation of the instruments, most failed immediately and sank, and only a few recorded more than a few shots.

XBT probes were deployed and measured the vertical temperature distribution in the water column (NOC 2008). The maximum depth reached was 875 m. In most cases the copper wire snapped when the probe reached a depth of about 200 m.

Land operations

The on-land phase lasted between October and December 2007 with the initial deployment of Refteks mostly completed in October, and the deployment of the Texans conducted from 17-21 December 2007 prior to and during the onshore-offshore seismic experiment (Fig. 10).

Montserrat has a very short runway in the north on which only small planes can land. There were a limited number of passenger flights scheduled from Antigua, and no air shipments for cargo. Shipping cargo by freighter from the United States required a substantial margin between shipping and expected arrival times due to unpredictable freight schedules. A local customs agent on Montserrat kept track of SEA-CALIPSO shipments and the receiving of the equipment, and provided useful advice on negotiating local bureaucracy.

The operational base of the experiment was a large rented villa (west of MVO, near OLVN on Fig. 10) that from October to December 2007 housed scouting and deployment teams and provided secure instrument storage. PASSCAL technicians used an apartment in the villa to test and work on instruments. In December, with the arrival of 35 land-based participants, the villa served as operational headquarters (HQ) for radio and phone communications with hiking teams and the ship, providing for changes in timing of hiking routes, and discussions of adjustments in shiptracks.

RefTek sites were accessible by vehicle or foot in the northern third of Montserrat, outside of the volcanic exclusion zone and including both Centre and Silver Hills (Fig. 12). Instrument locations were isolated as much as possible from vehicle traffic, electric wires, cliffs, or water waves that might interfere with seismic signals. Sites had to be reasonably secure from theft of the battery and solar panels. Final locations included the gardens and yards of private homes, local businesses, a Water Authority water storage tank, the MVO, and the airport. Teams visited each site in advance and received permission from the resident or official in charge. Land station coordinates were determined by direct GPS measurement, leading to uncertainties of about 5 m in horizontal position and 50 m in station altitude.

In the southern two-thirds of Montserrat, within the volcanic exclusion zone and including South Soufrière Hills and SHV, most of the RefTek locations were accessible only by small boat transport of people and instruments (Fig. 13). The limited access resulted in poorer coverage in the south than in the north (Fig. 10). Deployments required permissions on a given day from MVO, and radio or cell phone contact with MVO. Landing sites included the beaches south of Plymouth and along the Tar River delta, and with more difficulty, shoreline rocks near the southern point of Montserrat. Sites were accessible with relative ease in October but with great difficulty in December, due to strong winds and wave action.

The primary challenge in deploying the Texans during the experiment was that 209 of the seismometers had very limited battery capacity and had to be deployed in conjunction with the anticipated hours of airgun shooting, which could not be known with certainty beforehand. Within a few hours on either side of the experiment, five teams hiked over 5-10 km of steep, rough terrain, installing and/or collecting an instrument every 100 m. The duration of these treks ranged from several to as much as 9 hours. The design of the Texan is such that if battery power is lost, the timing fails and renders the data unusable. Thus, it was of crucial importance that the instruments be collected and data uploaded promptly, before the batteries died. Because the airgun shooting duration was expected to be similar to the Texan battery life, the hiking deployment was planned closely around the hours of the shooting. We had requested from PASSCAL tests of instruments adjusted for longer-life lithium batteries; however these modications affected the electronics systems and reliability of performance was reduced, so this approach was abandoned. Contingency plans were devised to accommodate staggered start/stop times for the standard instruments for several hours at the beginning and end of the shooting, if airgun shooting could exceed three days. These contingency plans were not used, but frequent communications between HQ and the ship were vital in adjusting to maritime developments that could influence land operations.

Texans were placed every 100 m over a total of ~20 km; for installation, each team was assigned one line accessible by road, and one hiking line. Texans were in place for approximately 90 h, accommodating both the 77 h of actual shooting and the approximate 100 h battery life. Although the 77 h of shooting time was less than that anticipated (approximately 100 h), the reduction of shooting time "resolved" our battery life problem. One line of easily accessible Texans was retrieved, the data uploaded, and instruments reinstalled mid-experiment for a quality check, to confirm that signals were being received, and to look at preliminary results. The road-based Texans were installed at the side of roadways, on public land where possible, thereby requiring the fewest possible number of permissions. Two lines required entering the exclusion zone and therefore access permission was needed from the MVO. Two Texans were installed by B Voight and R Herd on the northeast side of the volcano, at Whites Yard and inland from Spanish Point.

For the Centre Hills hiking lines, the difficulty of parts of this terrain would be hard to overstate (Fig. 3, 14-16). The Centre Hills are characterised by mountainous rainforest with steep ridges and valleys. Hikers were on precipitous, wet and slippery soil-veneered slopes, using trails made almost invisible by dense vegetation. Local guides (and one from East Anglia, UK) cleared paths with machetes prior and during the experiment and were vital in getting the groups up into the mountains. Safety considerations included carrying First Aid kits and radios for communication with headquarters and the MVO. All groups carried portable GPS units suited to forest cover, for navigation and to mark the instrument locations.

Ship-board operations

The offshore field campaign consisted of the 5-day seismic cruise JC19 on the RRS James Cook plus the OBS deployment from the vessel Beryx. The JC19 cruise lasted from 16 to 21 December and, as has been stated, comprised 77 hours of continuous shooting with an artificial seismic source and collection of MCS seismic data around the island of Montserrat. The cruise started and finished in Saint John's, Antigua, 30 nautical miles east of Montserrat. The shooting took place between 17 and 20 December.

The OBS deployment was accomplished from the 12-m vessel Beryx (Fig. 17), by a team hosted by the Institut Regional de Peche et Mer (IRPM) in Gourbeyre, Basse Terre, Guadeloupe, where it was given access to dry working space for the setup of the instruments. Guadeloupe is approximately 50 nautical miles south of Montserrat. The OBS deployment was scheduled to take place in the days 9th, 10th, 11th and 12th of December 2007, but was delayed due to the late delivery of the equipment. The equipment was delivered on 12 December and the instruments deployed in the days 13th, 15th and 16th of December. The OBS deployment locations had to be changed from the previously planned locations, mainly due to concerns about the safety of the team and the equipment because of rough seas caused by the presence of a tropical storm over Haiti that sent reinforced trade winds over the Lesser Antilles. The deployment was accomplished thanks to the skill of skipper Paul Gervain and dedicated OBIC staff. The OBS instrument recovery was accomplished on 21 and 22 December.

The RRS James Cook docked in Antigua on schedule, from 30 November to 3 December, where early preparations for the SEA-CALIPSO cruise were undertaken (Fig. 18, 19). Major items of equipment loaded on board were: (1) the 8-airgun array; (2) 12 XBT's (expendable bathythermographs) to measure the water column temperature; (3) the 600 m 48-channel digital streamer; (4) 48 sonobuoys donated by Lamont-Doherty Earth Observatory; (5) cetacean monitoring equipment supplied by Seiche Measurements Ltd for purposes of marine mammal environmental control; and (6) two PASSCAL Refteks for shot-time recording. The deck plan is shown in Fig. 20. The airgun and streamer engineers set up and tested their equipment at the port. This included synchronizing the streamer and airgun clocks, and supplying the streamer data logger with an electronic pulse from the airgun trigger mechanism (‘Long-Shot’ airgun controller). Much of the loading and testing of the equipment had to be carried out before the preceding JC18 cruise, also supported at Antigua port call. The turn-around time between cruises JC18 and JC19 was limited to a half day on 16 December, requiring efficiency in equipment offloading and loading, and testing.

On 16 December the airguns were installed and tested. The streamer winch had been damaged badly during transit, but a spare winch was made suitable for the cruise (Fig. 21). The cetacean monitoring equipment (Passive Acoustic Monitoring, PAM) was set up. A radio mast was erected on the ship to receive transmission from the sonobuoys, and the computers were set up in the ship's laboratory. Additionally, a RefTek (the land station seismometer type) data logger, and an OBS datalogger were set up in the ship laboratory. All data logging systems (streamer, sonobuoy, RefTek, OBS) recorded an electronic pulse from the airgun trigger mechanism for accurate timing. The depth indicators used to monitor the airgun depth were delayed at customs and consequently the ship was late leaving Antigua, so shooting began on the morning of the 17 December.

As previously mentioned, extremely rough sea conditions made OBS deployments east of Montserrat untenable, and sites to the the lee of the island were chosen to facilitate deployment and recovery of the instruments. This circumstance required modification of shiptracks, with consultations carried out between the offshore and onshore leadership groups. Both radial and quasi-circular tracks needed to be re-aligned with respect to the existing OBS positions.

When at sea shooting around Montserrat on 17-21 December, all equipment was monitored 24 h each day. The airguns were deployed by hoist from the rear deck of the RRS James Cook (Figs. 22, 23). One team of watchkeepers monitored airgun depths and misfires, streamer depth and quality, and ship navigation and speed, and deployed sonobuoys. Specialist engineers were on call for the streamer or airguns. A second team of watchkeepers monitored for cetaceans. During daylight hours this team both kept watch from the bridge, and monitored the PAM microphone array. At night just the PAM was monitored. In the case of a cetacean sighting, shooting was halted, a 20 min clearance period was enforced, and then the airguns were switched on using a “soft start” (turning on each gun 3 minutes apart).

The deployment involved 77 h of active shooting (Figs. 24, 25), with several short (31-37 min) interruptions, once to deviate ship-path for a yacht on a collision course, once to repair a gun logger, and three times due to sea mammals in the vicinity (Fig. 26). The possibility of serious interference of the shooting schedule by marine mammal detection was a worrisome concern, because frequent sightings would have had major impacts on both sea and land operations and the success of the experiment. The period of active shooting was also affected by several longer pauses required by ship command at the beginning and end of the 5 days of ship operations, to a degree not anticipated beforehand, and these pauses required adjustments to both land and sea operations. The cumulative effect of these pauses reduced the shooting time available and required modifications of the ship track, particularly for the final day. The decisions were developed by consultation between the offshore and onshore leadership groups.

As noted above many shipboard problems of varied complexity were encountered and efficiently resolved. These were critical to the success of the operation, to the credit of the dedicated and skilled National Marine Services technical staff under the meritorious leadership of Colin Day, the professionalism of the officers and crew of the RRS James Cook under the command of Master Philip Gauld, and the efficient work of the GeoPro airgun team.

Scientific results

This section focuses on five main topics: data and 2D modelling, the priminary 3D analyses of tomography, the 3D velocity model generated with further analysis, reflection imaging of deep structures, and offshore reflection profiling.

Data and 2D modelling

The data quality is generally high, with first arrivals recognisable at up to 50 km offset for the OBSs on both hydrophone and vertical geophone (Paulatto *et al*. 2010a). The horizontal components are also of high quality, suggesting that the instrument-seabed coupling was good. For the land stations, data quality depends strongly on the local noise conditions and host materials. Example data sections are shown in Fig. 27. Identified phases include crustal refracted P-wave arrivals and their multiples, refractions turning in the sediments, and wide-angle basement reflections. In the OBS data (Fig. 27a,b) two distinct P-wave refractors can be distinguished, with apparent velocities of 2.3 km s^{-1} (layer 1) and 4.0 – 6.0 km s^{-1} (layer 2) respectively, giving a first indication of the offshore velocity structure. Phases have been manually picked, from the vertical geophone or hydrophone data, depending on which one presented the best data. Picking uncertainties were estimated visually. For first arrivals at short offset uncertainties are between 20 ms and 40 ms and at longer offsets between 20 ms and 100 ms. Reflected phases that are masked by the first arrivals coda have uncertainties of 40 ms. Some gaps are present in the dataset due to short interruptions in shooting caused by sea mammals or other vessels in the vicinity and airgun maintenance.

A subset of the data was selected for the modelling presented in Paulatto *et al*. (2010a), consisting of four OBSs and four land stations, approximately aligned on a southeast to northwest line crossing Soufrière Hills and Centre Hills (black dotted line in Fig. 28). Records of the shots on the radial line to the southeast of the island and other isolated shots on the crossings between the selected profile and the shooting track in the northwest were analysed and travel times were inverted to obtain a provisional 2D seismic velocity profile through the island, with the further aim to guide the inversion of the full three-dimensional dataset.

The regularized inversion approach developed by Hobro *et al*. (2003) has been used. This method allows the data misfit and model roughness to be minimized at the same time to give a minimum-structure model, and it allows the simultaneous inversion of refractions, wide-angle reflections and multichannel seismic data.

The final 2D velocity model (Fig. 29b) extends 54 km in the horizontal direction and from the top of Soufrière Hills at almost 1000 m elevation to a depth of 10 km below sea level. The ray coverage reaches 10 km depth and is denser on the southeast of the island where shots were fired along a radial line coincident with the segment chosen for the 2D model (Fig. 29c). Layer 1 comprises the sediment layer offshore and volcanic edifice on land, and is characterised by a strong lateral velocity gradient in proximity of the coast. Velocities vary from 1.5 to 3.0 km s^{-1} offshore and from 2.5 to 5.5 km s^{-1} onshore. A high velocity core is imaged under the island, with the two highest velocity regions located under the volcanic edifices of Soufrière

Hills and Centre Hills, and also extending into layer 2. Offshore velocities in layer 2 vary from 4.0 km s^{-1} at the top to ~6.5 km s^{-1} at 10 km depth. Onshore velocities vary from 5.0 to 6.5 km s^{-1}. The interface between layer 1 and 2 is located at a depth of between 2.0 and 2.8 km. The thickness of layer 1 ranges from 1 km, far from the island, to a maximum value of 3.6 km under the Soufrière and Centre Hills, both of which have maximum elevations of about 1 km above sea level.

This velocity model reveals the presence of large lateral velocity variations beneath the volcanic edifice, extending over the entire depth range of the model. Layer 1 is interpreted as a sedimentary layer (Vp = 1.5 – 3.0 km s^{-1}) plus extrusive and intrusive volcanic material forming the island of Montserrat (Vp = 3.0 – 5.5 km s^{-1}). Since resolution below about 5.0 km is poor, interpretation of the velocity structure in layer 2 has to be cautious. Paulatto et al. (2010a) distinguish two different regions within layer 2: a well constrained upper sub-layer extending down to 5.0–7.0 km below sea level, with velocities between 3.5 and 6.0 km s^{-1}, and characterised by a strong vertical and lateral velocity gradient, and a lower sub-layer with velocities over 6.0 km s^{-1}, a lower velocity gradient, and extending to the bottom of the model which is at 10 km depth. Layer 1 plus the upper sub-layer of layer 2 correspond to the upper layer defined by Boynton *et al*. (1979), while the lower sub-layer corresponds to the top of the middle layer.

In layer 1 the predominant feature of the velocity field is the presence of high P-wave velocities beneath the island contrasting with the lower velocity sediments on the flanks and beneath the ocean floor. The velocity contours mirror the topography and suggest that the high velocity region has two cores, below Soufrière Hills and Centre Hills respectively.

Paulatto *et al*. (2010a) distinguish three regions within layer 1: a core, an apron, and the normal sedimentary cover, each characterised by different seismic velocities. The core has velocities similar to those found in the upper crust (Vp = 4.0 – 5.5 km s^{-1}), and broadly compatible with an andesitic composition (Christensen & Mooney 1995), as suggested by the surface geology (Harford et al. 2002). The interpretation of the high velocity core of layer 1 is based on the exposed geology of the Soufrière Hills Volcano, on the identification of numerous hypabyssal noritic xenoliths with hypabyssal textures in the lavas (Kiddle *et al*. 2008), and on geophysical evidence that indicates that the current eruption is fed from a shallow dyke (Mattioli *et al*. 1998; Hautmann *et al*. 2009). The exposed geology consists of andesite domes, breccias formed by rockfalls and mass wasting, and hydrothermally altered equivalents (e.g. Harford *et al*. 2002). These observations indicate that the core includes a pile of andesitic domes and a system of a dykes and sills that represent the feeders for several dome eruptions over the last 170 ka. Eruptions, flank collapses, rockfalls and erosion displace material from the top of the volcanoes and deposit it on the flanks and on the seabed, and this material, intermixed with pelagic sediments, makes up the lower-velocity apron around the cores (Le Friant *et al*. 2004, 2009). This region is exhibits a strong lateral velocity gradient and has velocities that are intermediate between the solid andesite and the submarine sediments (Vp = 2.5 – 4.0 km s^{-1}). Different degrees of compaction, grain size, water content and percentage of pelagic sediments could account for the range in seismic velocities observed. This kind of structure is not limited to the sub-aerial part of the island but continues downward to the bottom of layer 1, suggesting that the main eruption style for the island's entire history was similar to that exhibited by the current eruption.

Velocities in the sediment layer in the offshore region are those of normal oceanic sediments ($V_p = 1.5 - 3.0$ km s^{-1}) (cf. Hamilton 1980). The range of velocities observed is consistent with data from sediment cores collected in the region (Reid *et al*. 1996; Le Friant *et al*. 2008) that suggest that the main sediment components are hemipelagic calcareous and volcaniclastic sediments, interspersed with turbidites. The gradual decrease in velocity with increasing distance from the coast (Fig. 29b) is attributed to a variation in the volcaniclastic content, and to different volcaniclastic sedimentary facies having different physical characteristics. Coarse-grained sediments are expected to be more abundant close to the shelf slope, while fine-grained sediments are deposited farther away (e.g., Trofimovs *et al*. 2006).

The interface that separates layer 1 and 2 is interpreted as the paleo-seabed at the time when volcanic activity shifted from the outer to the inner Lesser Antilles Arc (~22 ka). Far from the island, where layer 1 thickness is about 1200 m, this interpretation gives a mean sedimentation rate of 5.4 cm ka^{-1}. This result is in agreement with sedimentation rate estimates from sediment cores in the Lesser Antilles (Reid *et al*. 1996; Le Friant *et al*. 2008). The interface is depressed under the island, suggesting that the load of the volcanic edifice may be causing flexure of the underlying lithosphere. There is also evidence in the coincident seismic reflection data collected (Kenedi *et al*. 2010) that a major extensional fault is crossed by this section, and could play a role in depressing the basement under the island. The interface is well constrained in the offshore region southeast of the island, where it clearly corresponds to a discontinuity in physical characteristics, but is only loosely constrained beneath the island, where there is no velocity contrast. It is not yet clear whether the reflector imaged beneath South Soufrière Hills (at x = 26 km in Fig. 29c) corresponds to the same feature as the reflector imaged offshore, separating the sediments from the igneous crust, or whether it is a distinct feature, possibly corresponding to a sill.

Preliminary three-dimensional seismic velocity model

In another preliminary study developed in early 2008 (Shalev *et al*. 2010), the first-arrival time data were inverted using the tomography code from Shalev & Lees (1998). The method develops a cubic b-spline description of the 3D volume, and applies an LSQR algorithm to invert the data. The study used 115,158 ray paths derived from 58 stations, including 25 Refteks, 19 Texans, 7 OBSs, and 7 MVO broadband stations in the exclusion zone (Fig. 30).

Starting conditions were two 1D velocity models (Shalev *et al*. 2010, Fig. 2), one each for land and for ocean, with the boundary between them defined as the bathymetric line at 200 m water depth. The target cube for the 3D inversion comprised 50 × 45 × 8 km, with a horizontal velocity grid spacing of 0.5 km in the land area, 1 km for the ocean near the land, and 5 km near the outer boundaries (Shalev *et al*. 2010, auxiliary material). Vertical grid spacing was 0.5 km to a depth of 5 km, and 1 km below 5 km. A smaller grid spacing of 0.25 km was tested for the center of the land area but showed no improvement.

To check for resolution of the 3D inversion, Shalev *et al*. (2010) ran checkerboard tests based on the starting 1D velocity models. A consistent recovery of the pattern was observed to a depth of over 4 km in the area of good ray coverage under the island, but below 5 km depth the resolution was unreliable (Shalev *et al*. 2010, auxiliary material). Although the acquisition geometry of the experiment was designed to target magma storage zones at >5 km depth under SHV, the actual seismic velocities beneath and surrounding Montserrat turned out to be faster than expected, thus turning back most of the refracting seismic energy at depths <5 km. The result for the dataset used in this preliminary study was that the first-arrival P-wave tomography produced a reliable image of the velocity structure only between 1 and 5 km in depth, and extending approximately to the shelf break.

Results of the tomographic inversion are shown in Figure 31. Notable features in the P-wave velocity structure are high-velocity anomalies below all three volcanic centres, at about 2 to 3 km depth. The most prominent of these is the anomaly below Centre Hills, with a similar but less intense anomaly under SHV (Figs. 31a, 32).

Other large and consistent anomalies are the low-velocity volumes on the flanks of the volcanic centres. There are three such anomalies, to the northeast, northwest, and southwest of Centre Hills. These anomalies are stable regardless of inversion parameters. The east-west cross section (Fig. 31d) shows both a high-velocity body under SHV and a low-velocity anomaly west of SHV. The suggestion from the image that the two anomalies are elongated downward and away from the center of the island could be an artifact of raypaths coming from the perimeter toward the center, but the geometric positions of the main high-amplitude anomalies is stable.

The fast anomalies beneath the three volcanic centres are interpreted to correspond mainly to dense crystallised andesite comprising dome cores, sills, dikes, or irregular shaped intrusions, and adjacent altered zones with silica precipitation, that are seismically faster than the surrounding material. The latter materials comprise lavas and volcaniclastic deposits, including talus, block-and-ash flow deposits, and lahars. The interpretation of crystalline cores are consistent with the work of Harford & Sparks (2001), who suggest that recurring intrusions solidify at depths up to 3 km under SHV, and by other evidence that suggests that dikes may rise to shallow depths under SHV (Mattioli *et al*. 1998; Costa *et al*. 2007; Hautmann *et al*. 2009; Linde *et al*. 2010; Voight *et al*. 2010; Chardot *et al*. 2010). The high velocities observed are consistent also with nodules in eruption products (Kiddle *et al*. 2010).

The locations of the low-velocity anomalies northeast of Centre Hills and west of SHV suggest a relationship with the volcanic centers (Fig. 32), and the features probably represent syn-volcanic apron deposits. An extension of such low-velocity features to 3–4 km depth could be problematic. There is good evidence from offshore seismic reflection profiles for buried volcaniclastic deposits to 2 km depth off the east coast of Montserrat (Kenedi *et al*. 2010). These low-velocity features could also result from hydrothermal alteration, which has been shown to reduce seismic velocities in oceanic rocks (Carlson 2001). Evidence for hydrothermal circulation beneath the Garibaldi-Richmond-St. Georges Hills region includes anomalous seismic activity (Rowe *et al*. 2004), surface hot springs and ponds, and hot water in boreholes (Chiodini *et al*. 1996). A recent MT study on Montserrat shows good correlation between these low velocity zones and low resistivity at 1–4 km depth (G. Ryan & P. Malin, unpublished data.

2009).

Enhanced three-dimensional seismic velocity model

In further analyses reported by Paulatto *et al*. (2012), first-arrival travel times were inverted to generate a 3D seismic velocity model using a tomography code based on the regularised least squares approach (Hobro *et al*. 2003). The algorithm allows a realistic multi-layer model parameterisation. The vertical components of 61 land stations were used in this study, selected to provide a regular coverage of the island and yielding 181,665 first arrival recordings (Fig. 33). This dataset is more comprehensive than that used in the preliminary work and was developed during a thorough PhD dissertation study by Paulatto in which special attention was given to data from all ten OBS stations, in addition to land stations.

Some characteristics of the upper crustal structure are evident in the raw data. Field recordings at OBS stations show delayed first arrivals and decreased signal-to-noise ratio for seismic waves undershooting SHV (Fig. 34), a signature often associated with the presence of magma bodies. The delay is matched closely by synthetic first arrivals for the final model but not by first arrivals from an earlier smoother model, suggesting that the source of the delay is captured in the final model. The delay is larger for offsets of 30–40 km, corresponding to rays turning at 6–7 km depth, and has a maximum of about 0.2 s. The reduced signal-to-noise ratio is likely due to the shadow zone of a low-seismic velocity body.

Seismic velocities were defined by interpolating a quadratic b-spline polynomial over a regular rectangular grid. The grid spacing was set to 1 km in all directions in the early inversion iterations, and the vertical grid spacing was reduced to 0.5 km after iteration 36 to allow stronger vertical velocity gradients. The starting model was based on OBS data alone and was therefore representative of the offshore structure but not the island structure. It was composed of three laterally homogeneous layers, separated by interfaces representing the seabed and sea surface. The top or first layer is an air layer with constant Vp = 0.34 km s^{-1}. The second layer is a water layer with Vp decreasing from 1.53 km s^{-1} at the surface to 1.49 km s^{-1} at 1 km depth. The third layer is a solid layer with initial laterally homogeneous velocity structure determined from a two-dimensional inversion of a subset of the data (Paulatto *et al*. 2010a).

A first estimate of the model resolution was obtained by calculating the ray density in each model cell. The deepest rays turn at about 12 km depth and the shallowest at a few hundred metres beneath the seabed (Fig. 35). The ray coverage is densest at about 3 km depth beneath the island and decreases beneath 5 km depth where most land-station rays reach their deepest point. Beneath this depth the model is constrained predominantly by rays undershooting the island, recorded at seafloor instruments.

Checkerboard tests (Zelt 1998; Seher *et al*. 2010) were carried out with patterns of varying lateral and vertical dimension. Each test consisted of inverting a synthetic dataset obtained by ray tracing in a perturbed model built by superimposing an 8% three-dimensional sinusoidal seismic velocity perturbation to the final model. The resolution is limited in the top 2 km by the irregular sampling and by the fact that most rays are sub-parallel, and is best between 2 and 6 km where the ray coverage is higher and rays cover a large range of azimuths. Between 6 and 7.5 km the resolution is still acceptable, but decreases rapidly beneath 7.5 km depth (Paulatto *et al*. 2012).

The final seismic velocity model (Fig. 36) shows that the three volcanic centres on Montserrat share a similar shallow structure, characterized by a prominent high-seismic-velocity core, likely comprising lava domes and intrusions, surrounded by a lower-seismic-velocity apron of volcaniclastic and pelagic sediments, in agreement with previous tomographic models (Paulatto *et al*. 2010a; Shalev *et al*. 2010). But at depths larger than 4 km, the new results show that the three volcanoes are strikingly different: beneath Centre Hills and Silver Hills the core seismic velocities remain higher than their surroundings, but beneath SHV we observe a low-velocity volume, or LVV. Calculation of the seismic velocity anomaly with respect to the structure of the older volcanic centres shows that the LVV is 6 to 8 km wide and at least 4 km high, with a volume of over 100 km^3. The top is at about 5 km depth but the base is not resolved since the resolution analysis shows that objects of the size of the LVV can be resolved at depths of up to 7.5 km but not greater. The volume of the LVV shallower than 7.5 km, with seismic velocity reduced by more than 0.5 km s^{-1}, is about 20 km^3.

An LVV could be caused by variations in lithology, by elevated temperatures, and/or by the presence of partial melt. Significant variations of lithology are unlikely as the three volcanoes have quite similar compositions (Harford *et al*. 2002). To understand the effect of smoothing introduced by seismic tomography and to test compatibility of our model with previous geological and geodetic constraints on the magma chamber properties, we integrated our tomographic results with numerical models of magma chamber growth (Paulatto *et al*. 2012). We modeled the three-dimensional temperature and melt distribution in the upper crust from incremental growth of a magma chamber by repeated injection of sills at specified depths (Annen *et al*. 2008). This conceptual model of magma emplacement is supported by observations of intrusive bodies elsewhere (Searle *et al*. 2003; de Saint-Blanquat *et al*. 2006; Michel *et al*. 2008) and by SEA-CALIPSO seismic imaging of horizontal reflectors beneath southern Montserrat that are interpreted as sills (Byerly *et al*. 2010).

To simulate the emplacement of a sill, the cells corresponding to the location and dimensions of the sill and the cells corresponding to a central conduit extending between the lower boundary of the domain and the depth of the sill are set to a temperature of 850◦C and to a melt fraction of 0.35, which are the estimated characteristics of SHV magma from petrology (Murphy *et al*. 2000). The cells beneath the intruded sill are shifted downwards to accommodate the new intrusion. This mechanism of floor depression is based on the assumption of mass exchange between a deeper reservoir and the shallow magma chamber we are modeling, and is observed in plutons (Cruden 1998). Two models that reflect best understanding of the recent volcanic history and productivity are shown in Paulatto *et al*. (2012, Fig. 11). The temperature and melt distributions predicted by these models were used to estimate seismic velocity anomalies, using the same methods employed in the inverse estimation of temperature and melt.

The resulting model anomalies (Fig. 37c,g) have much sharper edges and a larger magnitude than the observed seismic velocity anomaly. Several factors can contribute to smoothing in seismic tomography, but at the depth of the LVV, the main cause of smoothing is the limited bandwidth of the seismic signal. This effect was estimated by smoothing the synthetic magma chamber models with a depth-dependent three-dimensional Gaussian filter with width equal to the estimated Fresnel radius for a signal with dominant frequency of 6–25 Hz (Paulatto *et al*. 2012, *appendix*). The filter output estimates the sharpest model that can be recovered with travel-time tomography (Fig. 37d,h). The filtered synthetic magma chamber models show that only 10–30% of the actual anomaly amplitude is recovered by seismic tomography. The observed LVV is consistent with a magma chamber with size and geometry similar to model A (Fig. 12a-d), which has a volume with melt fraction > 0.30 of approximately 13 km^3 between 5.5 km and 7.5 km depth, and a maximum melt fraction just below 0.35. The total intruded volume is about twice this amount.

A larger magma chamber (~20 km^3) could be accommodated if it extended deeper than 7.5 km. The results of model B (Fig. 12e-h) show that a magma chamber with radius smaller than 1 km yields too small a seismic velocity anomaly to fit the tomographic results. Paulatto *et al*. (2012) conclude that the magma chamber has a radius of 1–2 km and extends from ~ 5.5 to at least 7.5 km depth.

Imaging deep reflectors

Reflecting imaging was the motivation for the design of the dense reflection spreads consisting of over 200 Texan recorders equipped with 4.5 Hz geophones. These deployments constituted three lines (Fig. 38), two effectively radiating NW and N from SHV and the third providing fan coverage for sources on and SE of SHV. These arrays were designed in part to “undershoot” SHV with airgun sources with the main aim to image reflections from the top of the magma chamber.

Unfortunately, despite careful application of processing and enhancement techniques, this main aim was not realized and analysis results were disappointing. Conventional CMP processing of the airgun shots recorded by the Texan arrays proved relatively ineffective at imaging crustal structure. The minimum source-receiver offsets that were imposed by bathymetric and other limitations on how close the ship could approach the island, and safety and time constraints on how close the receivers could be placed near SHV and Chances Peak left only relatively wide-angle reflections available for imaging. Imaging at such offsets is difficult under even ideal conditions, given the relatively close arrival times of true reflected energy with direct and refracted arrivals. Such discrimination is made even more difficult by interference from water bottom multiples that are generated by marine artificial sources at these water depths. A more serious problem with the array geometry was that the reflector midpoints corresponding to the actual source track/receiver deployments largely fell offshore, with relatively few actually sampling under either Montserrat in general or SHV in particular. For the “best” stack generated from the Belham Valley array (Fig. 38) best aligned to undershoot SHV, only a small fraction of the seismic section falls on the island, and the portion which does lacks upper crustal coverage due to the large minimum-offsets available. The data hint of some subhorizontal reflectors, but the quality of the data makes such inferences strained.

Although continuous, as opposed to windowed, recording was primarily imposed by the regular nature of the airgun source (one shot every 60 seconds), such recording also allowed the recording of natural sources, and in particular a number of microearthquakes that occurred near the summit of SHV. These earthquake recordings, processed using a selected subset of traditional multichannel reflection techniques, provide our most substantive indications of reflecting crustal structures near SHV.

The microearthquakes were recorded from 17 to 20 December 2007. Twenty local events were identified from the continuous data recording and correlated with events from the areal seismic network. Locations made with HypoEllipse (Lahr 1999) indicated that the epicenters were centered under the summit of SHV at relatively shallow depth, thus providing near-vertical reflection coverage for depth points relatively close to SHV (Fig. 38). The data from these microearthquakes were treated in the same manner as borehole shots in a conventional controlled source profile. Attention was focused on the Belham Valley line, which samples most closely to the SHV. Analysis concentrated on seven events that had a horizontal location error less than one kilometer, with the reported location accepted for processing purposes.

The raw earthquake gathers (e.g. Fig. 39) show clear indications of organized energy that cannot be attributed to direct P, S or surface wave energy, but rather suggest moveout consistent with reflected arrivals. However, individual reflections are difficult to trace undisrupted across the array, which we suspected was due to relative static shifts associated with the overlying crust. Starting with the raw data, elevation statics were applied to correct for changes in topography along the seismic lines, then the data were bandpass filtered from 1 to 8 Hz. To further improve reflection coherence, we applied a form of refraction statics. First P-wave arrivals were aligned to near-horizontal using linear moveout (LMO) corrections. Deviations of the first arrival time from horizontal were manually picked and used to apply a static shift to force alignment of the first arrival. The LMO correction was subsequently removed, hopefully with increased lateral alignment of reflections as well as first arrivals. A normal moveout correction (NMO) was then applied using an average velocity of 5 km s^{-1} from 0 s to 10 s to image reflection geometry at depth. Several additional coherency enhancement techniques were tested to further increase the visibility of reflected energy included FX-deconvolution, trace mixing, and FK-filtering.

The processed gathers for all seven events show strong similarities, e.g. subhorizontal reflectivity, despite being recorded for different earthquake sources (Byerly *et al*. 2010). But it is unclear whether one can defend a reflection-for-reflection correlation between the various gathers. We simply assert that the overall similarity in reflectivity argues that geological layering at a common depth, rather than noise, is being imaged. As shown in Byerly *et al*. (2010, auxiliary material), noise gathers do not replicate the key features of the microearthquake gathers, and thus we are confident that the coherent energy evident in our images originated from the microearthquake sources. The resulting individual earthquake gathers show consistent subhorizontal energy between 6 and 19 km depth beneath the NW flank of SHV. These amplitudes, which need enhancement just to be visible, provide little support for their interpretation as fluid bodies at depth. Our attempts to identify the polarity of these reflectors were unfruitful, and we are left with the conjecture that these reflectors represent either buried volcanic layering and/or later sills intruded into mid-crustal levels. The sill interpretation seems more consistent with the needed impedance contrasts to generate detectable reflections from depth. The Moho lies near 30 km (Sevilla *et al*. 2010), much deeper than any of the prominent reflections indicated by these images. Finally, the presence of sill-like features in the upper or middle crust beneath an active volcano is not surprising. Similar results were obtained using recorded ambient “noise” from the Texan recordings (L. Brown, written communication). The primary value of these studies is their demonstration that relatively high-resolution reflection imaging of crustal structure is feasible using microearthquake or ambient noise sources.

Offshore reflection profiling

The SEA-CALIPSO experiment included a 48-channel 600-m digital streamer used in a seismic reflection survey, to explore local submarine deposits and faults, and expand knowledge based on previous seismic and bathymetric studies (e.g. Feuillet *et al*. 2001, 2002). Although a low source frequency and long shot interval were selected to maximize the first-arrival tomography data and were thus less optimal for the reflection study, quite useful results were obtained (Kenedi *et al.* 2010). Here we present some key results from our survey and discuss their implications on the local tectonic and volcanic interactions.

The region examined and tectonic context are illustrated in Fig. 40 (cf. Fig. 1 for broader regional setting). The shot lines are numbered, and of these, selected sections are shown in Figs. 41-43 (for section locations see red profile lines on Fig. 40). The data were bandpass filtered between 4 Hz and 64 Hz, stacked, and migrated using sediment velocities from semblance analysis. Time to depth conversions used an average sediment velocity of 2200 m s^{-1} (Paulatto *et al*. 2010a).

On and west of Montserrat, young andesitic domes (<300 ka) and structurally uplifted areas (Harford *et al*. 2002) are aligned due to normal faulting as part of the extensional Montserrat-Havers fault system (MHFS) (Feuillet *et al.* 2010). The MHFS includes an ESE-trending lineament interpreted as the Belham Valley fault (BVF) (Harford *et al*. 2002) (Fig. 40). Normal faulting continues SE of Montserrat with a right step to the Bouillante-Montserrat fault system (BMF) (Fig. 40). Extension with approximately a N-S trend is prevalent in the region, which Feuillet *et al*. (2010) suggest is accommodated as oblique shear along a series of *en echelon* and mainly NE-dipping normal fault systems including the BMF, MHFS, and the Redonda fault system (RFS) (Fig. 40). Kenedi *et al.* (2010) propose that these systems also accommodate minor local shear that has resulted in rotation of older sediments and deformation of the footwall of the BVF and related faults.

Off the eastern shelf, reflection profiles are dominated by chaotic sediment packages of volcaniclastic debris. Eastward-tapering sediment lenses extend offshore from Silver Hills and Centre Hills (Lines 7 and 9; Figs. 40 and 41). The debris from Silver Hills (Line 7) extends ~10 km from the shelf and overlies strata that step down towards Montserrat. From Centre Hills also (Line 9), debris onlaps layered sediments that dip westward, from 1.5 s two-way travel time (twt) at km 12 to 2.2 s twt at km 5 (Fig. 41). The apparent dip (Line 9) and downward fault-step pattern (Line 7) towards the island are consistent with island subsidence or with rotation on the hanging wall of the MHFS faults (Fig. 40).

From Centre Hills the debris lenses have accumulated in stacks, the largest being ~10 km long (Fig. 41). The lenses are onlapped by and alternate with sub-horizontal strata. Kenedi et al. (2010) interpret the lenses as submarine fans from emplacements of volcaniclastic flows, caused largely by lava dome collapses and deposited over several hundred ka. Coarse submarine fans have formed in this way during the current volcanism and have produced tapering units that extend as far as 8 km offshore (Le Friant *et al*. 2009, 2010; Trofimovs *et al.* 2008, 2011).

Where fans are overlain by flat-lying sediment, sedimentation rates can be estimated. Off Silver Hills a large fan is covered by about 80 m of flat sediments, and since Silver Hills became extinct at about 1 Ma (Harford *et al*. 2002), the sedimentation rate was ~8 cm ka^{-1}. Off Centre Hills the sediments are 44 m thick., and assuming the Centre Hills became extinct at about 500 ka, the rate was approximately 9 cm ka^{-1}. Le Friant *et al*. (2008) report hemipelagic sedimentation rates 60 km offshore as 1-3 cm ka^{-1}, and at about 16 km offshore, Trofimovs *et al.* (2010) report 4–7 cm ka^{-1}. Our higher rates are consistent with a persistent near-shore source.

The N-S reflection profiles off the eastern shelf cut across the debris fans. Approximately 1-2 km offshore (Line 2, Fig. 42) a mounded feature is visible just below the sea floor between km 6 and km 11. SHV flow deposits 4-5 km off the shelf are indicated by the mound on Line 23 between kms 10 and 20. A 6 km-wide channel is visible in Line 2 at km 11 to 15, which is interpreted as an embayment associated with a previously described gravity flow (Le Friant *et al*. 2004) (*see* Fig. 40). The southern slope of the embayment is consistent with the fault scarp north of Roche's Bluff (located on Fig. 40), subsequently modified by landsliding.

Off the west coast, north-dipping fault scarps offset the ocean floor on profiles approximately 6 and 14 km offshore (Lines 21 and 15, Figs.43 and 40). The western scarp offset at km 10 of Line 15 is at least 40 m. The MHFS fault scarp and S-tilted footwall block are clear features also on the nearby profile gwa058 of Feuillet *et al*. (2010). To the north several faults break the ocean floor, indicating recent activity. A normal fault-bounded step in the morphology near km 16 on Line 15 is associated with the Redonda fault system (RFS) (Fig. 40). Further north, buried scarps have created basins of folded, syn-rift sediments, and beyond km 23, faulting is buried by about 100 m of flat basin-filling sediments.

In the south, both profiles reveal complex footwall deformation. At km 4-10 of Line 15 a series of small basins have formed on the tilted footwall, which is an ascending slope over about 1300 m of elevation. On the elevated footwall of Line 21 (at km 1), a minor graben is infilled by subhorizontal sediment (Fig. 43).

At km 3-6 on Line 21, sediments appear to dip to the south and onlap onto a major N-dipping normal fault (Fig. 43). This fault is not the same as the principal scarp fault of Line 15, but is *en-echelon* and south of it by about 2 km (Fig. 40 and Feuillet *et al*. 2010, Fig. 2). The fault may coincide with an along-strike projection of the Belham Valley fault (BVF, Fig. 40).

These images have led to some new tectonic interpretations of southern Montserrat, via integration of our new data with older studies and the work of Feuillet *et al*. (2010). Kenedi *et al.* (2010) agree with the regional model of Feuillet *et al*. (2010) that the major fault systems RFS, MHFS and BMF are mainly normal and arranged in a right-stepping *en echelon* structure, and also that on the large scale, this section of the arc accommodates regional left-lateral shear. They disagree with the interpretations of some onshore features discussed in Feuillet *et al*. (2010), and include a discussion of the SHV feeder dike in relation to the complexity of local tectonic and magmatic stresses.

Feuillet *et al*. (2010) re-introduced an old idea (e.g. Rea 1974) that Garibaldi and St. Georges Hills are volcanic cones and suggest they were fed by vents in a fissure parallel to the BVF. However the field evidence does not support this hypothesis. St. Georges, Garibaldi, and Richmond Hills are composed mainly of distal block-and-ash-flow and pumice-and-ash flow deposits, and epiclastic beds (Harford *et al.* 2002). The 3D tomography (Shalev *et al*. 2010) indicates low P-wave velocity material under St. Georges and Garibaldi Hills, quite dissimilar to the high velocity cores under SHV and Centre Hills. Thus the morphology of these hills is not primary; they are fault-bounded tectonic uplifts that have been deformed by (mostly) normal faults, and deposits have been tilted beyond the sedimentary depositional-slope limits.

A related issue is the BVF, which, in contrast to Feuillet *et al*. (2010) but following Harford *et al*. (2002), we interpret as a N-dipping normal fault. This is consistent with our interpretation of Garibaldi and St. Georges Hills as tectonic uplifts; in addition, these onshore blocks seem analogous to the prominent elevated footwalls seen offshore on Lines 15 and 21 (Fig. 43; cf. Feuillet *et al*. 2010, Fig. 3, profiles gwa 055 and 058). The N-dipping fault in our marine profile Line 21 (Fig. 43, ~km 3), is aligned with the BVF as an along-strike projection, and the north-dip on the offshore profile supports a similar interpretation for the BVF. Finally, 3D tomography (Shalev *et al*. 2010) suggests that the contact of the P-wave velocity anomaly boundary under St. Georges Hill dips roughly 50° N.

Regionally, southern Montserrat is part of a transtensional regime with extensional overprinting. Transtensional deformation zones involve rotation, local compression, and uplift (Dewey *et al*. 1998], which is consistent with the uplifted blocks and also westward-dipping sediments off the east coast. Locally, southern Montserrat includes a right-step between the MHFS and the BMF, *en echelon* normal fault systems in sinistral slip; thus uplift may have been encouraged by a minor contractional component (Deng *et al.* 1986; Cunningham & Mann 2007). The marine reflection profiles and related onshore data (e.g. Miller *et al.* 2010) indicate that on Montserrat the interplay among local faulting, volcanism, and stresses is complex. The regional transtensional system of *en echelon* faults (cf. Feuillet *et al.* 2010) has influenced volcanism, while the local fault step suggests both a component of compression near SHV and complicated and evolving stress regimes and fault movements.

Discussion and lessons learned

Scientific issues

The SEA-CALIPSO study is a rare active source tomographic experiment of an active andesitic island stratovolcano, and the first to present a detailed image of an island arc volcano in the Lesser Antilles. The current and future results of this research should help scientists to better understand volcanism at Montserrat, and provide insights on how regions of intermediate composition are developed within primarily basaltic crust at interoceanic arcs. This research enables comparisons of the Lesser Antilles arc with other arcs such as the Marianas, Izu-Bonin, Kuriles and Aleutians, and provides constraints for dynamic models of magma flow and explosive volcanism.

Our experiment used as many as 180,000 raypaths in damped smoothed inversions over a 47 x 54-km target area to produce 2D and 3D images of the P-wave seismic velocity (Paulatto *et al*. 2010a,b; Shalev *et al*. 2010). In the preliminary work, 2D inversions of a subset of data using first arrivals and wide-angle reflections revealed a heterogeneous high-velocity body underneath the island, representing the cores of volcanoes and subjacent intrusions (Fig. 29; Paulatto *et al*. 2010a,b; Voight *et al*. 2010). An interface at about 2 km depth was identified, and interpreted as the paleoseafloor probably depressed under the island from volcanic loading.

The better-constrained 3D inversions described in this paper show that high-velocity cores, interpreted as crystallized intrusions, underlie each of the volcanic centres (Figs. 31, 32, 36; Shalev *et al*. 2010; Paulatto *et al*. 2012). Such cores underlie the extinct centres to depths of nearly 8 km but occur only above 5 km under SHV (Fig. 36). A low-velocity volume (LVV) underlies SHV at depths between about 5 and nearly 8 km and is interpreted as a reservoir of partly crystallized magma that feeds the current eruption (Fig. 44). Two shallow areas of low velocity in the northeast and southwest flanks of the island reflect volcaniclastic deposits and hydrothermal alteration (Fig. 32).

Related research using receiver functions define the Mohorovic crust-mantle discontinuity at about 30 km in depth at this location (Sevilla *et al*. 2010). Offshore reflection profile lines reveal deep wedges of volcaniclastic debris and important tectonic details that illuminate the intimate connection between tectonics, volcanism, and sedimentation in volcanic arcs (Figs. 40-43).

Integration of seismic tomography with thermal numerical models allowed us to go beyond simple static constraints on present-day melt distribution (Fig. 37; Paulatto *et al*. 2012). In our models the magma chamber formed by repeated intrusion of andesite sills over a few thousand years, although our results are non-unique inasmuch as different emplacement histories can produce similar melt and temperature distributions. A single longer series of sill injections with a slower accretion rate could give a similar present-day seismic anomaly as two shorter series, with a faster accretion rate separated by a repose period. Magma chamber growth over several tens of thousand years or more induces thermal anomalies that are too cool and too broad to fit the tomography data. Over-accretion and under-accretion can give similar results, but the latter seems more consistent with field observations of exhumed granitic plutons (Wiebe & Collins1998). In rapidly growing magma chambers the emplacement dynamics are likely to be more complex, so under-accretion represents a simplified model. In our preferred model the magma chamber would become almost completely solidified 37,000 years after the last emplacement (Paulatto *et al*. 2012, Fig. 11). Shallow magma chambers of similar volume to our model can become solid over a few thousand to a few tens of thousand years if they are not continuously replenished by new influx (Annen *et al*. 2008, 2009).

These results reinforce the hypothesis that typical arc-volcano magma chambers are transient features, which only exist during active phases. Our experiment highlights the indication that even a shallow magma chamber as large as 13 km^3 is difficult to detect and constrain with seismic tomography, and that associated low-seismic-velocity anomalies may be significantly underestimated. Deeper or smaller magma chambers may prove impossible to detect with travel-time seismic tomography.

Further, where an LVV is detected, melt content is only poorly constrained by seismic data solely, and an adequate interpretation must rely on independent constraints. The melt fraction estimated under SHV from the velocity anomaly alone is only 3–10%, similar to tomography-based estimates at other magmatic systems (Menke *et al*. 2002; Haslinger *et al.,* 2001). This estimate is too low. However, we show that with the use of thermal models, and by taking into consideration the smoothing imposed by limited seismic resolution (Fig. 37), that the observed LVV under SHV is consistent with the presence of a magma chamber with more than 30% melt as more clearly indicated by the observed petrology. Thus the approach developed in this research, based on integrating seismic tomography with numerical models of magma chamber formation and incorporating petrologic and geodetic constraints, can reveal the characteristics and dynamics of magmatic systems with a level of detail that none of these methods alone has achieved (Paulatto *et al*. 2012).

Finally, we comment here on reflecting imaging. This was the main motivation for our deployment of dense reflection spreads in three main lines (Fig. 10), designed to “undershoot” SHV with airgun sources and to image reflections from the top of the magma chamber. Unfortunately, despite careful application of processing and enhancement techniques, this main aim was not realized and analysis results were disappointing. The conventional CMP processing of the airgun shots recorded by the Texan arrays proved relatively ineffective at imaging crustal structure, for the several reasons discussed previously. In retrospect there seems to be little that could have been done on this small island to improve the reflection geometry, given the resources available and the constraints that existed. Placing receivers closer to SHV, or moving the ship much closer to the island, were not realistic possibilities. More near-vertical reflection geometries were needed. However the continuous recording employed in this experiment enabled us to test two relatively unconventional but potentially promising approaches to reflection imaging near volcanoes, including using natural earthquake sources to produce reflection seismic sections (Byerly *et al*. 2010), and seismic interferometry, extracting surface waves and body waves from cross-correlating seismic noise (L. Brown, written communication).

Operational issues

Here we highlight five topics: (1) inspiration and perspiration; (2) experiment timing and equipment issues; (3) communications; (4) impact of potential volcano activity on the experiment; and (5) our interactions with local residents.

The success of our experiment owed a great deal to a large number of competent and enthusiastic people from diverse institutions who proved they were able to work hard and very well together toward a common goal over a several year period, planning carefully and assisting each other, and responding creatively to a number of difficult technical problems that arose. The team was ably supported by professional technical teams at PASSCAL, Scripps, OBIC, and NERC Marine Services, aided by the MVO, and generously assisted with supplemental funding from several sources to meet specific problems. The lesson is to devise promising research and then to populate the research team with the best expertise possible, seeking to include experienced individuals who can set egos aside in favor of benefiting the common effort.

Our initial concept was to record both natural earthquakes, and signals from a three-day active source experiment using an airgun array towed by a research vessel around Montserrat, taking opportunistic advantage of a previously-planned NERC ship operation scheduled in May 2005. Due to ship schedule delays, the cruise availability for us was withdrawn for 2005 and needed to be rescheduled for 2007. Although disappointing for us at the time, in retrospect this delay proved to be absolutely vital to the success of our experiment. We were able to develop more thorough plans, acquire additional ship time, and obtain additional financial support. We were able to double the size of the land seismometer array, leading to improved tomographic resolution. We added a digital streamer which provided the local sediment thickness data needed to account for travel-time delays in signals from the airgun shots, and in addition to provide useful reflection profiles indicating sediment type and structure. And of critical importance, we were able to include an OBS component in the experiment. The OBS array expanded the source-receiver offsets and this was the most significant factor in our achieving the resolution at depth needed to image the magma chamber. The sum of these components resulted in a vastly improved and successful experiment.

Well-planned and redundant communication systems also were vital to success. The requirement of the successful land operation was to have all seismometers recording data when the airgun shooting took place, whereas the precise timing of ship operations could not be firmly known beforehand. Significant changes in ship activity out of the control of the Chief Scientist occurred near the beginning and end of the experiment, but redundant communications enabled the necessary flexible adjustments to land operations and reprogramming of instruments. Similarly, near the end of the shooting phase of the experiment, some final adjustments needed to be made to the ship track, and good communications facilitated discussion between land and sea teams in prioritising the options. A clear discussion of all experimental plans in advance, and involving both land-based and ship-based staff and ship officers, is useful for developing contingency flexibility and avoiding misunderstandings.

Fortunately for us the activity at the Soufrière Hills Volcano was low during this experiment. The only volcano-related incident was that one scouting mission by boat had to be abandoned due to the observation of rockfalls down the crater valley on the east flank. Nonetheless, the experiment required precautions compatible with the possibility of the volcano erupting. Participants went into the volcanic exclusion zone multiple times by boat, car, and foot; each time, HQ and MVO were involved by radio or mobile phone communication. In some cases, MVO staff was required as an escort.

In the unlikely event of a large-ash producing eruption, HQ and MVO were kept informed about the Centre Hills hikers' timing and locations.

Finally, as a generalization, the residents of Montserrat have had an uneasy relationship with scientists connected to monitoring and research on the Soufrière Hills Volcano. Volcanologists have been responsible for forecasting what the volcano might do and have provided scientific advice to the authorities since the eruption began in 1995. Both the unpredictable behaviour of the volcano and misunderstandings between the public, authorities and volcanologists have led to tensions involving part of the population on occasion (Haynes *et al.* 2006). Locally there is a strong desire that the volcano will go back to sleep, volcanologists will go away, and tourists will return. Despite these issues the leaders of the on-land operations of SEA -CALIPSO were met with interest and cooperation from almost all Montserratians. People agreed to locate seismometers on their properties for three months, and no stations were vandalized. There was some concern locally about the airgun shooting, which people feared would kill marine life and deafen SCUBA divers. These concerns did not materialise. At our request the Marine Authority on island also sent out multiple warnings to local fisherman and local vessels about our cruise, to minimize the possibility of vessels impinging on ship tracks and causing interruptions to airgun shooting. The overall cooperation of the Montserrat authorities, civic leaders and population in our endeavor has been greatly appreciated.

Acknowledgements

Funding was provided by NSF, NERC, Discovery Channel TV, the British Geological Survey and the Foreign and Commonwealth Office of the UK.

Robin Reichlin, Leonard Johnson, Russ Kelz, Sonia Esperanca, and Sandy Shor at NSF provided very strong support and responded when necessary to special needs. Helen Beadman at NERC provided enthusiastic help in scheduling, and essential financial and logistic support for the cruise. Shipboard operations owed a great deal to the skill and dedication of the National Marine Services technical staff under the outstanding leadership of Colin Day, the professionalism of the officers and crew of the RV James Cook under the command of Master Philip Gauld, the efficient work of the GeoPro airgun team under the direction of Leonid Akentiev, and the skilled assistance of W. Sutherland and others representing Scripps. The excellent contributions of Gail Hough, Murray Grigor, Peter Learey, Jess Trofimovs to the shipboard science team was much appreciated. Michael Unwin and Caroline Weir provided skilled service in regard to mitigation of harm to marine animals. The late John Diebold at Lamont-Doherty provided sound and timely advice on airgun technology at a critical period in our planning, and also donated equipment. The challenging OBS deployment was accomplished thanks to the skill of skipper Paul Gervain of the Institut Régional de Pêche Marine, Guadeloupe, and the dedicated OBIC staff. On-land operations were greatly aided by the PASSCAL group in Socorro, Jim Fowler, Bruce Beaudoin, and Mike Fort, and expert field teams included in authorship. Necessary on-land assistance was provided by K Byerly, C Chen, K Jeffcoat, R Malin, L Malin, Dagan Smith, J Taron, J Walton , and J Winston. Excellent support was provided by MVO, especially Vicki Hards, Silvio de Angelis, and Michael Strutt. Catherine McClintock at PSU greatly assisted various CALIPSO funding efforts. We thank Fusion Petroleum Technologies, Inc., for aid in data processing the offshore seismic lines. Neil

X, Alex Keily and Max Williams of Darlow Smithson Productions provided media services, leading to the television documentary "*Engineering Volcanoes*" produced for Discovery Channel. Tom Dawkins of Montserrat contributed our artistic Logo.

Appendix

Cruise diary

Abbreviated diary. All times are local, 4 hours behind GMT time.

<u>Monday 3rd to Saturday 15th December</u>

The GeoPro engineers set up and tested the airgun array and controller on the James Cook during the cruise JC18, preceding JC19.

<u>Friday 7th December</u>

The OBS deployment team of C. McCoy, A. Burchell, M. Paulatto and C. Pearce flies to Guadeloupe through Paris Orly. A car is hired. Arrive at Marine de Rivi´ere Sens, Gourbeyre, Basse Terre and check in at the Hotel La Crosi´ere.

<u>Saturday 8th December</u>

First meeting with Paul Gervain at IRPM and inspection of the vessel Beryx and the workshop. We are informed by the shipping agent that our container with all the OBS instrumentation is still held at the Customs office awaiting clearance. Since the office is closed during the weekend the first possible day for delivery is Monday.

<u>Sunday 9th to Tuesday 11th December</u>

Corrected documentation is supplied through the shipping agent. The container is released the on late afternoon Tuesday 11th.

<u>Wednesday 12th December</u>

The container is delivered at 12:00. We set up the lab at IRPM and start the assemblage and initialization of the instruments. At 15:00 the team leaves port on the Beryx and performs the acoustic release test in about 1000 m of water off the west coast of Guadeloupe. The test is successful. However, even in the lee of the island, the sea is rough and most of the team soon feels the effects of sea sickness. We are back in port at about 18:00.

Thursday 13th December

The OBS team sails at 07:30 on the Beryx with four instruments on board. The plan is to deploy them at planning sites 8, 9, 10 and 6. The working conditions on board are very poor. The sea is rough especially when the boat leaves the lee of the island and since the waves come from the east while our course is mainly north-south, the roll of the boat is particularly unpleasant. Soon all the scientific crew is seasick and almost unable to work. The deployment of instruments in these conditions and from such a small boat is a particularly tricky operation, with the risks of injuring the crew or damaging the instrument. The experience of the skipper is essential to the success of the operation. Three out of four instruments are deployed (sites 8, 9 and 10). We are back in port at 19:00.

Friday 14th December

No deployments. Instead all the remaining instruments are assembled and programmed so that they are ready to be deployed, and the operations at sea are simplified and limited to lowering them in the water and log keeping. A new OBS array plan is designed by M. Paulatto and C. Peirce and approved by T. Minshull, with more instruments now to the west, on the lee side of Montserrat, and no instruments to the east. Originally planned sites 1-5 are abandoned and new sites 11-16 are added (see figures 5 and 6). REVISE FIGS

Saturday 15th December

M. Paulatto and C. Pearce fly to Antigua to join the RRS James Cook. C. McCoy and A. Burchell leave port onboard the Beryx at 06:00 to deploy instruments on sites 11, 12, 15 and 16. Since the weather is slightly improved, the vessel less crowded and the operations better organised, the deployment goes smoothly. Return to port at 19:00. Pre-cruise meeting in Saint John’s, Antigua.

Sunday 16th December

C. McCoy and A. Burchell onboard the Beryx deploy OBS instruments on sites 6, 7 and 14. Leave port at 06:00, return to port at 19:00. All instruments deployed.

The RRS James Cook arrives in port in Saint John’s, Antigua, at 09:00 as scheduled. The scientific party boards the ship at 12:00 approximately, after immigration and customs formalities. All equipment is loaded and arranged on deck and in labs. The MCS streamer winch is severely damaged and needs a new hydraulic motor, and a replacement is sought. GPS antennas for data-logger synchronisation are installed. P. Malin and M. Grigor set up a Reftek datalogger in the deck lab to record shot timing. S. Dean, C. Peirce and M. Paulatto set up an OBS data logger with the same purpose. GeoPro airfreight is delivered at 18:00. The ship leaves port at 19:30, heading to a waypoint south of Antigua.

Monday 17th December

Start of gun deployment at 07:00. At 7:35 deployed Passive Acoustic Monitoring (PAM) equipment and start marine mammal monitoring. At 10:12 beginning of shooting with soft start. Guns are activated sequentially from gun 8 to gun 1 to increase source power gradually. At 10:18 the soft start sequence is interrupted due to a yacht on ship’s course. A second soft start commences at 10:24. Soft start completed at 10:46. At 10:43 - 12:48, streamer deployment. At 14:06. shooting and acquisition system deployment is complete, and MCS acquisition can start. The speed of ship over ground is 4.5 knots. The captain decides that the ship will not sail over the shallow shelf around Montserrat, as had been originally planned. We note that if the ship turns at 5° per minute or more the streamer is pulled too close to the guns. Thus 2° per minute turns are adopted. The shooting track is modified accordingly and a provisional version is passed on to the ship's officers. At 14:11, gun 8 is shut down. At 15:54 the ship's speed is reduced by 1 knot due to overheating of thrusters. At 18:54 - 23:43, starboard gun array is shut down and brought on deck for repairs. At 19:52 - 19:59, soft start. The gun controller is rebooted at 20:01, possibly due to power failure. After another soft start is performed, guns are back on full power at 20:59. Guns are shut down at 22:45 due to dolphins in the vicinity. XBT probes keep failing after a few hundred meters and wires get tangled on the guns and streamer.

Tuesday 18th December

Continue shooting. Gun 3 is shut down at 07:13. Speed is increased to 4.5 knots. At 13:02 the portside gun array is shut down and serviced to fix gun 3. Guns are redeployed and soft start begins at 15:30. Starboard gun array is shut down and serviced at 21:08. All guns are shut down at 22:05 due to a yacht near the ship's course. Shooting restarts at 22:44.

Wednesday 19th December

Continue shooting. Shooting track is adjusted to allow maneuvering in proximity of Redonda. From 04:00, gun 8 is repeatedly shut down and turned on again, until 06:24 when it is shut down indefinitely. All guns are shut down at 10:14 for dolphins. Soft start at 10:46. Problems with portside guns at 11:57. Portside array shut down and serviced at 14:41, soft start begins at 18:03, with full array firing at 18:14. Some MCS data plots are produced on board by S. Dean.

Thursday 20th December

Continue shooting. Starboard gun array shut down at 07:24 for service. Soft start begins at 07:43 with full array firing at 07:52. All guns shut down at 09:32 due to marine mammal. Soft start at 10:10, with full array firing at 10:30. Some errors on portside guns, possibly caused by an air leak between 10:53 and the end of shooting. A yacht crosses the ship's track at 13:23. The ship is forced to slow down and turn to avoid collision. All guns are shut down at 15:00. Guns and streamer are retrieved.

Friday 21st December

The RRS James Cook returns to port in Saint John's, Antigua. OBS instruments recovery accomplished. C. McCoy and A. Burchell leave Guadeloupe on the Beryx at 06:00. Instruments 07, 11, 12, 15, 16 are recovered. The team spends the night on the boat anchored in a cove on Montserrat. Arrive at anchorage at 19.00.

Saturday 22nd December

The Beryx leaves Montserrat anchorage at 03:00. Instruments 06, 08, 09, 10 are recovered. Return to port at 18:00. M. Paulatto flies back to Guadeloupe from Antigua, to help with instrument recovery and packing.

Sunday 23rd - Monday 24th December

Container packing. C. McCoy flies back to the U.K.

Thursday 27th December

A. Burchell and M. Paulatto fly back to the U.K.

References

ANNEN, C. 2009. From plutons to magma chambers: thermal constraints on the accumulation of eruptible silicic magma in the upper crust. *Earth and Planetary Science Letters*, **284**, 409-416.

ANNEN, C., PICHAVANT, M., BACHMANN, O., BURGISSER, A. 2008. Conditions for the growth of a long-lived shallow crustal magma chamber below Mount Pelee volcano (Martinique, Lesser Antilles Arc). *Journal of Geophysical Research*, **113**, B07209, doi:10.1029/2007JB005049.

ASPINALL, W.P., MILLER, A.D., LYNCH, L.L., LATCHMAN, J.L., STEWART, R.C., WHITE, R.A., POWER, J.A. 1998. Soufriere Hills eruption, Montserrat, 1995 – 7: volcanic earthquake locations and fault plane solutions. *Geophysical Research Letters*, **25**(18), 3397-3400.

BAILEY, R. C. & GARCES, P. B. 1988. On the theory of air-gun bubble interactions. *Geophysics*, **53**, 192-200.

BARCLAY, J., CARROLL, M.R., RUTHERFORD, M.J., MURPHY, M.D., DEVINE, J.D., GARDNER, J., SPARKS, R.S.J. 1998. Experimental phase equilibria: constraints on pre-eruptive storage conditions of the Soufriere Hills magma. *Geophysical Research Letters* **25**, 3437-3440.

BARCLAY, J., HERD, R.A., EDWARDS, B., KIDDLE, E., DONOVAN, A. 2010. Caught in the act: implications for the increasing abundance of mafic enclaves during the eruption of the Soufriere Hills Volcano, Montserrat. *Geophysical Research Letters*, **37**, L00E09, 5 PP., 2010 doi:10.1029/2010GL042509.

BYERLY, K., BROWN, L., VOIGHT, B., MILLER, V. 2010. Reflection imaging of deep structure beneath Montserrat using microearthquake sources, Geophys. Res. Lett., 37(L00E20), doi:10.1029/2009GL041,995.

CARLSON, R. L. 2001. The effects of temperature, pressure, and alteration on seismic properties of diabase dike rocks from DSDP/ODP Hole 504B. *Geophysical Research Letters*, **28**(20), 3979–3982, doi:10.1029/2001GL013426.

CHARDOT, L. & 13 OTHERS 2010. Explosion dynamics from strainmeter and microbarometer observations. Soufriere Hills Volcano, Montserrat:

2008-2009. *Geophysical Research Letters*, **37**, L00E24, doi: 10.1029/2010GL044661.

CHIODINI, G., CIONI, R., FRULLANI, A., GUIDI, M., MARINI, L., PRATI, F., RACO, B. 1996. Fluid geochemistry of Montserrat Island, West Indies. *Bulletin Volcanology*, **58**, 380–392, doi:10.1007/s004450050146.

CHRISTOPHER, T., EDMONDS, M., HUMPHREYS, M.C.S., HERD, R.A. 2010. Volcanic gas emissions from Soufriere Hills Volcano, Montserrat 1995-2009, with implications for mafic magma supply and degassing. *Geophysical Research Letters*, **37**, LE00E04, doi:10.1029/2009GL041325.

COFFIN, M. F., GAHAGAN, L.M., LAWYER, L.A. 1998. Present-day Plate Boundary Digital Data Compilation., Tech. Rep. 174, University of Texas.

COSTA, A. MELNIK, O., SPARKS, R.S.J., VOIGHT, B. 2007. Control of magma flow in dykes on cyclic lava dome extrusion. *Geophysical Research Letters*, **34,** L002303, doi:10.1029/2006GL027466.

CRUDEN, A. R. 1998. On the emplacement of tabular granites. *Journal Geological Society,* **155**, 853–862.

CUNNINGHAM, W.D. & MANN, P. 2007. Tectonics of strike‑slip restraining and releasing bends. *Geological Society Special Publication*, **290,** 1–12, doi:10.1144/ SP290.1.

DE SAINT-BLANQUAT, M. & OTHERS 2006. Mechanisms and duration of non-tectonically assisted magma emplacement in the upper crust: The Black Mesa pluton, Henry Mountains, Utah. *Tectonphysics*, **428(**1), 1–31.

DENG, Q., DANING, W., ZHANG, P., CHEN, S. 1986. Structure and deformational character of strike‑slip fault zones. *Pure and Applied Geophysics*, **124**, 203–223, doi:10.1007/BF00875726.

DEWEY, J.F., HOLDSWORTH, R.E., STRACHAN, R.A. 1998. Transpression and transtension zones. *Journal Geological Society*, **135**, 1–14.

DRUITT, T.H., & KOKELAAR, B.P. (eds.) *The eruption of Soufriere Hills Volcano, Montserrat, Montserrat, from 1995-1999*. Geological Society, London, Memoirs, **21**, 645 pp.

EDMONDS, M., AIUPPA, A., HUMPHREYS, M., MORETTI, R. , GIUDICE, G., MARTIN, R.S., HERD, R.A., CHRISTOPHER, T. 2011. Excess volatiles supplied by mingling of mafic magma at an andesite arc volcano. *Geochemistry, Geophysics and Geosystems,* **11**,Q04005, doi:10.1029/2009GC002781.

ELSWORTH, D., MATTIOLI, G., TARON, J., VOIGHT, B., HERD, R. 2008. Implications of magma transfer between multiple reservoirs on eruption cycling. *Science,* **322**,246-248, doi:10.1126/science.1161297.

EVANGELIDIS, C.P., MINSHULL, T.A., HENSTROCK, T. 2004. Three-dimensional crustal structure at Ascension Island from active source tomography. *Geophysical journal International* 159, 311-325.

FEUILLET, N., MANIGHETTI, I., TAPPONNIER, P., JACQUES, E. 2002. Arc parallel extension and localization of volcanic complexes in Guadeloupe, Lesser Antilles. *Journal of Geophysical Research*, **107**(B12), 2331, doi:10.1029/2001JB000308.

FEUILLET, N., LECLERC, F., TAPPONNIER, P., BEAUDUCEL, F., BOUDON, G., LE FRIANT, A., DEPLUS, C., LEBRUN, J-F., NERCESSIAN, A., SAUREL,J-M., CLEMENT, V. 2010. Active faulting induced by slip partitioning in Montserrat and link with volcanic activity: new insights from the 2009 GWADASEIS marine cruise data. *Geophysical Research Letters*, **37**, L00E15, doi:10.1029/2010GL042556.

FOROOZAN, R., ELSWORTH, D., VOIGHT, B., MATTIOLI, G. 2010. Dual reservoir structure at Soufriere Hills Volcano inferred from continuous GPS observations and heterogeneous elastic modelling. *Geophysical Research Letters*, **37**, doi:10.1029/2010GL042511.

FOROOZAN, R., ELSWORTH, D., VOIGHT, B., MATTIOLI, G. 2011. Magmatic metering controls the stopping and restarting of eruptions. *Geophysical Research Letters*, **38**, L05306, doi:10.1029/2010GL046591.

GERARDIN, N., FEUILLARD, M., VIODE, J.P. 1991. Réseau régional sismique de l'arc des Petites Antilles: Sismicité superficielle (1981 – 1988), *Bulletin Societe Geol. Gr.,* **162**, 1003-1015.

HARFORD, C.L., SPARKS, R.S.J. 2001. Recent remobilisation of shallow-level material on Montserrat revealed by hydrogen isotope composition of amphiboles. *Earth and Planetary Science Letters,* **185**, 285-297.

HARFORD,C.L., PRINGLE, M.S., SPARKS, R.S.J., YOUNG, S.R. 2002. The volcanic evolution of Montserrat using ^{40}Ar/^{39}Ar geochronology. In: DRUITT, T.H., & KOKELAAR, B.P. (eds.) *The eruption of Soufriere Hills Volcano, Montserrat, Montserrat, from 1995-1999*. Geological Society, London, Memoirs, **21**, 93-113.

HASLINGER, F., THURBER, C., MANDERNACH, M., OKUBO, P. 2001. Tomographic image of P-velocity structure beneath Kilauea's East Rift Zone and South Flank: Seismic evidence for a deep magma body. *Geophysical Research Letters*, **28**(2), 375–378

HAUTMANN, S., GOTTSMANN, J., SPARKS, R.S.J., COSTA, A., MELNIK, O., VOIGHT, B. 2009. Modelling ground deformation caused by oscillating overpressure in a dyke conduit at Soufriere Hills Volcano, Montserrat. *Tectonophysics*, **471**,87-95.

HAUTMANN, S., GOTTSMAN, J., SPARKS, R.S.J., MATTIOLI, G.S., SACKS, I.S., STRUTT, M.H. 2010. Effect of mechanical heterogeneity in arc crust on volcano deformation with application to Soufriere Hills Volcano, Montserrat, West Indies. *Journal of Geophysical Research*, **115**, B09203, doi:10.1029JB006909.

HAYNES, K., 2006. Volcanic island in crisis: investigating environmental uncertainty and the complexity it brings. *The Australian Journal of Emergency Management*, **21**, 21-28, 2006.

HUMPHREYS, M.C.S., EDMONDS, M., CHRISTOPHER, T., HARDS, V. 2009b. Chlorine variations in the magma of Soufriere Hills Volcano, Montserrat: Insights from Cl in hornblende and melt inclusions. *Geochimica et Cosmochimica Acta*, 73, 5693-5708, doi: 10.1016/j.gca.2009.06.014.

KENEDI, C.L., SPARKS, R.S.J., MALIN, P., VOIGHT, B., DEAN, S.,

MINSHULL, T., PAULATTO, M., PEIRCE, C., SHALEV, E. 2010. Contrasts in morphology and deformation offshore Montserrat: New insights from the SEA-CALIPSO marine cruise data. *Geophysical Research Letters,* **37**, L00E25, doi:10.1029/2010GL043925

KIDDLE, E., EDWARDS, B, LOUGHLIN, S., PETTERSON, M., SPARKS, R.S.J., VOIGHT, B. 2010. Crustal structure beneath Montserrat, Lesser Antilles, constrained by xenoliths, seismic velocity structure and petrology. *Geophysical Research Letters*, **37**, L00E11, doi:10.1029/2009GL042145.

LAHR, J.C. 1999. HYPOELLIPSE: A computer program for determining local earthquake hypocentral parameters, magnitude, and first-motion pattern (Y2K compliant version). *U. S. Geological Survey Open File Repor*t 99-23.

LEES, J. M. 2007. Seismic tomography of magmatic systems. *Journal of Volcanology and Geothermal Research,* **167**(1–4), 37–56, doi:10.1016/j. jvolgeores.2007.06.008.

LE FRIANT, A., HARFORD, C.L., DEPLUS, C., BOUDON, G., SPARKS, R.S.J., HERD, R.A., KOMOROWSKI, J-C. 2004. Geomorphological evolution of Montserrat, (West Indies): importance of flank collapse and erosional processes. *Journal of the Geological Society,* **161**, 171-182, doi:10.1144/0016-764903-017.

LE FRIANT, A., LOCK, E.J., HART, M.B., BOUDON, G., SPARKS, R.S.J., LENG, M.J., SMART, C.W., KOMOROWSKI, J-C., DEPLUS, C., FISHER, J.K. 2008. Late Pleistocene tephrochronology of marine sediments adjacent to Montserrat, Lesser Antilles volcanic arc. *Journal of the Geological Society*, **165**, 279-289, doi: 10.1144/0016-7692007-019.

LE FRIANT, A., DEPLUS, C., BOUDON, G., SPARKS, R.S.J., TROFIMOVS, J., TALLING, P. 2009. Submarine deposition of volcaniclastic material from the 1995 – 2005 eruptions of Soufriere Hills volcano, Montserrat. *Journal of the Geological Society, London*, **166**, 171-182, doi: 10.1144/0016-76492008-047.

LE FRIANT, A., DEPLUS, C., BOUDON, G., FEUILLET, N., TROFIMOVS, J., KOMOROWSKI, J-C., SPARKS, R.S.J., TALLING, P.,

LOUGHLIN, S., PALMER, M., RYAN, G. 2010. Eruption of Soufriere Hills (1995-2009) from an offshore perspective: insights from repeated swath bathymetry surveys. *Geophysical Research Letters*, **37**, L11307 doi:10.1029/2010GL0435580

LINDE, A.T., SACKS, S, HIDAYAT, D., VOIGHT, B., CLARKE, A., ELSWORTH, D., MATTIOLI, G., MALIN, P., SHALEV, E., SPARKS, S., WIDIWAJAYANTI, C. 2010. Vulcanian explosion at Soufriere Hills Volcano, Montserrat on March 2004 as revealed by strain data. *Geophysical Research Letters*, **37**, L00E07, doi:10.1029/2009GL041988.

MATTIOLI, G.S., DIXON, T.H., FARINA, F., HOWELL, E.S., JANSMA, P.E., SMITH, A.L. 1998. GPS measurement of surface deformation around Soufrière Hills Volcano, Montserrat from October 1995 to July 1996. *Geophysical Research Letters*, **25**(18), 3417–3420, doi:10.1029/98GL00931.

MATTIOLI, G.S.& Y OTHERS 2004. Prototype PBO instrumentation of CALIPSO Project captures world-record lava dome collapse on Montserrat. *EOS, Transactions American Geophysical Union,* **85** (34), 317-325.

MATTIOLI, G., HERD, R.A., STRUTT, M.H., RYAN, G.,WIDIWIJAYANTI, C., VOIGHT, B. 2010. Long-term surface deformation of Soufriere Hills Volcano, Montserrat from GPS geodesy: inferences from simple elastic inverse models. *Geophysical Research Letters*, **37**, L00E13, doi:10.10292009GL042268.

MELNIK, O. & SPARKS, R.S.J. 2002. Modelling of conduit flow dynamics during explosive activity at Soufrière Hills Volcano, Montserrat. *In:* Druitt, T.H. and Kokelaar, B.P. (eds) *The eruption of the Soufrière Hills Volcano, Montserrat 1995 to 1999*. Geological Society, London. Memoir 21, 307-318.

MELNIK, O. & COSTA, A. (this volume). Dual chamber-conduit models of non-linear dynamic behaviour at Soufriere Hills Volcano, Montserrat.

MELNIK, O., SPARKS, R.S.J. 2005. Controls on conduit magma flow dynamics during lava dome building eruptions. *Journal of Geophysical Research,* **110,** B02209, doi:10.1029/2004JB003183.

MENKE, W., WEST, M., TOLSTOY, M. 2002. Shallow-crustal magma chamber beneath the axial high of the Coaxial segment of Juan de Fuca

Ridge at the source site of the 1993 eruption. *Geology*, **30**(4), 359–362.

MICHEL, J., BAUMGARTNER, J., PUTLITZ, B., SCHALTEGGER, U., OVTCHAROVA, M. 2008. Incremental growth of the Patagonian Torres del Paine laccolith over 90 k.y, *Geology*, **36**, 459–462.

MILLER, V., VOIGHT, B., AMMON, C.J., SHALEV, E., THOMPSON, G. 2010. Seismic expression of magma-induced crustal strains and localized fluid pressures during initial eruptive stages, Soufriere Hills Volcano, Montserrat. *Geophysical Research Letters*, **37**, L00E21, doi:10.1029/2010GL043997.

MINSHULL, T.A., PIERCE, C., SINHA, M.C. 2005. Multi- disciplinary, sub-seabed geophysical imaging. Sea Technology, **46**(10), 27–31.

MURPHY, M.D., SPARKS, R.S.J., BARCLAY, J., CARROLL, M.R., BREWER, T.S. 2000. Remobilization of andesite magma by intrusion of mafic magma at the Soufriere Hills Volcano, Montserrat, West Indies. *Journal of Petrology*, **41**, 21–42.

NOC 2008, Cruise Report JC19 RRS James Cook and Vessel Beryx, National Oceanography Centre, Southampton, 211 pp.

OKAYA, D. & X OTHERS 2002. Double-sided onshore-offshore seismic imaging of plate boundary: super-gathers across South Island, New Zealand. *Tectonophysics*, **355**, 243-263.

PAULATTO, M. & 13 OTHERS 2010a. Upper crustal structure of an active volcano from refraction/reflection tomography, Montserrat, Lesser Antilles. *Geophysical Journal International*, doi:10.1111/j.1365-246X.2009.04445.x

PAULATTO, M., MINSHULL, T.A., HENSTOCK, T.J. 2010b. Constraints on an intrusive system beneath the Soufriere Hills Volcano, Montserrat, from finite difference modelling of a controlled source seismic experiment. *Geophysical Research Letters*, **37**, L00E01, doi: 10.1029/2009GL041805.

PAULATTO M., ANNEN, C., HENSTOCK,T.J., KIDDLE, E., MINSHULL, T.A., SPARKS, R.S.J. AND VOIGHT, B. 2012. Magma chamber properties from integrated seismic tomography and thermal modelling at Montserrat. *Geochemistry, Geophysics, Geosystems* **13**, Q01014,doi:10.1029/2011GC003892.

PERRET, F., 1939. The volcano-seismic crisis at Montserrat 1933-1937. *Publication of the Carnegie Institution*, **212**, 76pp.

POWELL, C.F. 1938. The Royal Society expedition to Montserrat, B.W.I.: Final Report. *Philosophical Transactions Royal Society London, A*, **237**, 1-34.

POWER, J.A., WYSS, M., LATCHMAN, J.L. 1998. Spatial variations in the frequency-magnitude distribution of earthquakes at Soufriere Hills volcano, Montserrat, W.I. *Geophysical Research Letters*, **25**, 3653-3656.

REA, W.J. 1974. The volcanic geology and petrology of Montserrat, West Indies. *Journal of the Geological Society of London,* **130**, 341-366.

ROWE etal 2004 Rowe, C. A., C. H. Thurber, and R. A. White (2004), Dome growth behavior at Soufrière Hills Volcano, Montserrat, revealed by relocation of volcanic event swarms, 1995–1996. *Journal of Volcanology and Geothermal Research,* **134**(3), 199–221, doi:10.1016/j.jvolgeores.2004.01.008.

RUTHERFORD, M.J., DEVINE, J.D. 2003. Magmatic conditions and magma ascent as indicated by hornblende phase equilibria and reactions in the 1995-2002 Soufriere Hills magma. *Journal of Petrology*, **44**,1433-1454.

SEARLE, M.P., SIMPSON, R.L., LAW, R.D., PARRISH, R.R., WATERS, D.J. 2003. The structural geometry, metamorphic and magmatic evolution of the Everest massif, High Himalaya of Nepal-South Tibet, *Journal of the Geological Society*, **160**, 345–366.

SEHER, T., SINGH, S.C., CRAWFORD, W.C., ESCARTIN, J., 2010. Upper crustal velocity structure beneath the central Lucky Strike Segment from seismic refraction measurements, *Geochemistry Geophysics and Geosystems,* **11**, Q05001, doi:10.1029/ 2009GC002894.

SEVILLA, W.I., AMMON, C.J., VOIGHT, B., DE ANGELIS, S. 2010. Crustal structure beneath the Montserrat region of the Lesser Antilles island arc. *Geochemistry, Geophysics and Geosystems*, **11**,Q06013, doi:10.1029/2010GV003048.

SHALEV, E., LEES, J.M. 1998. Cubic b-splines tomography at Loma Prieta. *Bulletin of the Seismological Society of America,* **88**, 256-269.

SHALEV, E. & 10 OTHERS 2010. Three-dimensional seismic velocity tomography of Montserrat from SEA-CALIPSO offshore/onshore experiment. *Geophysical Research Letters,* **37**, L00E17, doi:10.1029/2010GL042498.

SHEPHERD, J.B., TOMBLIN, J.F., WOO, D.A. 1971. Volcano-seismic crisis in Montserrat, West Indies 1966-67. *Bulletin of Volcanology*, **35**, 143-163.

SPARKS, R.S.J., YOUNG, S.R. 2002. The eruption of Soufriere Hills Volcano, Montserrat (1995-1999): overview of scientific results. In: DRUITT, T.H., & KOKELAAR, B.P. (eds.) *The eruption of Soufriere Hills Volcano, Montserrat, from 1995-1999*. Geological Society, London, Memoirs, **21**,45-69.

STRANDENES, S., VAAGE, S., ZALLBERG-METESELAAR, G., SODAL, A. 1991. Comparison of airgun clusters. *Society of Exploration Geophysicists, Abstracts*, **61**, 792-795.

TROFIMOVS, J., SPARKS, R.S.J., TALLING, P.J. 2008. Anatomy of a submarine pyroclastic flow and associated turbidity current: July 2003 dome collapse, Soufriere Hills volcano, Montserrat, West Indies. *Sedimentology*, **55**, 617-634.

TROFIMOVS, J. & X OTHERS 2010. Evidence for carbonate platform failure during rapid sea-level rise; ca 14000 year old bioclastic flow deposits in the Lesser Antilles. *Sedimentology,* **57**, 735-759, doi:10.1111/j.1365-3091.2009.01117.x

TROFIMOVS J. & 11 OTHERS 2011. Submarine pyroclastic flow deposits formed during the 20th May 2006 dome collapse of the Soufriere Hills Volcano, Montserrat. *Bulletin of Volcanology*, doi:10.1007/s00445-011-0533-5.

VOIGHT, B. & 19 OTHERS 1999. Magma flow instability and cyclic activity at Soufriere Hills Volcano, Montserrat, B.W.I. *Science*, **283**, 1138-1142.

VOIGHT, B. & 17 OTHERS 2006. Unprecedented pressure increase in deep magma reservoir triggered by lava-dome collapse. *Geophysical Research Letters*, **33**, L03312, doi:10.1029/2005GL024870.

VOIGHT, B. & SPARKS, R.S.J. 2010. Introduction to special section on the eruption of Soufriere Hills Volcano, Montserrat, the CALIPSO Project, and the SEA-CALIPSO arc –crust imaging experiment. *Geophysical Research Letters*, **37**, L00E23, doi: 10.1029/2010GL044254.

VOIGHT, B. & 10 OTHERS 2010a. Active source seismic experiment peers under Soufriére Hills Volcano. *Eos Trans. AGU*, **91**(28), 245, doi:10.1029/2010EO280002.

VOIGHT, B., WIDIWIJAYANTI, C., MATTIOLI, G., ELSWORTH, D., HIDAYAT, D., STRUTT, M. 2010b. Magma-sponge hypothesis and stratovolcanoes: Case for a compressible reservoir and quasi-steady deep influx at Soufriere Hills Vocano, Montserrat. *Geophysical Research Letters*, **37**, L00E05, doi:10.1029/2009GL041732.

VOIGHT, B. & 14 OTHERS. 2010c. Unique strainmeter observations of Vulcanian explosions, Soufriere Hills Volcano, Montserrat, July 2003. *Geophysical Research Letters*, **37**, L00E18, doi:10.1029/2010GL042551.

WADGE, G., HERD, R., RYAN, G., CALDER, E.S., KOMOROWSKI, J-C. 2010. Lava production at Soufriere Hills Volcano, Montserrat: 1995-2009. *Geophysical Research Letters*, **37**, L00E03, doi:10.1029/2009GL041466.

WIDIWIJAYANTI, C., CLARKE, A., ELSWORTH, D., VOIGHT, B. 2005. Geodetic constraints on the shallow magma system at Soufrière Hills Volcano, Montserrat. *Geophysical Research Letters*, **32**, L11309. doi:10.1029/2005GL022846.

WIEBE, R., & COLLINS, W.J. 1998. Depositional features and stratigraphic sections in granitic plutons: implications for the emplacement and crystallization of granitic magma chambers, *Journal of Structural*

Geology, **20**, 1273–1289.

ZANDOMENEGHI, D., BARCLAY, A., ALMENDROS, J., IBANEZ GODOY, J.M., WILCOCK, W.S.D., BEN ZVI, T. 2009. Crustal structure of Deception Island volcano from P wave seismic tomography: Tectonic and volcanic implications. *Journal of Geophysical Research*, **114**, B06310, doi:10.1029/2008JB006119.

ZELLMER, G.F., HAWKESWORTH, C.J., SPARKS, R.S.J., THOMAS, L.E., HARFORD, C., BREWER, T.S., LOUGHLIN, S. 2003a. Geochemical evolution of the Soufrière Hills volcano, Montserrat, West Indies. *Journal of Petrology*, **44**, 1349-1374.

ZELLMER, G.F., SPARKS, R.S.J., HAWKESWORTH, C.J., WIEDENBECK, M. 2003b. Magma emplacement and remobilization timescales beneath Montserrat: insights from Sr and Ba profiles across plagioclase phenocrysts. *Journal of Petrology*, **44**, 1413-1432.

ZELT, A.C. 1998. Lateral velocity resolution from 3-d seismic refraction data. *Geophysical Journal International*, **135**, 1101–1112.

Captions

Fig. 1. Seafloor bathymetry and tectonic setting for Montserrat and SEA-CALIPSO experiment (after Feuillet *et al*. 2010). Topography and insular shelf bathymetry from Le Friant *et al*. (2004). Bathymetry from AGUADOMAR and GWADASEIS cruises. Contours at 100 m interval. Active faults: black lines with ticks. Seismicity from PDE USGS. Double black arrows: local direction of extension. Large scale sinistral shear direction is indicated. Half black arrow with bars: regional scale tilt of the MHFS footwall. Dashed lines with names: location of seismic profiles in Feuillet *et al*. (2010). In white, submarine volcanoes. Top right inset: N225°E illuminated bathymetry and topography. Sinistral offsets of volcanic complexes are indicated by white dashed lines with a double arrow. The numbers in kilometers indicates the offsets. Dashed black lines: location of bathymetric profiles in Feuillet *et al*. (2010, Fig. S2). Bottom left inset: volcano tectonic map of Montserrat. Volcanic complex ages from Harford *et al*. (2002). In orange, Soufrière Hills domes: CaP, Castle Peak; CP, Chances

Peak; GaP, Galways Peak; GP, Gages Peak; PMt, Perches Mt. In white, South Soufrière Hills dome: FM, Fergus Mountain. In grey: GH, Garibaldi Hill; SGH, St Georges Hill. Kinsale-SP F., Kinsale-St Patrick fault; MHFS, Montserrat Havers Fault System; RH, Richmond Hill; SSH, South Soufrière Hills Inferred or less active faults are indicated by dashed lines.

Fig. 2. Evolution of ship-track plans. (a) Sketch from 2004 showing original concept of shiptracks (shotlines), with a Texan array onshore. (b) Bathymetric map showing the OBS deployment sites planned for 2007, and actual shiptrack. Anticipated OBS sites are shown offshore as crossed-circles. Land stations include Refteks (red dots) and Texan arrays (blue lines). DEM from Le Friant *et al*. (2004). (c) Similar figure showing final OBS station array and shiptrack positions. Note substantially changed OBS site locations. [NOTE TO REVIEWER, WE ARE REDRAFTING THIS FIG TO IMPROVE CLARITY]

Fig. 3. Bolt 'Long Life' airgun units assembled on a rigid frame and connected to the ship by electric cables and high-pressure tubes. Two frames were used, towed side-by-side with a separation of 9 m. (R.S.J. Sparks photo)

Fig. 4. Schematics of the gun array. Gun numbers and volumes in cu. in. are shown. The total volume is 2600 cu. in.

Fig. 5. An LC2000 four-component Ocean Bottom Seismometer (OBS). Instrument was designed by Scripps Institution of Oceanography. M. Paulatto photo.

Fig. 6. Two LC2000 Ocean Bottom Seismometers being readied for deployment in December 2007, with M. Paulatto in Guadaloupe onboard the vessel Beryx.

Fig. 7. The RefTek RT130 seismometer recorder, with 3-component Mark Products model L22, 2.0 Hz geophone. B. Voight photo.

Fig. 8. The RefTek RT125A seismometer, with cable to a single vertical component Mark Products L40 (or L28) 4.5 Hz sensor. B. Voight photo.

Fig. 9. The RefTeks were deployed from October through December, powered by deep cycle batteries with solar panel recharging. Site installation at Air Studios. B. Voight photo.

Fig. 10. Deployed instruments, on topographic base map of Montserrat. Inset table provides key. Refteks: blue squares, with unrealized stations shown by orange squares. Texan arrays: strings of yellow or green circles. The northern SW-NE Texan array was considered in planning stages, but not used. MVO seismograph sites: white triangles. CALIPSO strainmeter sites: white dots. Hazard zone safe-unsafe boundary: blue line. MVO: purple rectangle. Main Centre Hills trail: brown line.

Fig.11. Schematics of the ship, airgun array position, and streamer geometry used in SEA-CALIPSO experiment (after NOC 2008).

Fig. 12. Installation of typical RefTek seismometer station in October 2007.

Fig. 13. Loading RefTek equipment aboard the vessel Daily Bread at Little Bay in north Montserrat, for deployment along the south coast in October 2007.

Fig. 14. The rugged terrain of the Centre Hills, mountainous rainforest with steep ridges and valleys. Hikers carried Texans just before airgun shooting, using trails on precipitous wet soil-veneered slopes that could be almost invisible because of the dense vegetation. Shortly before the experiment some trails were cleared with machetes.

Fig. 15. Installing Texans on top of Katy Hill (near the words “Centre Hills” on Fig. 10), on the north-south Texan array line, in dense cloud-forest vegetation. A. Belousov photo.

Fig. 16. Oblique view of Montserrat island toward the southeast. The volcanic centres of Silver Hills, Centre Hills, and SHV run from north to south (left to right). Texan array lines are shown by colored triangles, with two arrays intersecting across the top of the Centre Hills (cf. Fig. 10). The array in green is radial to the Soufriere Hills Volcano, and roughly follows the Belham River valley. Refteks are shown by white triangles. Shiptracks are shown offshore, and the island of Guadaloupe, to the south, is at top of image. Image is from NASA, 2009.

Fig. 17. The 34-m vessel Beryx, based in Gourbeyre, Basse Terre, Guadeloupe, and used for OBS deployments.

Fig. 18. RRS James Cook (a) at sea and (b) in St. Johns, Antigua harbor.

Fig. 19. Loading equipment and supplies on the RRS James Cook at Antigua port call.

Fig. 20. Ship deck plan for the JC19 cruise.

Fig. 21. Streamer winch in operation on deck of RRS James Cook. J. Hammond photo.

Fig. 22. Hoist operations on stern rear deck of the RRS James Cook. J. Hammond photo.

Fig. 23. Airgun array being prepared for deployment off the stern of the RRS James Cook. J. Hammond photo.

Fig. 24. Shooting on a radial track offshore eastern Montserrat. Airgun explosion bubbles may be seen behind the hoist. The Tar River valley leading up to the Soufriere Hills Volcano is in the distance with the volcano summit covered by cloud cap. R.S.J. Sparks photo.

Fig 25. Synchronized explosions from the dual airgun clusters, offshore Montserrat.

Fig. 26 (a, b). Marine mammals alongside the RRS James Cook. The possibility of serious interference of the shooting schedule due to marine mammal detection was a serious concern, because frequent sightings and shooting shutdowns could have had major impacts on both sea and land operations and the success of the experiment.

Fig. 27. Examples of seismic data plotted as common receiver gathers (after Paulatto *et al*. 2010a). Panels correspond to the radial shooting line from point A (right end of the panels) to site O10 (left end), shown in Fig. 28, recorded on the eight instruments used in the 2D inversion. (a)-(d) Hydrophone channel recordings of OBS stations O09, O10, O12 and O11. (e)-(f) Vertical geophone recordings of Texan stations B94 and C46. (g)-(h) Vertical component recording of Reftek 130 stations M11 and M30. Synthetic traveltimes calculated through the final velocity model are

superimposed on the data (blue: layer 1 refractions; green: layer 2 refractions; red: basement reflections). The white gap present in all panels corresponds to an interruption in shooting due to marine mammals in the vicinity of the guns. A minimum-phase filter with corner frequencies 3-5-20-25 Hz was applied to the data. Amplitudes are normalized with a factor inversely proportional to offset.

Fig. 28. Bathymetric map of Montserrat with SEA-CALIPSO station array and shot positions. The black dashed line marks the position of the 2D tomographic section presented in this study. The digital elevation model was obtained by merging the GEBCO 08 Grid (http://www.gebco.net) with a detailed elevation model of Montserrat and the surrounding sea floor from Le Friant *et al*. (2004). After Paulatto *et al*. (2010a)

Fig. 29. (a) Starting model for 2D inversion process. (b) Final 2-layer model, paler areas are not sampled by rays inverted in the final step. (c) Ray coverage of final model. Segments of the basement interface that are sampled by wide angle reflections are highlighted in red. (d) Velocity uncertainty estimate. (e) Depth uncertainty estimate for basement interface. Station positions are marked by red dots. Vertical exaggeration is 2:1. After Paulatto *et al*. (2010a).

Fig. 30. Map of 3D tomography area showing bathymetry, topography contours, ship track, and station locations used in the Shalev *et al*. (2010) study, and average time residuals for shots and land based recorders. Black triangles mark the seismic stations included in the tomographic inversion. The stations offshore are ocean bottom seismometers. Colors stand for the average residuals (time computed minus time observed) in seconds where red represents slow and blue represents fast. On land, the colors contour the average residuals; on water, colors represent the average residual for each shot. The width of the ship track line is proportional to the number of seismic stations that recorded an airgun blast from a particular point on the track.

Fig. 31. P-wave tomography results displayed as perturbation from the average velocity at each depth. Blue represents faster velocities and red represents slower velocities. Map view slices through the target volume at depths (a) 2.0, (b) 3.5, and (c) 5.0 km. The black line marks the location of (d) the cross section across the SHV. The outline of Montserrat is a white line on all map view slices. After Shalev *et al*. (2010).

Fig. 32. Three-dimensional iso-surfaces of velocity anomalies, after Shalev *et al*. (2010). The blue surfaces define anomalies that are >6% faster than average. The red surfaces represent anomalies that are >6% slower than average. (a) Map view. (b) View from the east southeast. (C) View from the south-southwest.

Fig. 33. Topographic map of survey area with recording array and shot positions. Contour interval is 200 m. Shiptrack shown by red line with shot numbers labelled every 100 shots. Locations of the sections shown in Fig. 36 are marked with black dashed lines. SH: Silver Hills; CH: Centre Hills; SHV: Soufriere Hills Volcano. Reftek stations in blue, Texans in red, MVO stations in white. The stations corresponding to example data in Paulatto *et al*. (2012, Figs. 2,3) are highlighted in red. The panel on the right shows the location of Montserrat in the Lesser Antilles. Plate boundaries from Coffin *et al*. (1998). Digital elevation model from Le Friant *et al*. (2004) and the GEBCO 08 Grid (http://www.gebco.net).

Fig. 34. Field recordings showing delayed first arrivals and reduced signal-to-noise ratio beneath SHV, after Paulatto *et al*. (2012). (a) Map with location of instruments and data sections. Ship track in orange, shots corresponding to sections shown in Figs. 34b–34f are highlighted in red. (b) Section through SHV, corresponding to dashed line in (a), showing topography and ray trajectories. The approximate extent of the low velocity volume is marked with a dashed red circle. (c–f) Data corresponding to shots highlighted in Fig. 34a. First arrivals with error bars in blue. Travel-times for final model in red. Travel-times for preliminary smoothed model in pink (Paulatto *et al*. 2012, Fig. 5, iteration 36). The traces highlighted in green correspond to shots noted by green stars in Fig. 34a.

Fig. 35. Ray density. (a) W-E section. (b) S-N section. (c-d) horizontal sections at 2 and 7 km depth respectively. After Paulatto *et al*. (2012).

Fig. 36. Final seismic velocity model. (a–c) W-E sections through the three major volcanic centers. The high-seismic-velocity cores of the volcanoes are marked with white dashed lines representing 0.25 km/s seismic velocity anomaly contour with respect to the average seismic velocity of the island. (d) S-N section. Dashed frame marks the section of a model shown in Paulatto *et al*. (2012, Figs. 10–12). (e, f) Horizontal sections at 2 and 7 km depth below sea level respectively. The coastline and the 200 m depth contour are marked with thick black lines. The white circles bound the area over which the reference model for seismic velocity anomalies was

calculated. Lighter areas have no ray coverage. After Paulatto *et al*. (2012).

Fig. 37. Models of magma chamber accretion and predicted seismic velocity anomaly (after Paulatto *et al*. 2012). Model A: two successive events of under-accretion of 300-m-thick sills with 2 km radius at 400-year intervals, each starting at 5 km depth and lasting 4000 years, with a 15,000-year repose period. (a) Present-day temperature distribution, corresponding to 4000 years after start of second intrusion event. (b) Melt fraction. (c) calculated P-wave velocity anomaly. (d) P-wave velocity anomaly of filtered model. (e–h) Model B: same as Figs. 37a–37d for sills with 1 km radius.

Fig. 38. (a) On left, map of Montserrat showing the locations of the Texan seismic arrays (triangles), along with the best located microearthquakes used in this study (stars). The CDP reflection points corresponding to the Belham Valley recordings of a typical event are shown as circles. (b) On right, schematic cross-section illustrating depths of the sources relative to the recording spread, together with a resulting image (source gather). After Byerly *et al.* (2010).

Fig. 39. Example microearthquake gather illustrating the processing steps used to enhance possible deep reflections. (a) Raw data. (b) Data with bandpass filter and elevation statics. (c) Alignment using first arrivals and linear moveout. (d) Display with NMO. (e) NMO, FX-decon and trace mix (applied twice). After Byerly *et al.* (2010).

Fig. 40. Montserrat bathymetry and tectonic model. Grey curved line: Track of the RRS James Cook. Lines in red (7, 9, 2, 23, 15, 21) are discussed in this paper. Red circles: volcanic centers. Black fault symbols: normal faults from profiles, apparent dip as indicated. Thick dashed lines: major fault of the fault systems, including BVF and possible extension to RB. Large black arrows: extension direction (after Feuillet *et al*. 2001). Dotted lines: Gravity flow deposits 1–5 of Le Friant *et al*. (2004). Red squares: tectonic uplifts. Thin dashed lines: cross sections (P52, P56) along deposits from Le Friant *et al*. (2004). Orange fault north of the map: inferred from 1985–1986 Redonda earthquake mechanisms (Girardin *et al*. 1991; Feuillet *et al*. 2002). BMF, Bouillante‑Montserrat fault system; BVF, Belham Valley fault; CH, Centre Hills; GH, Garibaldi Hill; MHFS, Montserrat‑Havers fault system; RB, Roche's Bluff; RFS, Redonda fault system; RH, Richmond Hill; RHF, Richmond Hill fault; RI, Redonda Island; SGH, St. Georges Hill; SH, Silver Hills; SHV, Soufrière Hills Volcano. Bathymetry map from Institut de

Physique du Globe de Paris and M. Paulatto, NOCS. After Kenedi *et al.* (2010).

Fig. 41. Seismic reflection profiles and annotated interpretations of radial Lines 7 and 9. Solid lines: strong reflectors and sediment packages. Short dashed lines: faults. Thin dashed line: bottom multiple. Intersection with Lines 2 and 23 indicated at top. After Kenedi *et al.* (2010).

Fig. 42. Seismic reflection profiles and annotated interpretations of Lines 2 and 23, parallel to the east coast. Description as in Fig. 41. Intersection with Lines 7 and 9 indicated at top. Vertical lines at the top: boundaries between the major volcanic centres. After Kenedi *et al.* (2010).

Fig. 43. Seismic reflection profiles and annotated interpretations of Lines 15 and 21, off the west coast. Description as in Fig. 41. After Kenedi *et al.* (2010).

Fig. 44. Schematic N-S (from right to left) cross-section through Montserrat, illustrating insights from the SEA-CALIPSO experiment. The volcanic centres shown are, right to left, the extinct Silver Hills and Centre Hills complexes, underlain by solidified intrusions and magma chambers, and the Soufriere Hills Volcano, underlain by some solidified intrusions at shallow level, but with a partly molten magma chamber below 5 km depth. Contours of P-wave velocity are shown schematically and can be compared with Fig. 36.

SEACALmemoirFINALfigs

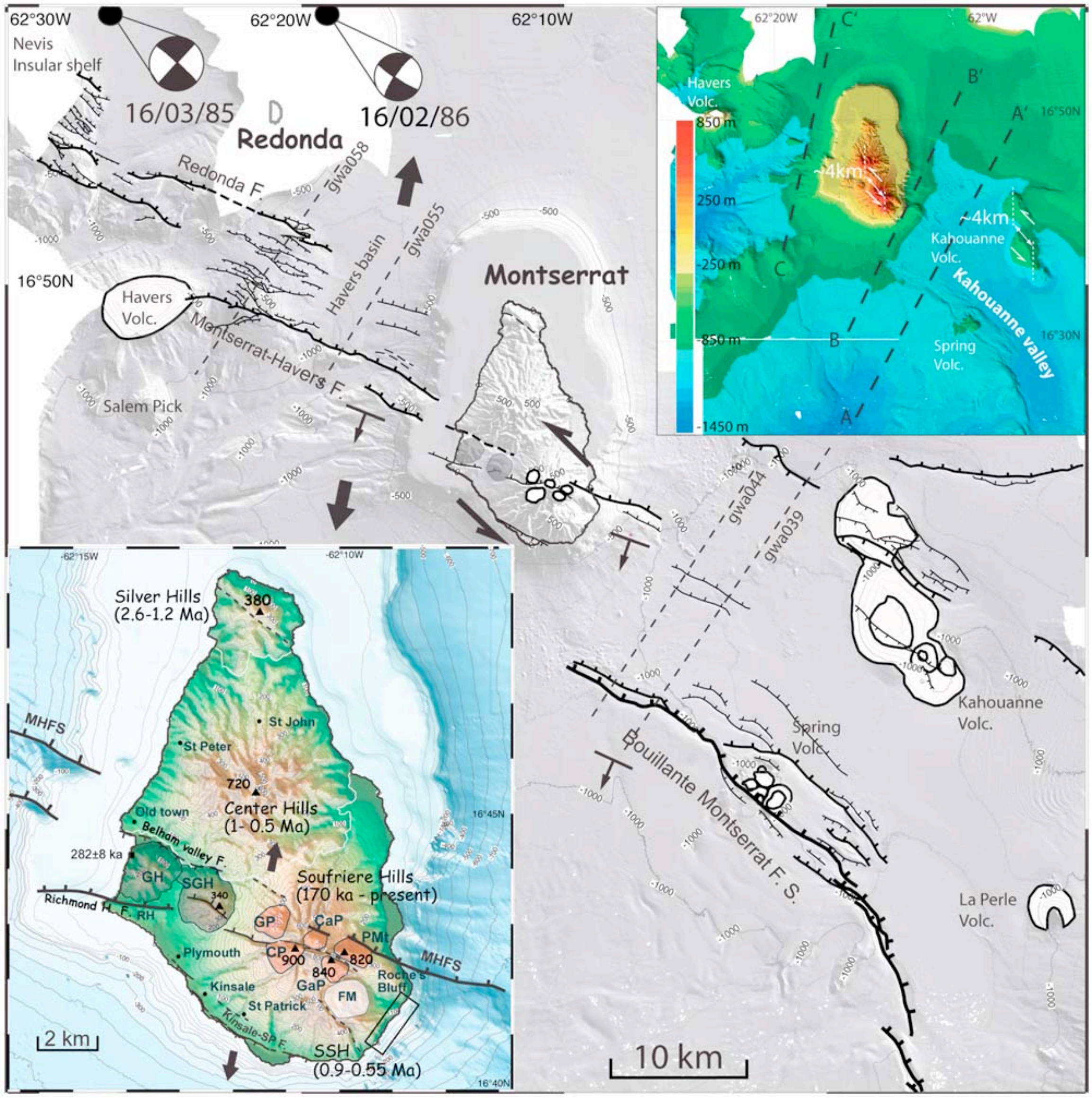

Fig. 1. Seafloor bathymetry and tectonic setting for Montserrat and SEA-CALIPSO experiment (after Feuillet *et al*. 2010). Topography and insular shelf bathymetry from Le Friant *et al*. (2004). Bathymetry from AGUADOMAR and GWADASEIS cruises. Contours at 100 m interval. Active faults: black lines with ticks. Seismicity from PDE USGS. Double black arrows: local direction of extension. Large scale sinistral shear direction is indicated. Half black arrow with bars: regional scale tilt of the MHFS footwall. Dashed lines with names: location of seismic profiles in Feuillet *et al*. (2010). In white, submarine volcanoes. Top right inset: N225°E illuminated bathymetry and topography. Sinistral offsets of volcanic complexes are indicated by white dashed lines with a double arrow. The numbers in kilometers indicates the offsets. Dashed black lines: location of

bathymetric profiles in Feuillet *et al*. (2010, Fig. S2). Bottom left inset: volcano tectonic map of Montserrat. Volcanic complex ages from Harford *et al*. (2002). In orange, Soufrière Hills domes: CaP, Castle Peak; CP, Chances Peak; GaP, Galways Peak; GP, Gages Peak; PMt, Perches Mt. In white, South Soufrière Hills dome: FM, Fergus Mountain. In grey: GH, Garibaldi Hill; SGH, St Georges Hill. Kinsale-SP F., Kinsale-St Patrick fault; MHFS, Montserrat Havers Fault System; RH, Richmond Hill; SSH, South Soufrière Hills Inferred or less active faults are indicated by dashed lines.

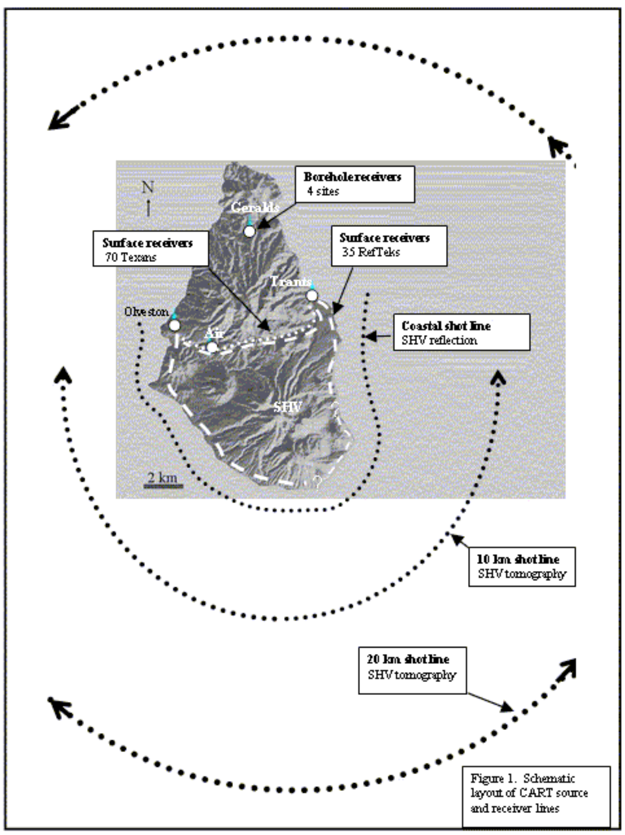

Fig 2a

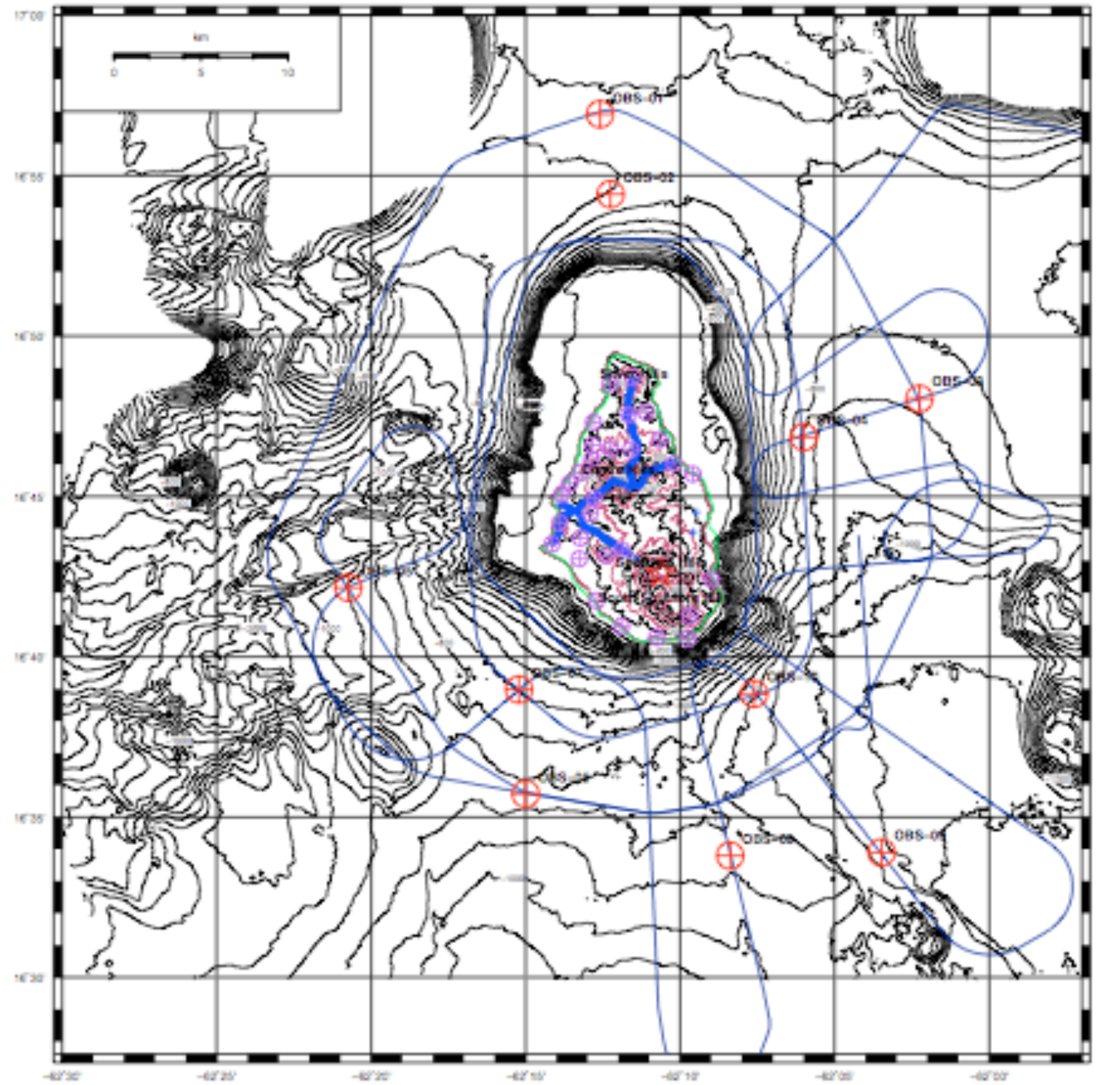

Fig 2b

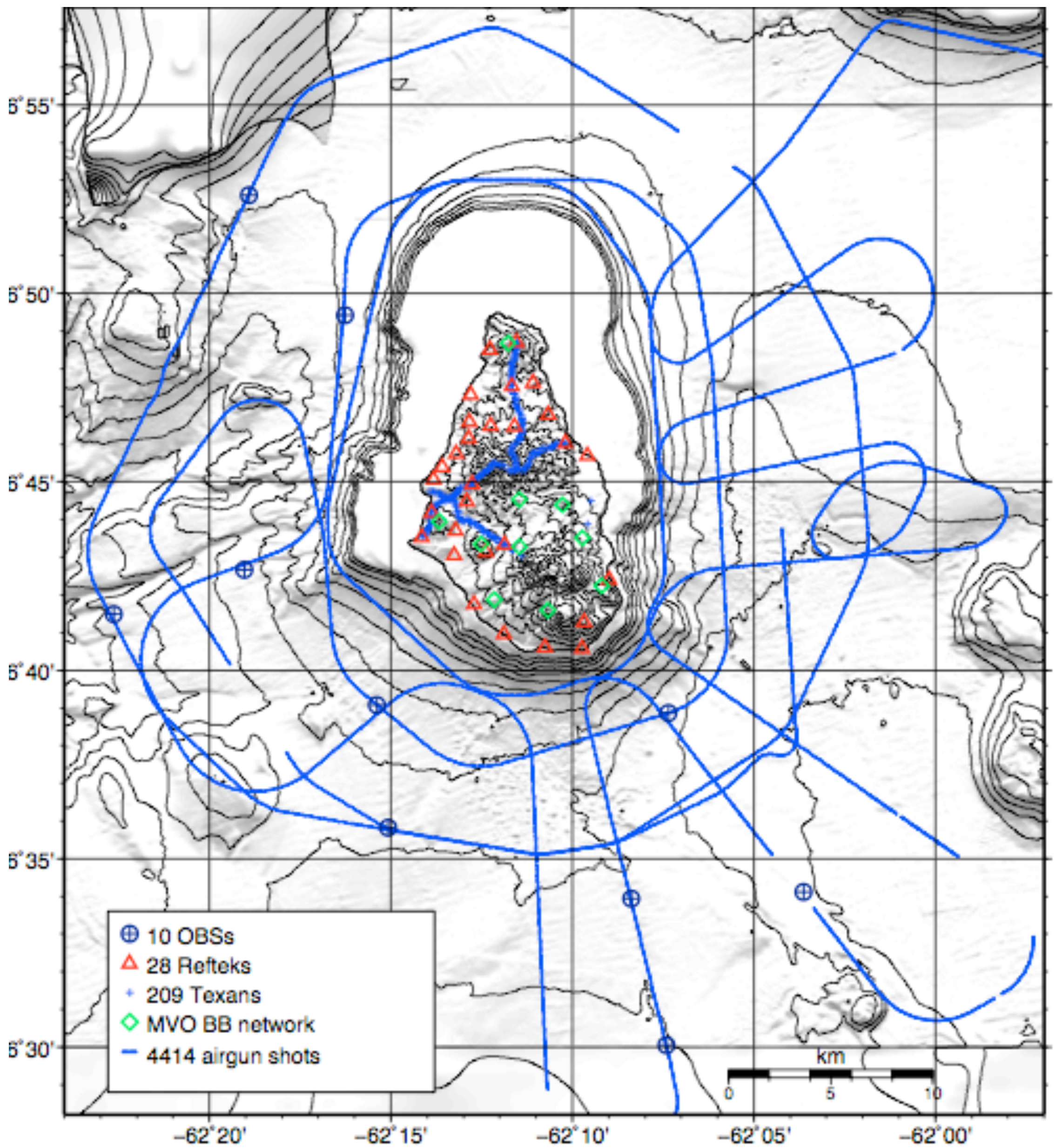

Fig. 2. Evolution of ship-track plans. (a) Sketch from 2004 showing original concept of shiptracks (shotlines), with a Texan array onshore. (b) Bathymetric map showing the OBS deployment sites planned for 2007, and actual shiptrack. Anticipated OBS sites are shown offshore as crossed-circles. Land stations include Refteks (red dots) and Texan arrays (blue lines). DEM from Le Friant *et al*. (2004). (c) Similar figure showing final OBS station array and shiptrack positions. Note substantially changed OBS site locations. [NOTE TO REVIEWER, WE ARE REDRAFTING THIS FIG TO IMPROVE CLARITY]

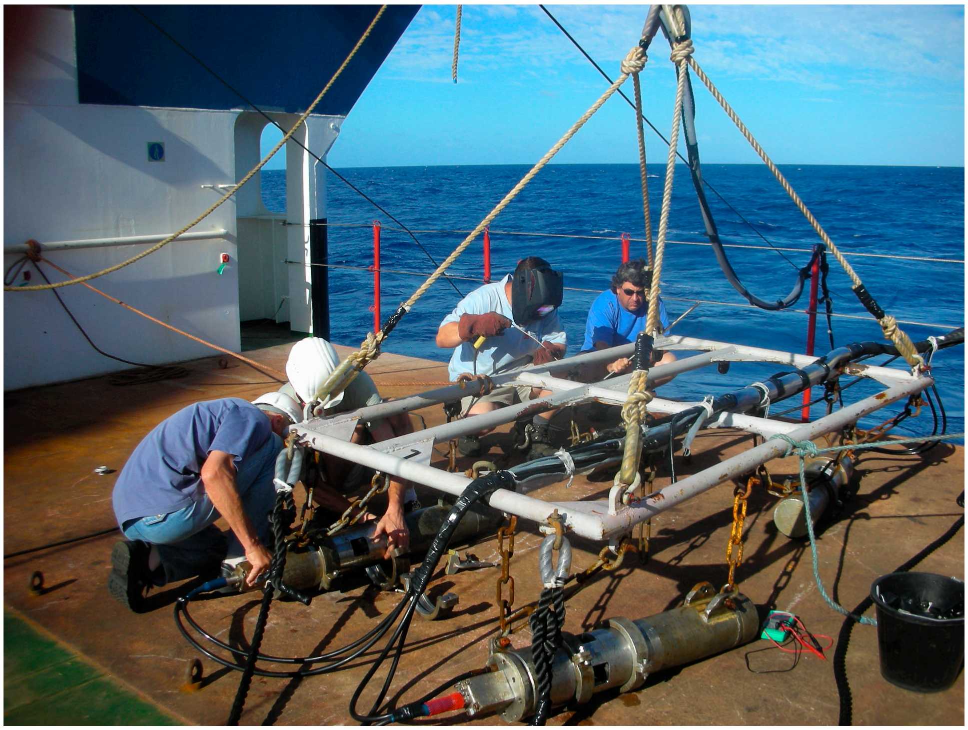

Fig. 3. Bolt 'Long Life' airgun units assembled on a rigid frame and connected to the ship by electric cables and high-pressure tubes. Two frames were used, towed side-by-side with a separation of 9 m. (S. Sparks photo)

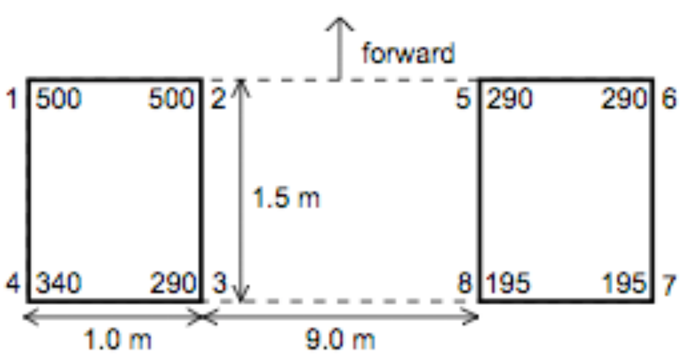

Fig. 4. Schematics of the gun array. Gun numbers and volumes in cu. in. are

shown. The total volume is 2600 cu. in.

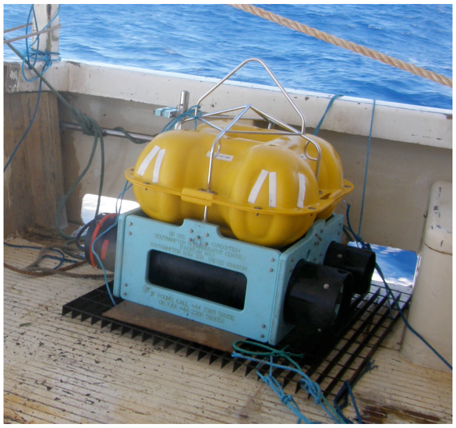

Fig. 5. An LC2000 four-component Ocean Bottom Seismometer (OBS). Instrument was designed by Scripps Institution of Oceanography. M. Paulatto photo.

Fig. 6. Two LC2000 Ocean Bottom Seismometers being readied for deployment in December 2007, with M. Paulatto in Guadaloupe onboard the vessel Beryx.

Fig. 7. The RefTek RT130 seismometer recorder, with 3-component Mark Products model L22, 2.0 Hz geophone. B. Voight photo.

Fig. 8. The RefTek RT125A seismometer, with cable to a single vertical component Mark Products L40 (or L28) 4.5 Hz sensor. B. Voight photo.

Fig. 9. The RefTeks were deployed from October through December, powered by deep cycle batteries with solar panel recharging. Site installation at Air Studios. (B. Voight photo).

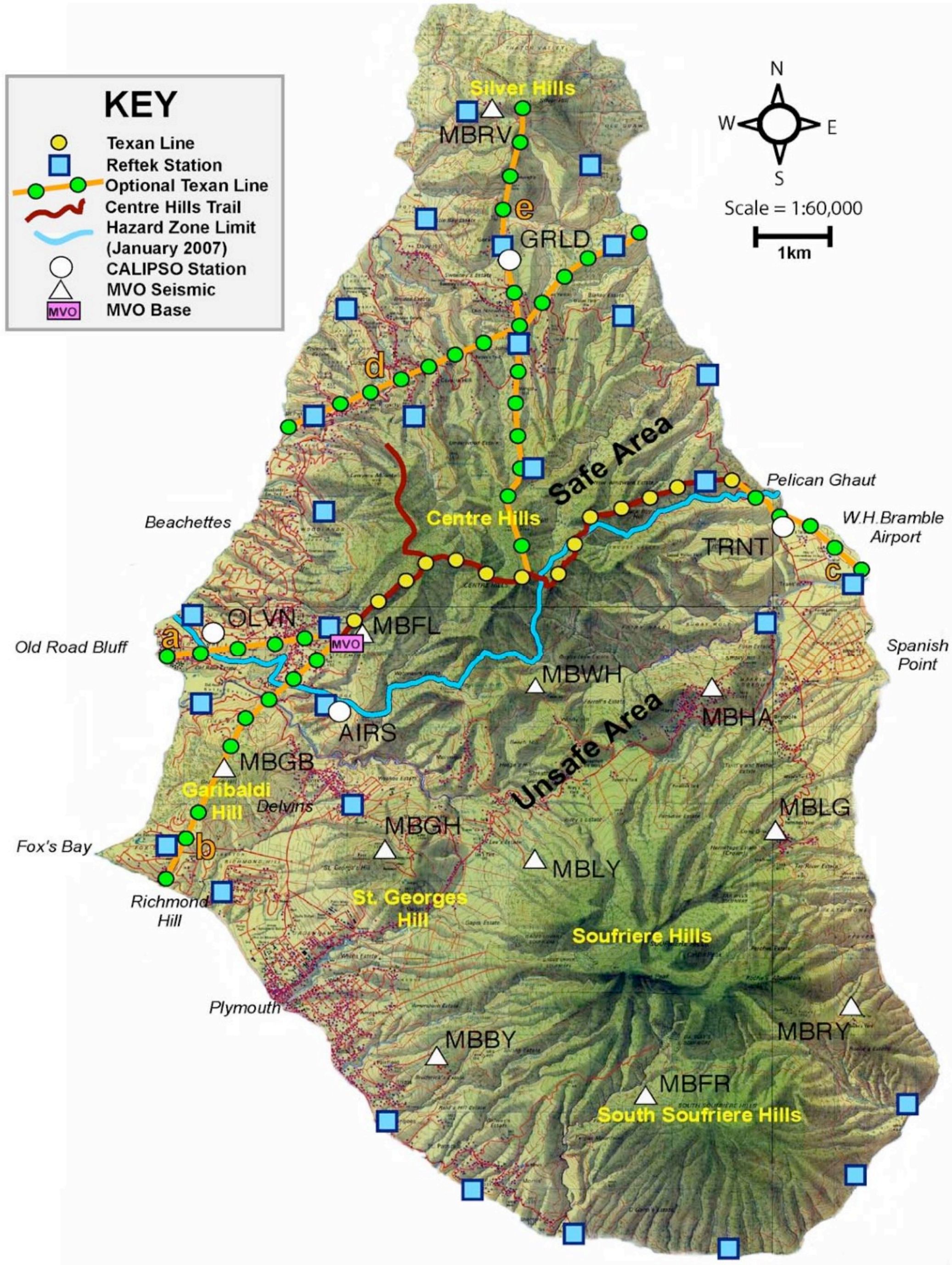

Fig. 10. Deployed instruments, on topographic base map of Montserrat. Inset table provides key. Refteks: blue squares, with unrealized stations shown by orange squares. Texan arrays: strings of yellow or green circles. The northern SW-NE Texan array was considered in planning stages, but not used. MVO seismograph sites: white triangles. CALIPSO strainmeter sites:

white dots. Hazard zone safe-unsafe boundary: blue line. MVO: purple rectangle. Main Centre Hills trail: brown line.

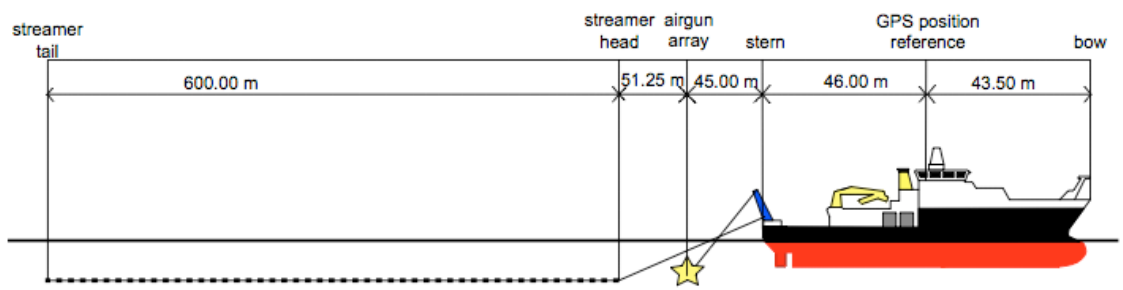

Fig.11. Schematics of the ship, airgun array position, and streamer geometry used in SEA-CALIPSO experiment (after NOC 2008).

Fig. 12. Installation of typical RefTek seismometer station in October 2007.

Fig. 13. Loading RefTek equipment aboard the vessel Daily Bread at Little Bay in north Montserrat, for deployment along the south coast in October 2007.

Fig. 14. The rugged terrain of the Centre Hills, mountainous rainforest with steep ridges and valleys. Hikers carried Texans just before airgun shooting, using trails on precipitous wet soil-veneered slopes that could be almost invisible because of the dense vegetation. Shortly before the experiment some trails were cleared with machetes.

Fig. 15. Installing Texans on top of Katy Hill (near the words "Centre Hills" on Fig. 10), on the north-south Texan array line, in dense cloud-forest vegetation. A. Belousov photo.

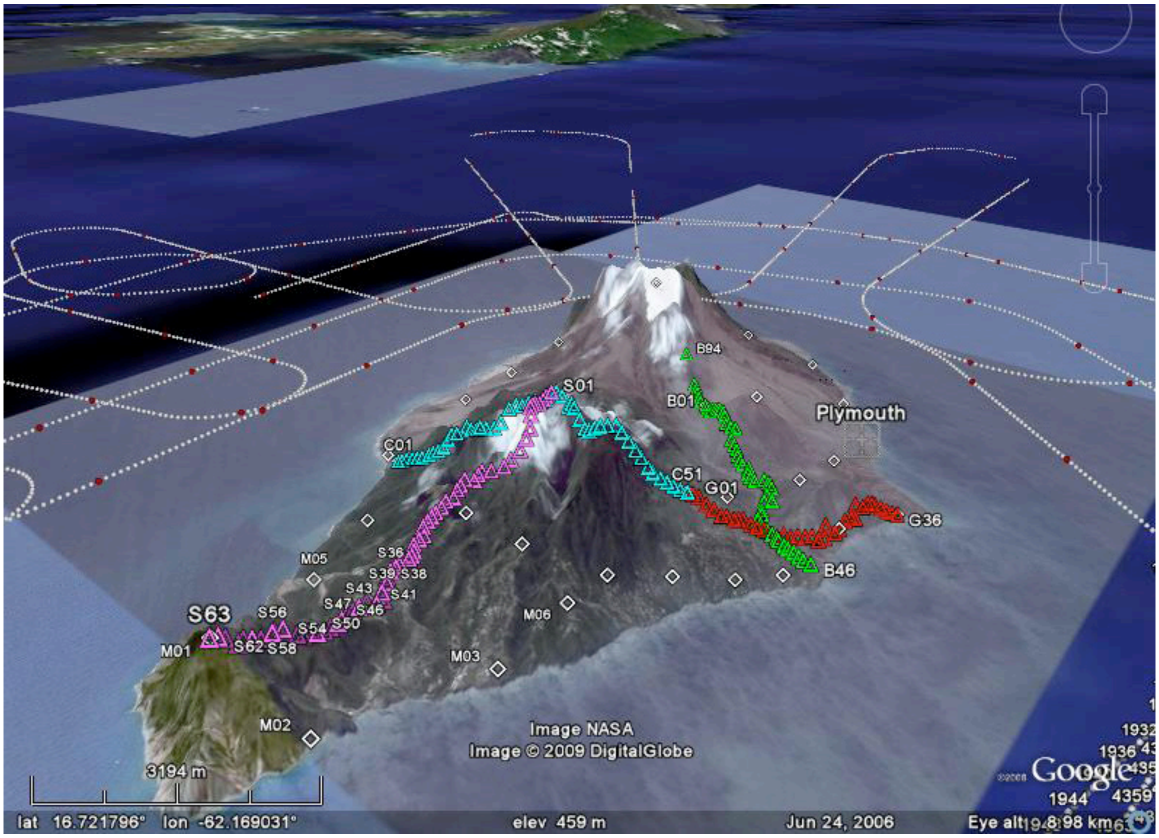

Fig. 16. Oblique view of Montserrat island toward the southeast. The volcanic centres of Silver Hills, Centre Hills, and SHV run from north to south (left to right). Texan array lines are shown by colored triangles, with two arrays intersecting across the top of the Centre Hills (cf. Fig. 10). The array in green is radial to the Soufriere Hills Volcano, and roughly follows the Belham River valley. Refteks are shown by white triangles. Shiptracks are shown offshore, and the island of Guadaloupe, to the south, is at top of image. Image is from NASA, 2009.

Fig. 17. The 34-m vessel Beryx, based in Gourbeyre, Basse Terre, Guadeloupe, and used for OBS deployments.

Fig. 18. RRS James Cook (a) at sea and (b) in St. Johns, Antigua harbor.

Fig. 19. Loading equipment and supplies on the RRS James Cook at Antigua port call.

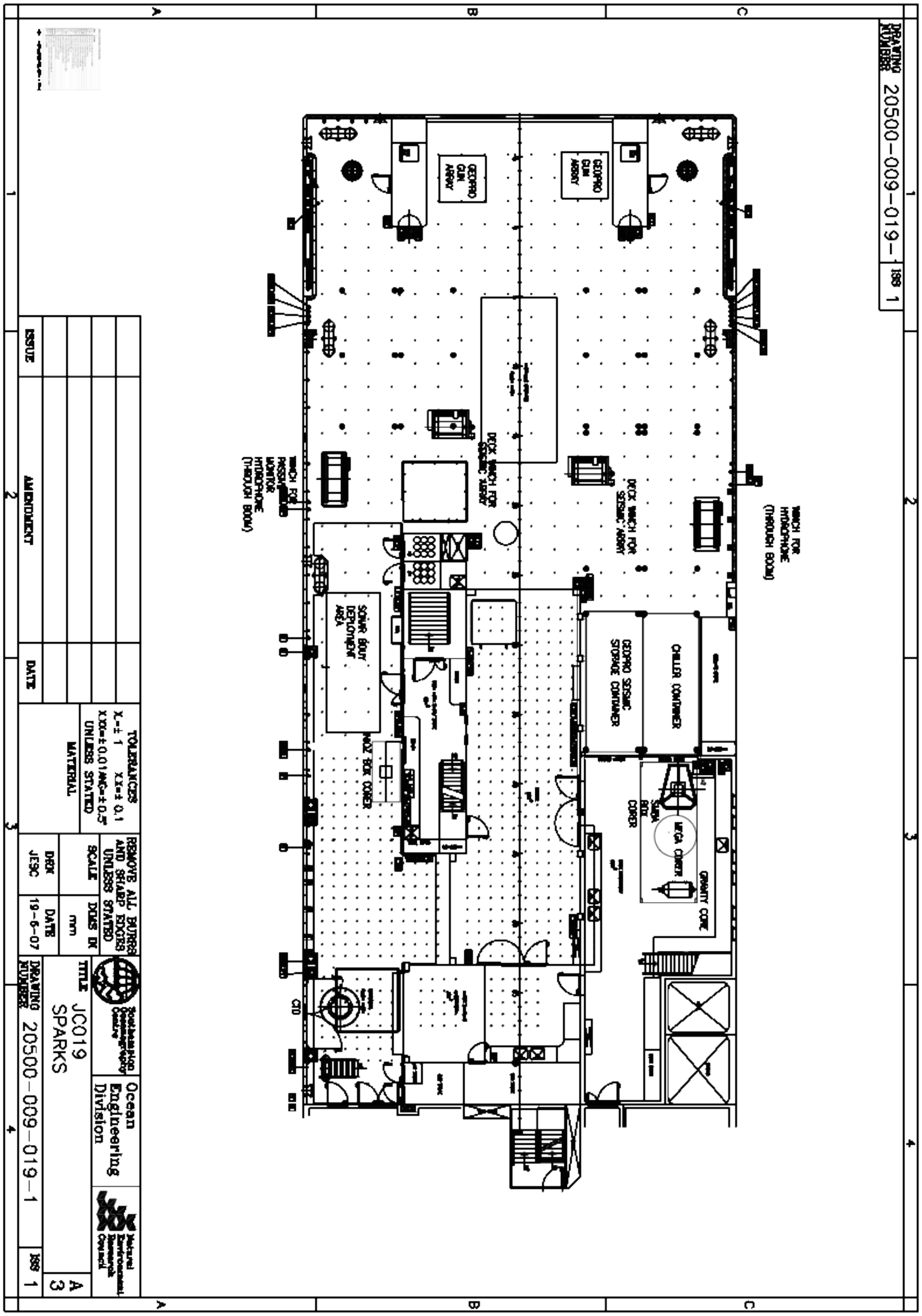

Fig. 20. Ship deck plan for the JC19 cruise.

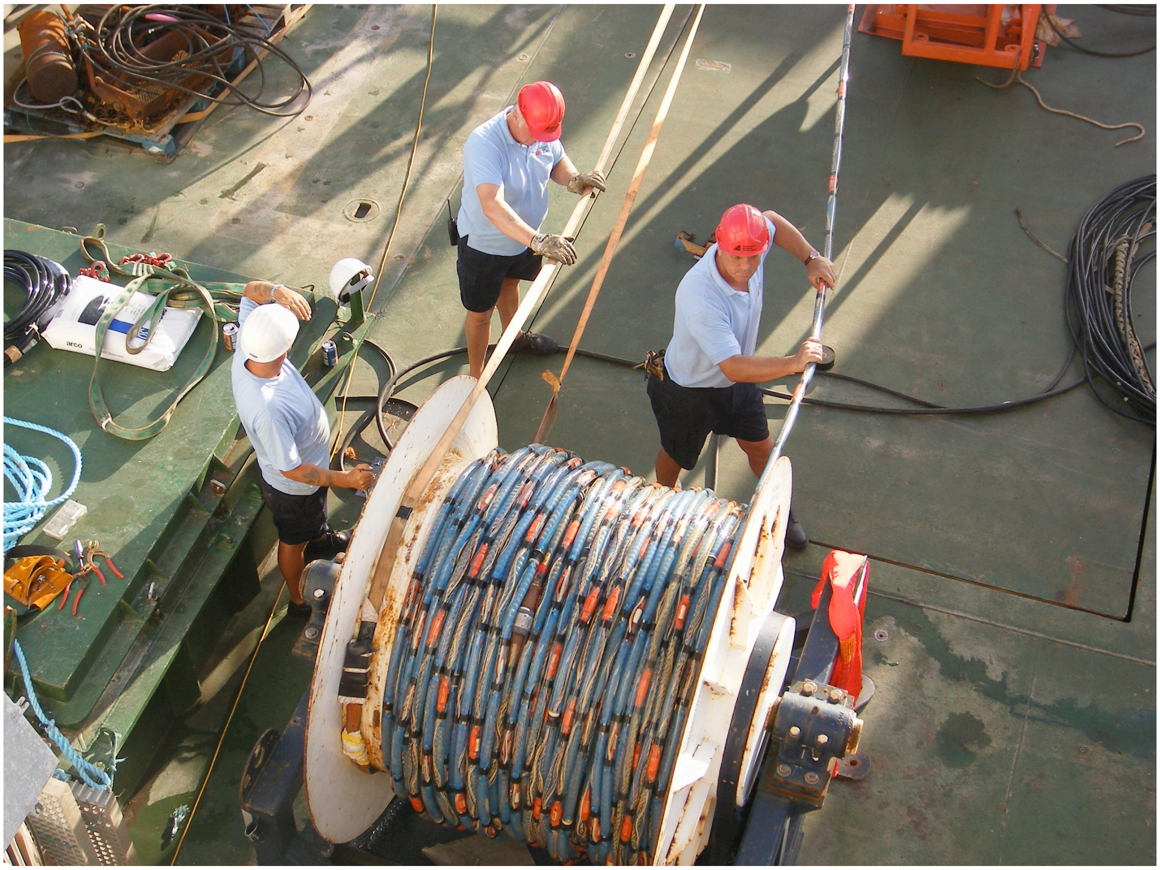

Fig. 21. Streamer winch in operation on deck of RRS James Cook. J. Hammond photo.

Fig. 22. Hoist operations on stern rear deck of the RRS James Cook. J. Hammond photo.

Fig. 23. Airgun array being prepared for deployment off the stern of the RRS James Cook. J. Hammond photo.

Fig. 24. Shooting on a radial track offshore eastern Montserrat. Airgun explosion bubbles may be seen behind the hoist. The Tar River valley leading up to the Soufriere Hills Volcano is in the distance with the volcano summit covered by cloud cap. Sparks photo.

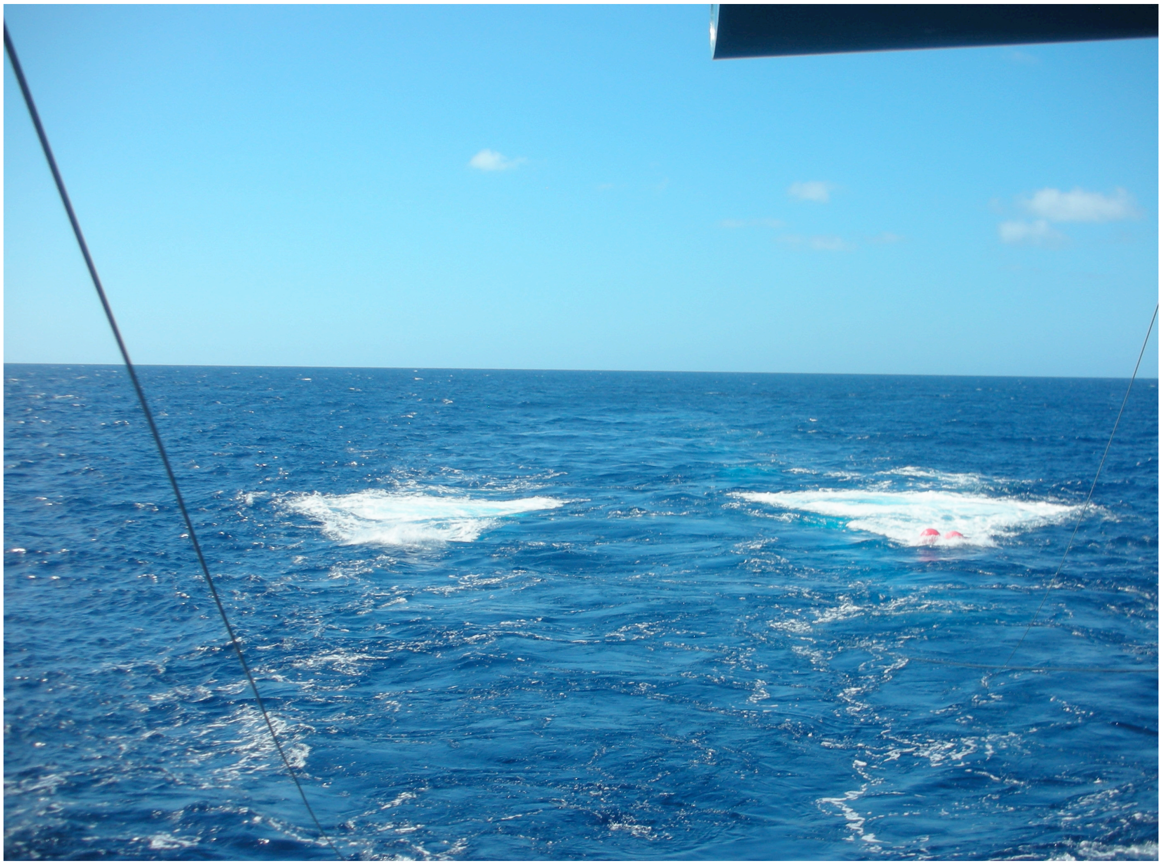

Fig 25. Synchronized explosions from the dual airgun clusters, offshore Montserrat.

Fig. 26 (a, b). Marine mammals alongside the RRS James Cook. The possibility of serious interference of the shooting schedule due to marine mammal detection was a serious concern, because frequent sightings and shooting shutdowns could have had major impacts on both sea and land operations and the success of the experiment.

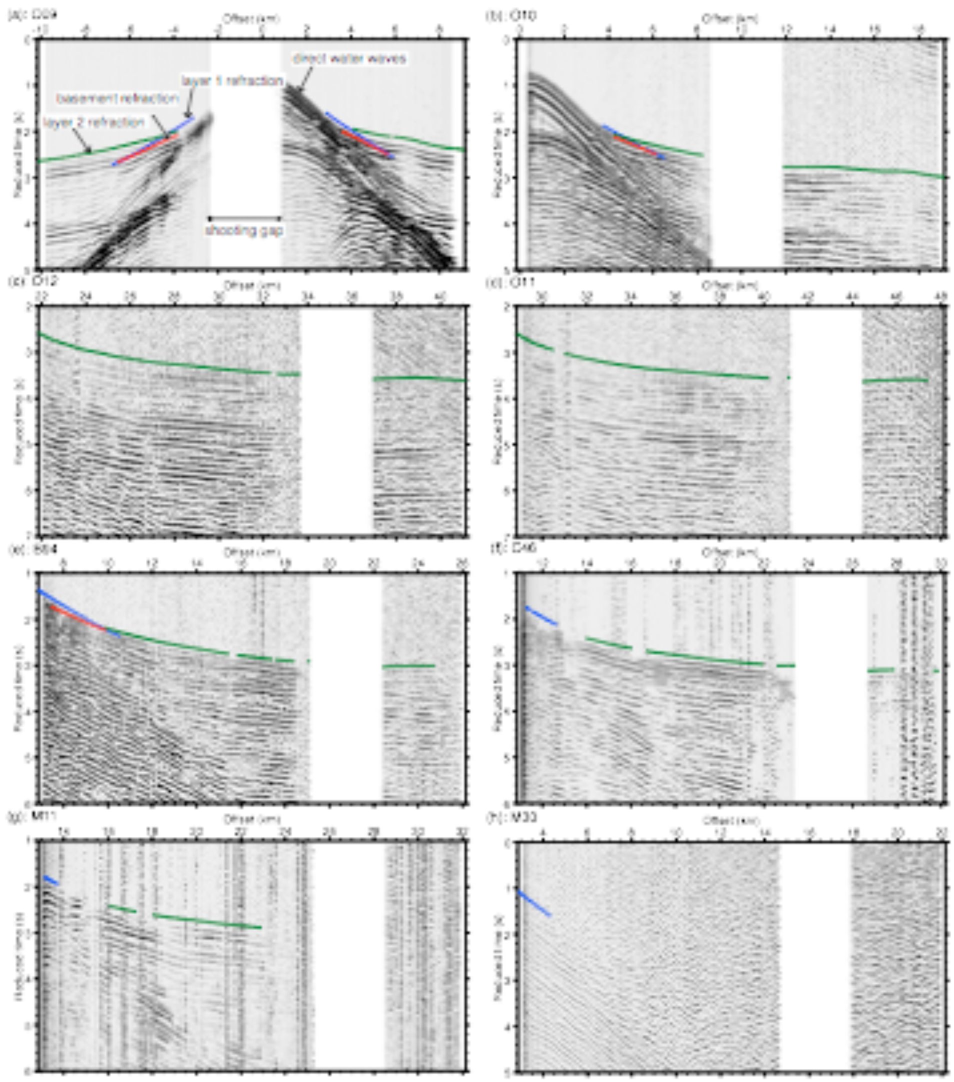

Fig. 27. Examples of seismic data plotted as common receiver gathers (after Paulatto *et al*. 2010a). Panels correspond to the radial shooting line from point A (right end of the panels) to site O10 (left end), shown in Fig. 28, recorded on the eight instruments used in the 2D inversion. (a)-(d) Hydrophone channel recordings of OBS stations O09, O10, O12 and O11. (e)-(f) Vertical geophone recordings of Texan stations B94 and C46. (g)-(h) Vertical component recording of Reftek 130 stations M11 and M30.

Synthetic traveltimes calculated through the final velocity model are superimposed on the data (blue: layer 1 refractions; green: layer 2 refractions; red: basement reflections). The white gap present in all panels corresponds to an interruption in shooting due to marine mammals in the vicinity of the guns. A minimum-phase filter with corner frequencies 3-5-20-25 Hz was applied to the data. Amplitudes are normalized with a factor inversely proportional to offset.

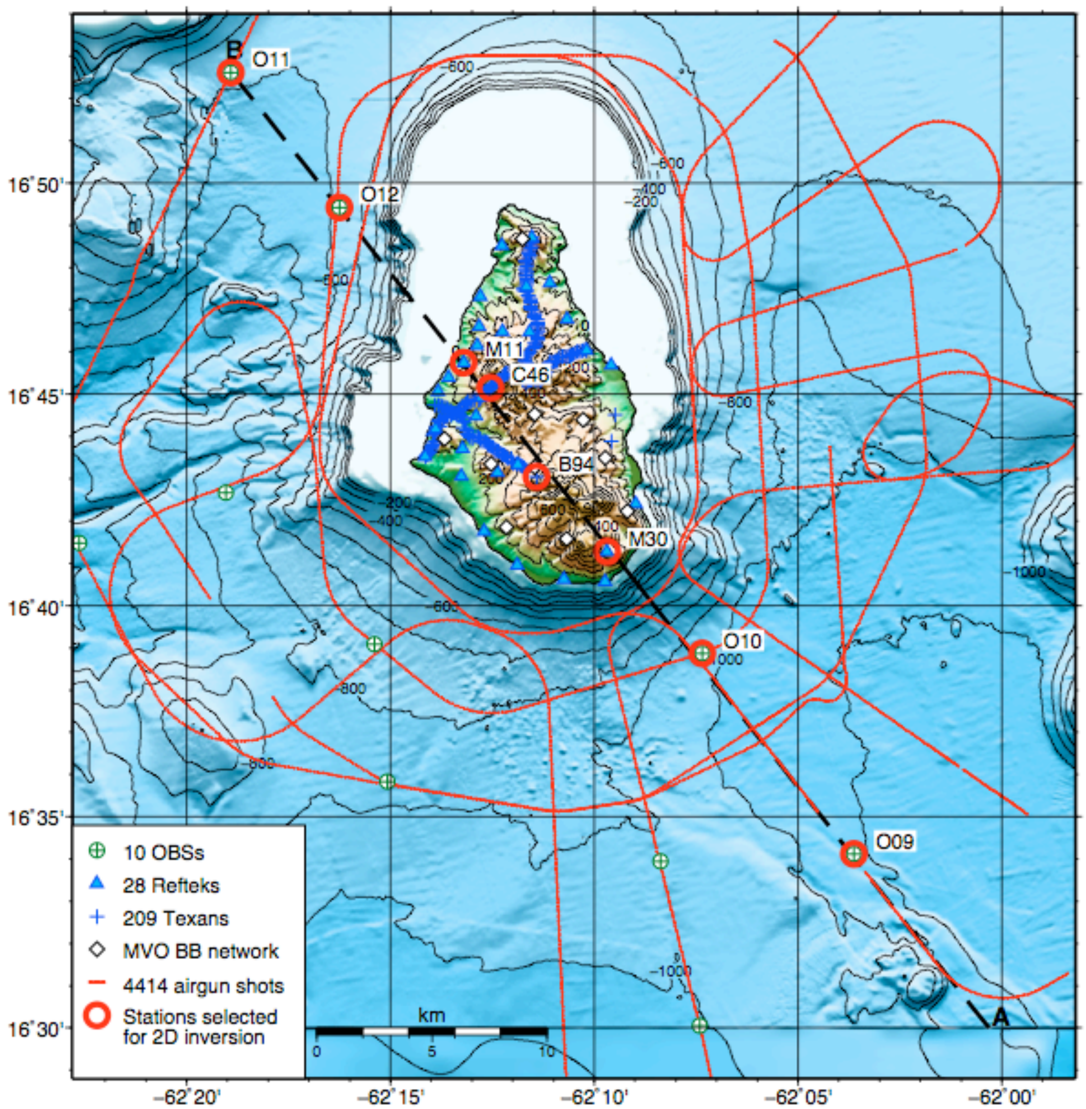

Fig. 28. Bathymetric map of Montserrat with SEA-CALIPSO station array and shot positions. The black dashed line marks the position of the 2D tomographic section presented in this study. The digital elevation model was

obtained by merging the GEBCO 08 Grid (http://www.gebco.net) with a detailed elevation model of Montserrat and the surrounding sea floor from Le Friant *et al*. (2004). After Paulatto *et al*. (2010a)

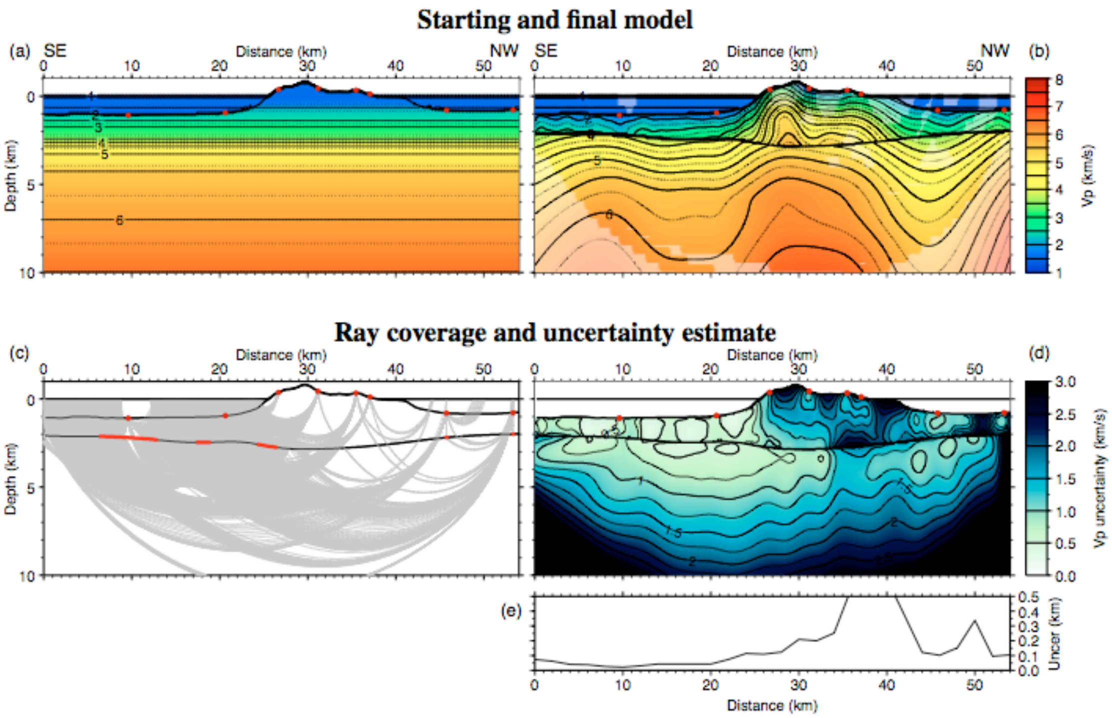

Fig. 29. (a) Starting model for 2D inversion process. (b) Final 2-layer model, paler areas are not sampled by rays inverted in the final step. (c) Ray coverage of final model. Segments of the basement interface that are sampled by wide angle reflections are highlighted in red. (d) Velocity uncertainty estimate. (e) Depth uncertainty estimate for basement interface. Station positions are marked by red dots. Vertical exaggeration is 2:1. After Paulatto *et al*. (2010a).

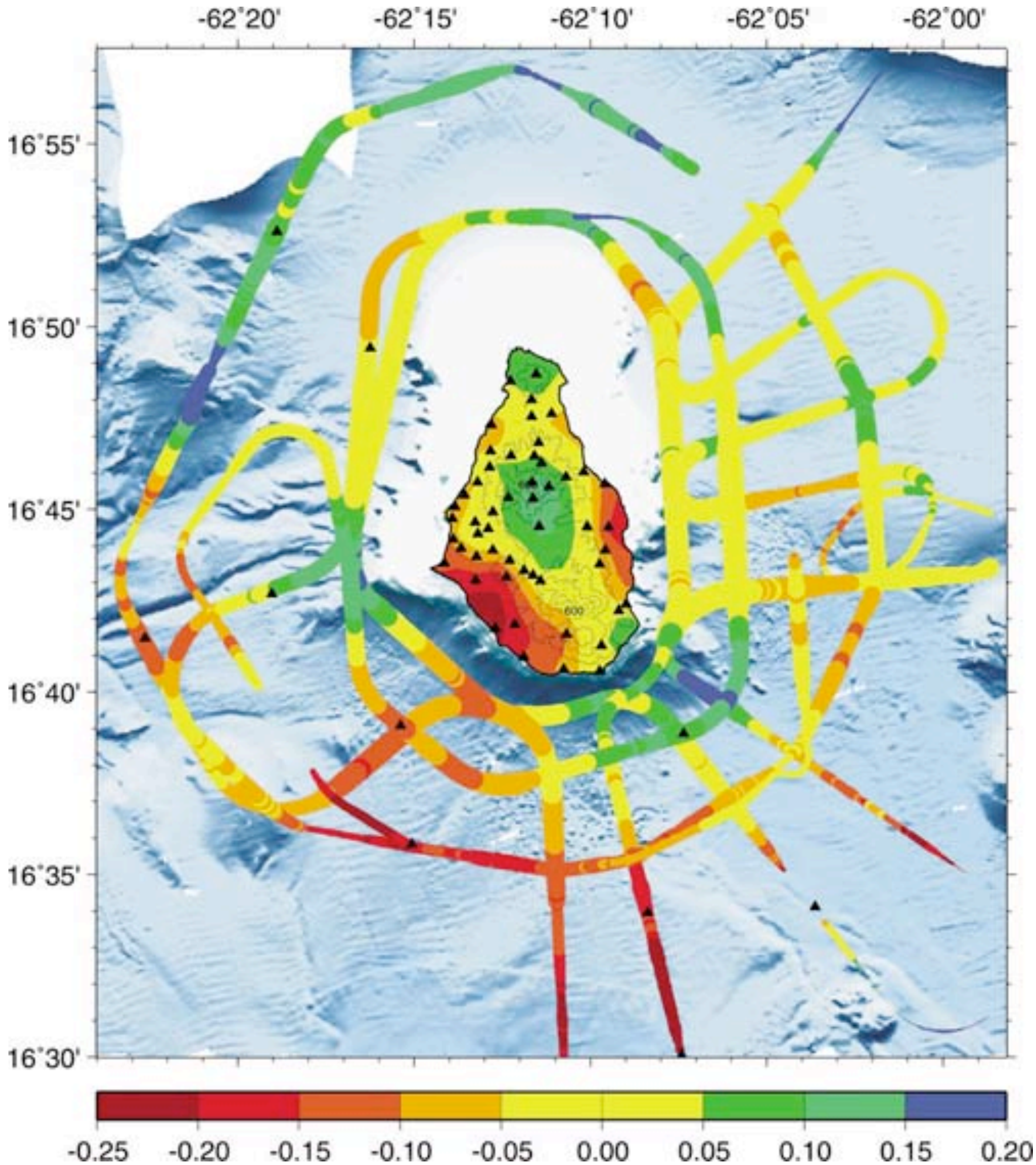

Fig. 30. Map of 3D tomography area showing bathymetry, topography contours, ship track, and station locations used in the Shalev *et al*. (2010) study, and average time residuals for shots and land based recorders. Black triangles mark the seismic stations included in the tomographic inversion. The stations offshore are ocean bottom seismometers. Colors stand for the average residuals (time computed minus time observed) in seconds where red represents slow and blue represents fast. On land, the colors contour the average residuals; on water, colors represent the average residual for each

shot. The width of the ship track line is proportional to the number of seismic stations that recorded an airgun blast from a particular point on the track.

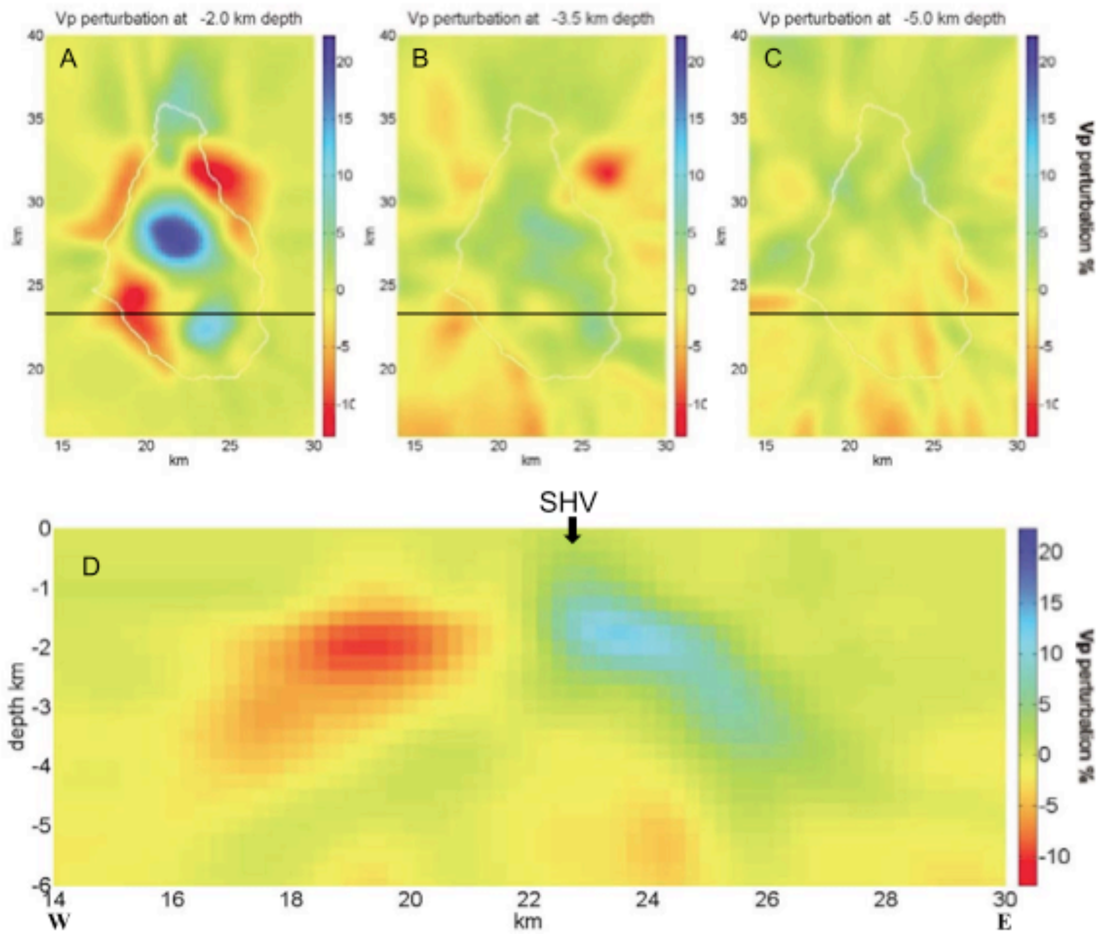

Fig. 31. P-wave tomography results displayed as perturbation from the average velocity at each depth. Blue represents faster velocities and red represents slower velocities. Map view slices through the target volume at depths (a) 2.0, (b) 3.5, and (c) 5.0 km. The black line marks the location of (d) the cross section across the SHV. The outline of Montserrat is a white line on all map view slices. After Shalev *et al*. (2010).

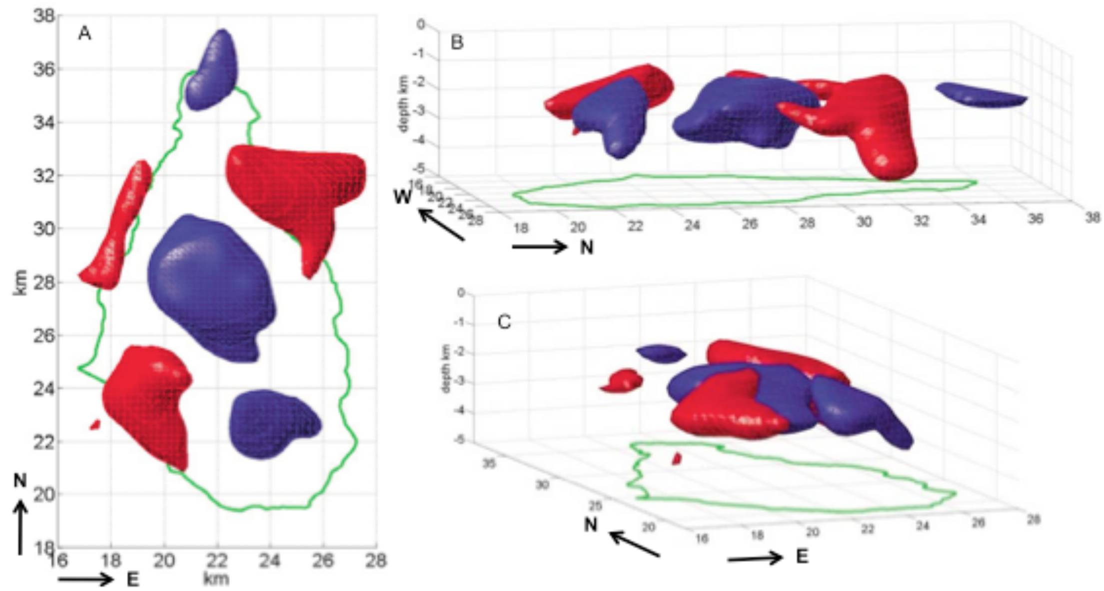

Fig. 32. Three-dimensional iso-surfaces of velocity anomalies, after Shalev *et al*. (2010). The blue surfaces define anomalies that are >6% faster than average. The red surfaces represent anomalies that are >6% slower than average. (a) Map view. (b) View from the east southeast. (C) View from the south-southwest.

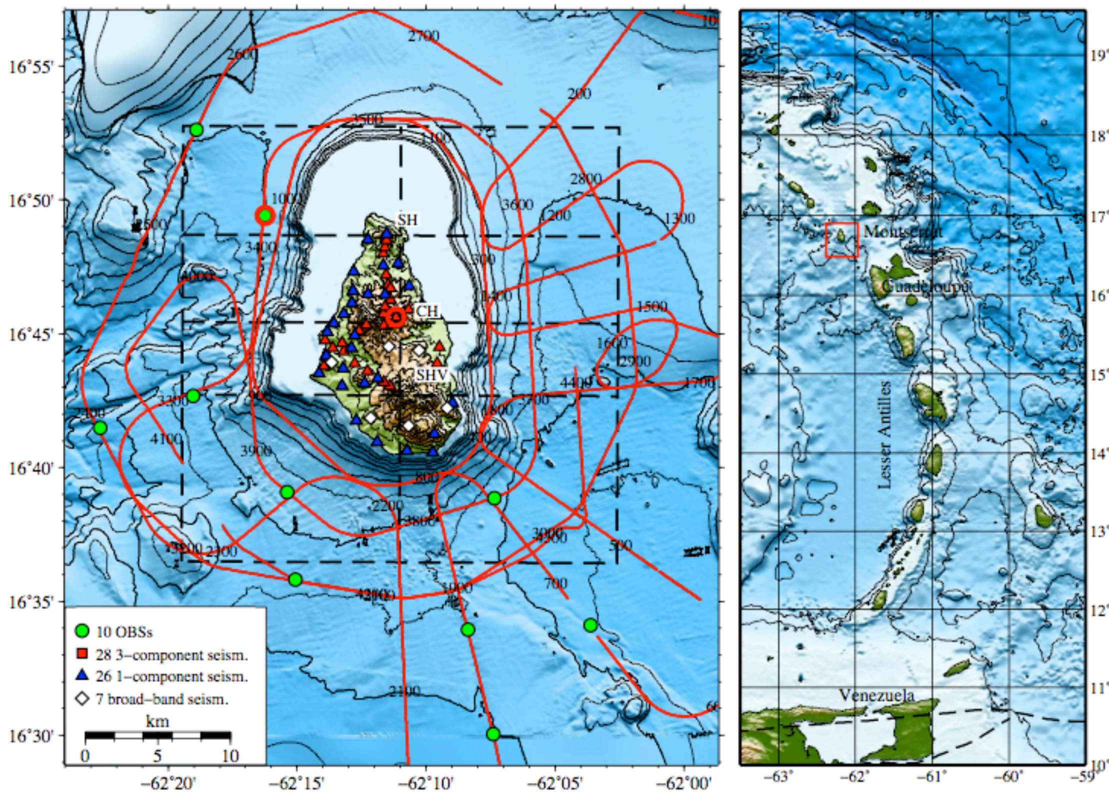

Fig. 33. Topographic map of survey area with recording array and shot positions. Contour interval is 200 m. Shiptrack shown by red line with shot numbers labelled every 100 shots. Locations of the sections shown in Fig. 36 are marked with black dashed lines. SH: Silver Hills; CH: Centre Hills; SHV: Soufriere Hills Volcano. Reftek stations in blue, Texans in red, MVO stations in white. The stations corresponding to example data in Paulatto *et al*. (2012, Figs. 2,3) are highlighted in red. The panel on the right shows the location of Montserrat in the Lesser Antilles. Plate boundaries from Coffin *et al*. (1998). Digital elevation model from Le Friant *et al*. (2004) and the GEBCO 08 Grid (http://www.gebco.net).

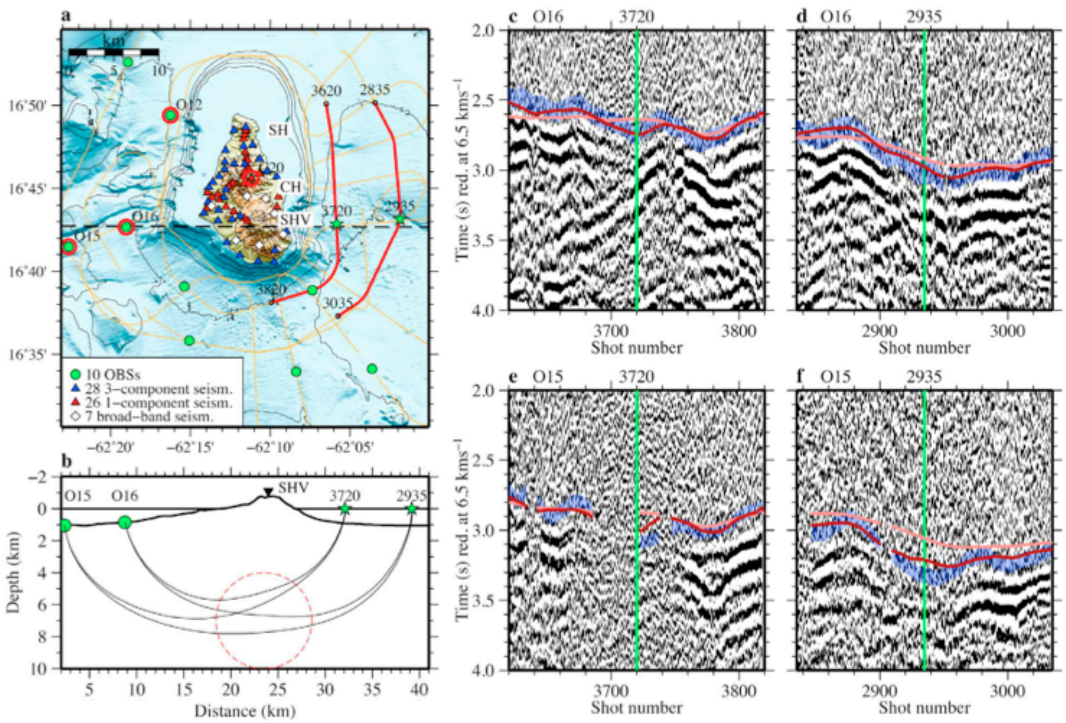

Fig. 34. Field recordings showing delayed first arrivals and reduced signal-to-noise ratio beneath SHV, after Paulatto *et al*. (2012). (a) Map with location of instruments and data sections. Ship track in orange, shots corresponding to sections shown in Figs. 34b–34f are highlighted in red. (b) Section through SHV, corresponding to dashed line in (a), showing topography and ray trajectories. The approximate extent of the low velocity volume is marked with a dashed red circle. (c–f) Data corresponding to shots highlighted in Fig. 34a. First arrivals with error bars in blue. Travel-times for final model in red. Travel-times for preliminary smoothed model in pink (Paulatto *et al*. 2012, Fig. 5, iteration 36). The traces highlighted in green correspond to shots noted by green stars in Fig. 34a.

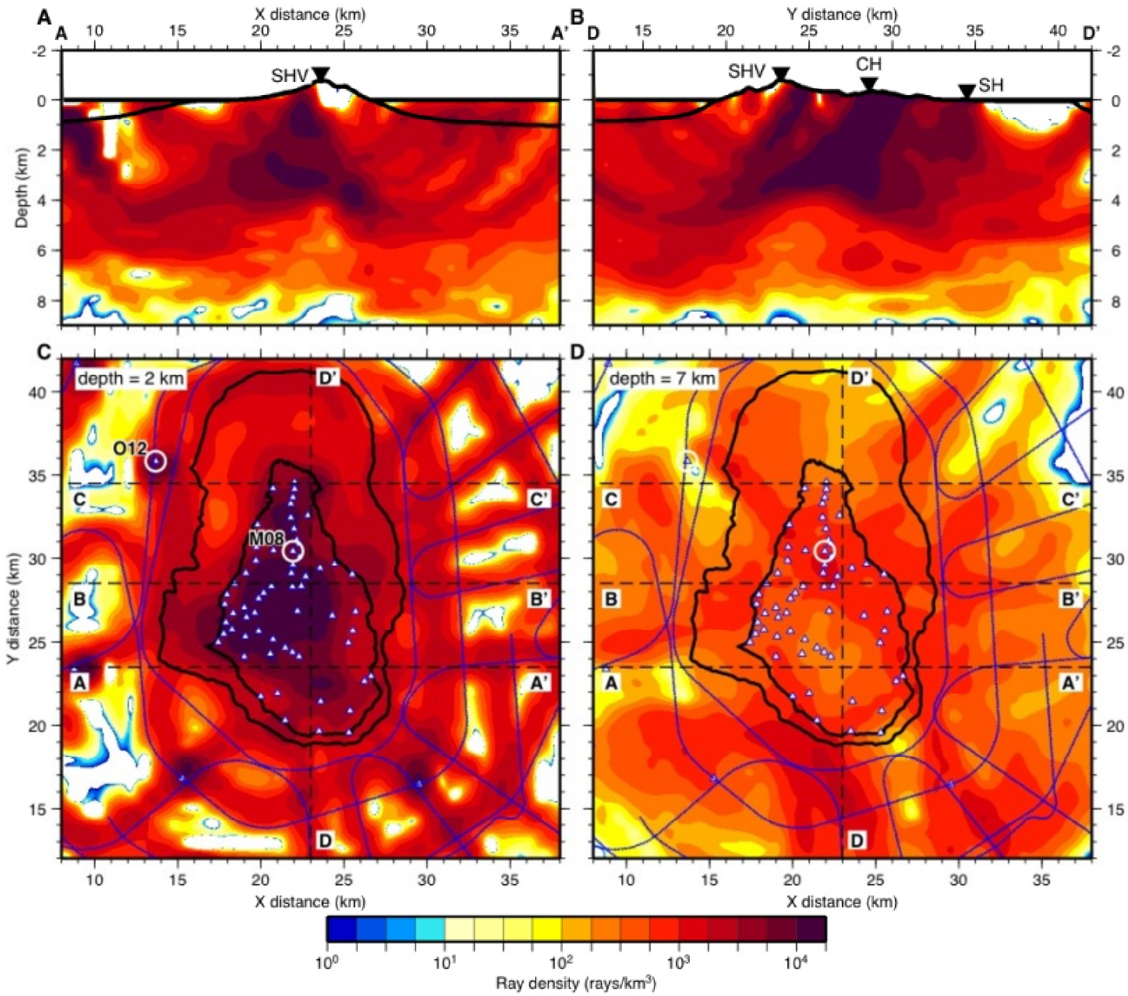

Fig. 35. Ray density. (a) W-E section. (b) S-N section. (c-d) horizontal sections at 2 and 7 km depth respectively. After Paulatto *et al*. (2012).

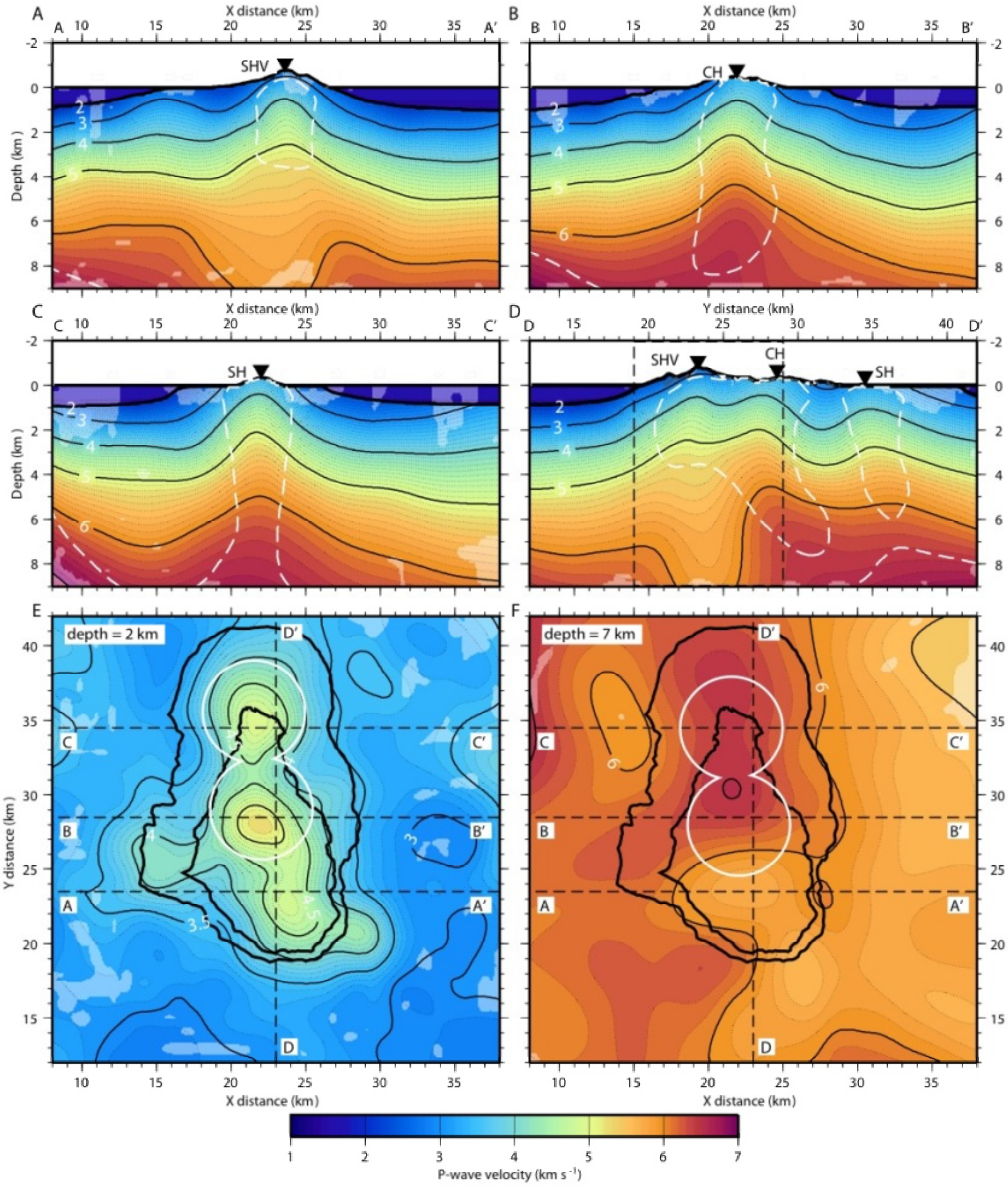

Fig. 36. Final seismic velocity model. (a–c) W-E sections through the three major volcanic centers. The high-seismic-velocity cores of the volcanoes are marked with white dashed lines representing 0.25 km/s seismic velocity anomaly contour with respect to the average seismic velocity of the island. (d) S-N section. Dashed frame marks the section of a model shown in Paulatto *et al*. (2012, Figs. 10–12). (e, f) Horizontal sections at 2 and 7 km depth below sea level respectively. The coastline and the 200 m depth contour are marked with thick black lines. The white circles bound the area

over which the reference model for seismic velocity anomalies was calculated. Lighter areas have no ray coverage. After Paulatto *et al*. (2012).

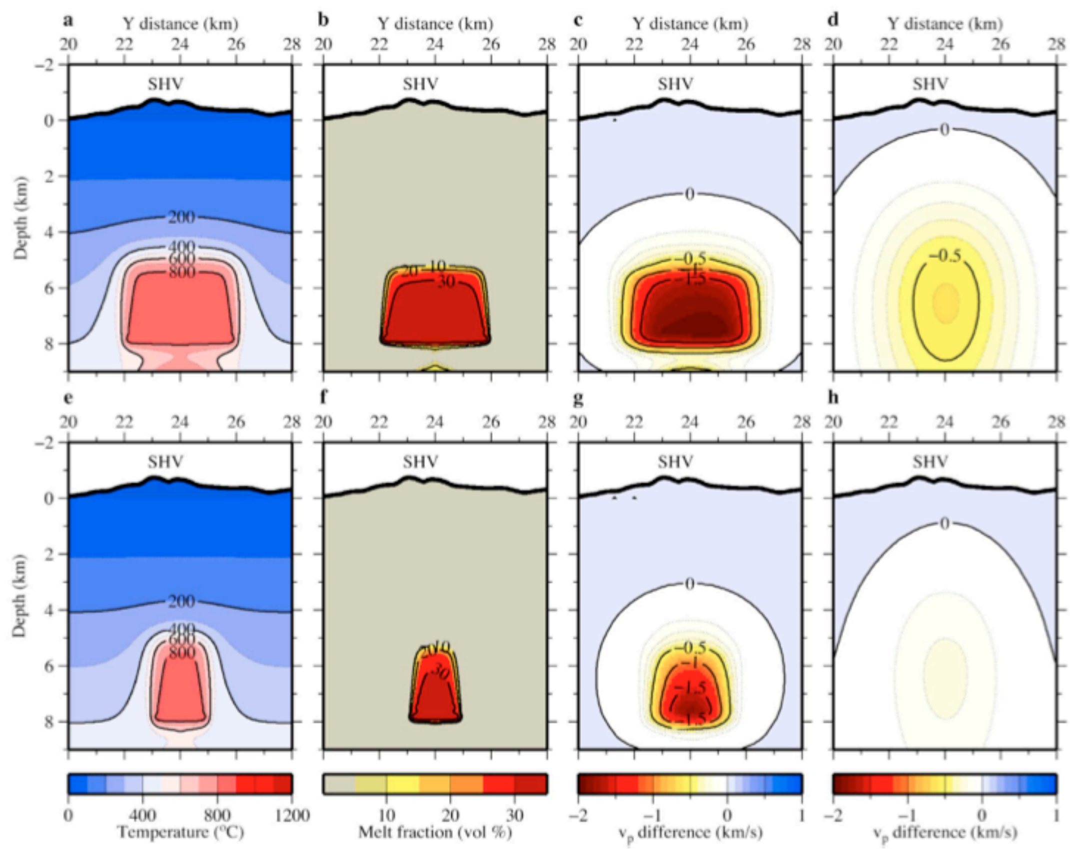

Fig. 37. Models of magma chamber accretion and predicted seismic velocity anomaly (after Paulatto *et al*. 2012). Model A: two successive events of under-accretion of 300-m-thick sills with 2 km radius at 400-year intervals, each starting at 5 km depth and lasting 4000 years, with a 15,000-year repose period. (a) Present-day temperature distribution, corresponding to 4000 years after start of second intrusion event. (b) Melt fraction. (c) calculated P-wave velocity anomaly. (d) P-wave velocity anomaly of filtered model. (e–h) Model B: same as Figs. 37a–37d for sills with 1 km radius.

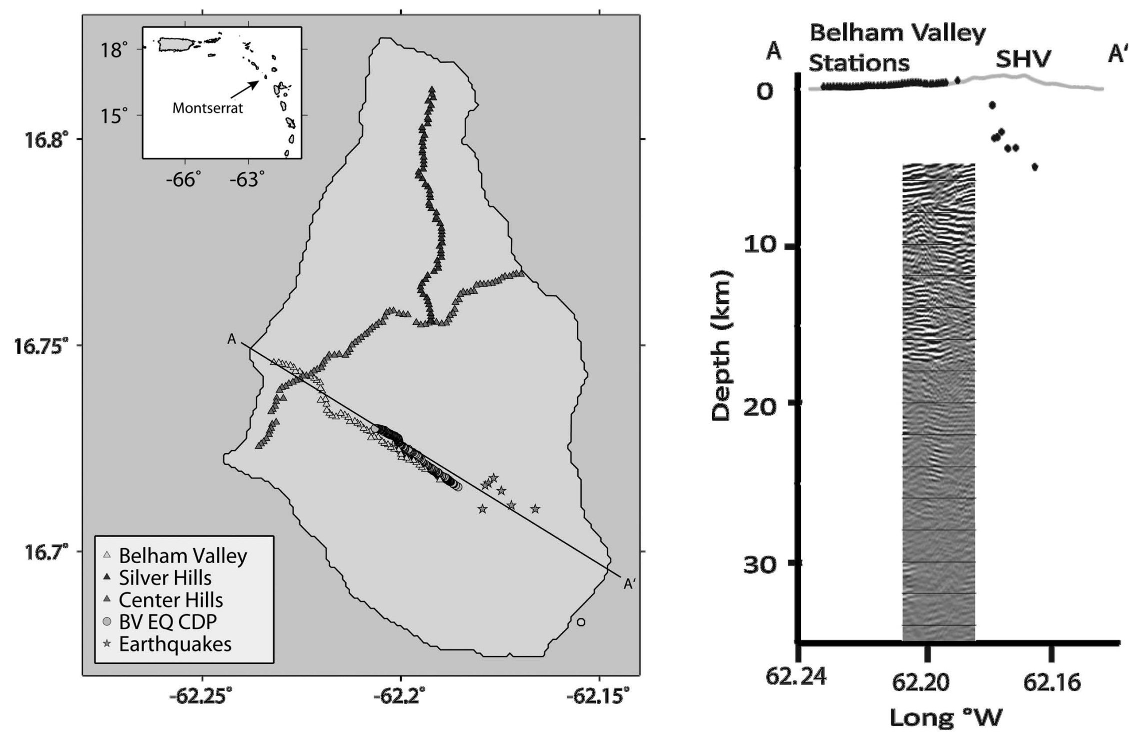

Fig. 38. (a) On left, map of Montserrat showing the locations of the Texan seismic arrays (triangles), along with the best located microearthquakes used in this study (stars). The CDP reflection points corresponding to the Belham Valley recordings of a typical event are shown as circles. (b) On right, schematic cross-section illustrating depths of the sources relative to the recording spread, together with a resulting image (source gather). After Byerly *et al.* (2010).

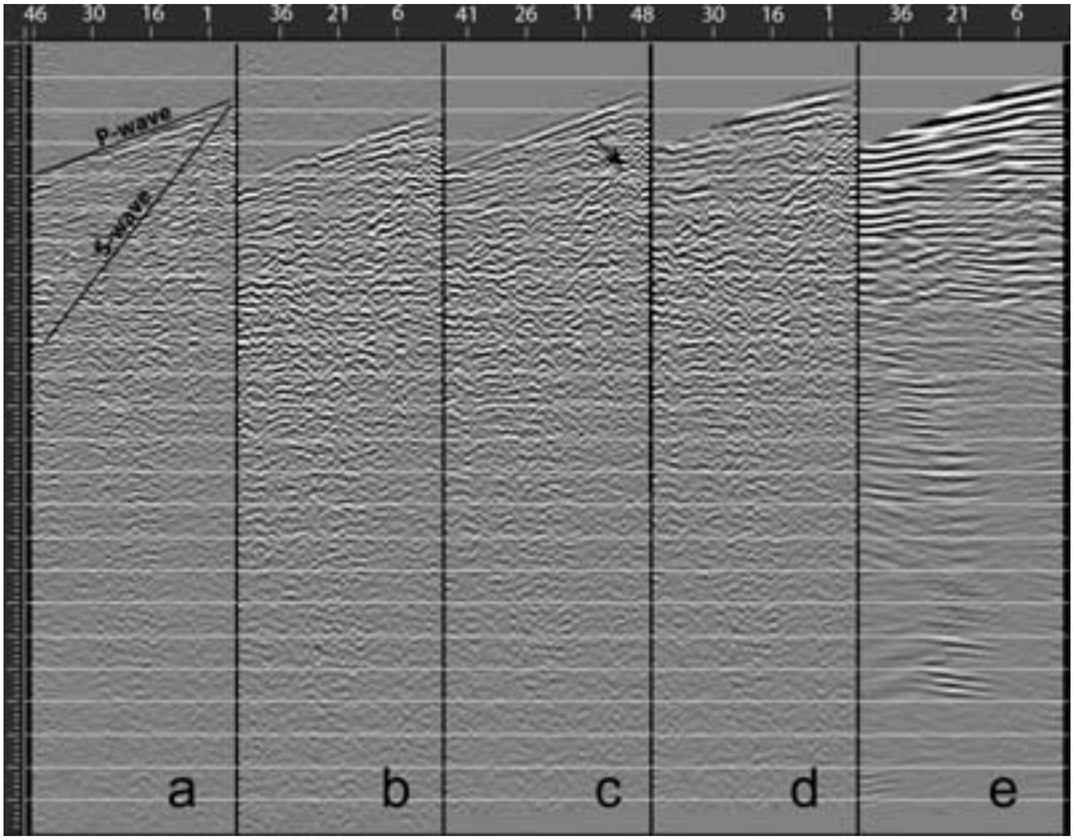

Fig. 39. Example microearthquake gather illustrating the processing steps used to enhance possible deep reflections. (a) Raw data. (b) Data with bandpass filter and elevation statics. (c) Alignment using first arrivals and linear moveout. (d) Display with NMO. (e) NMO, FX-decon and trace mix (applied twice). After Byerly *et al.* (2010).

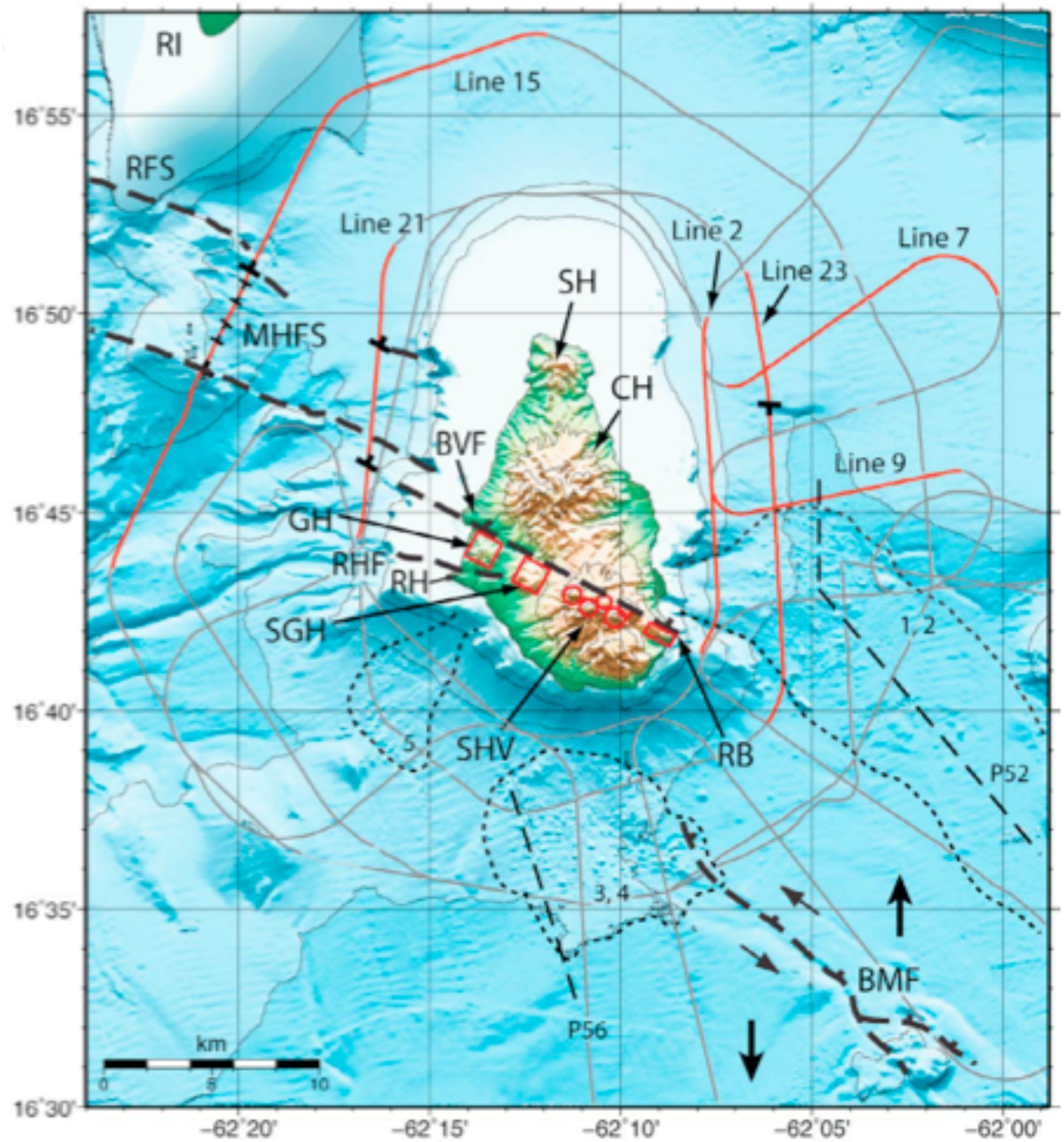

Fig. 40. Montserrat bathymetry and tectonic model. Grey curved line: Track of the RRS James Cook. Lines in red (7, 9, 2, 23, 15, 21) are discussed in this paper. Red circles: volcanic centers. Black fault symbols: normal faults from profiles, apparent dip as indicated. Thick dashed lines: major fault of the fault systems, including BVF and possible extension to RB. Large black arrows: extension direction (after Feuillet *et al*. 2001). Dotted lines: Gravity flow deposits 1–5 of Le Friant *et al*. (2004). Red squares: tectonic uplifts. Thin dashed lines: cross sections (P52, P56) along deposits from Le Friant *et al*. (2004). Orange fault north of the map: inferred from 1985–1986 Redonda earthquake mechanisms (Girardin *et al*. 1991; Feuillet *et al*. 2002). BMF, Bouillante-Montserrat fault system; BVF, Belham Valley fault; CH, Centre

Hills; GH, Garibaldi Hill; MHFS, Montserrat-Havers fault system; RB, Roche's Bluff; RFS, Redonda fault system; RH, Richmond Hill; RHF, Richmond Hill fault; RI, Redonda Island; SGH, St. Georges Hill; SH, Silver Hills; SHV, Soufrière Hills Volcano. Bathymetry map from Institut de Physique du Globe de Paris and M. Paulatto, NOCS. After Kenedi *et al.* (2010).

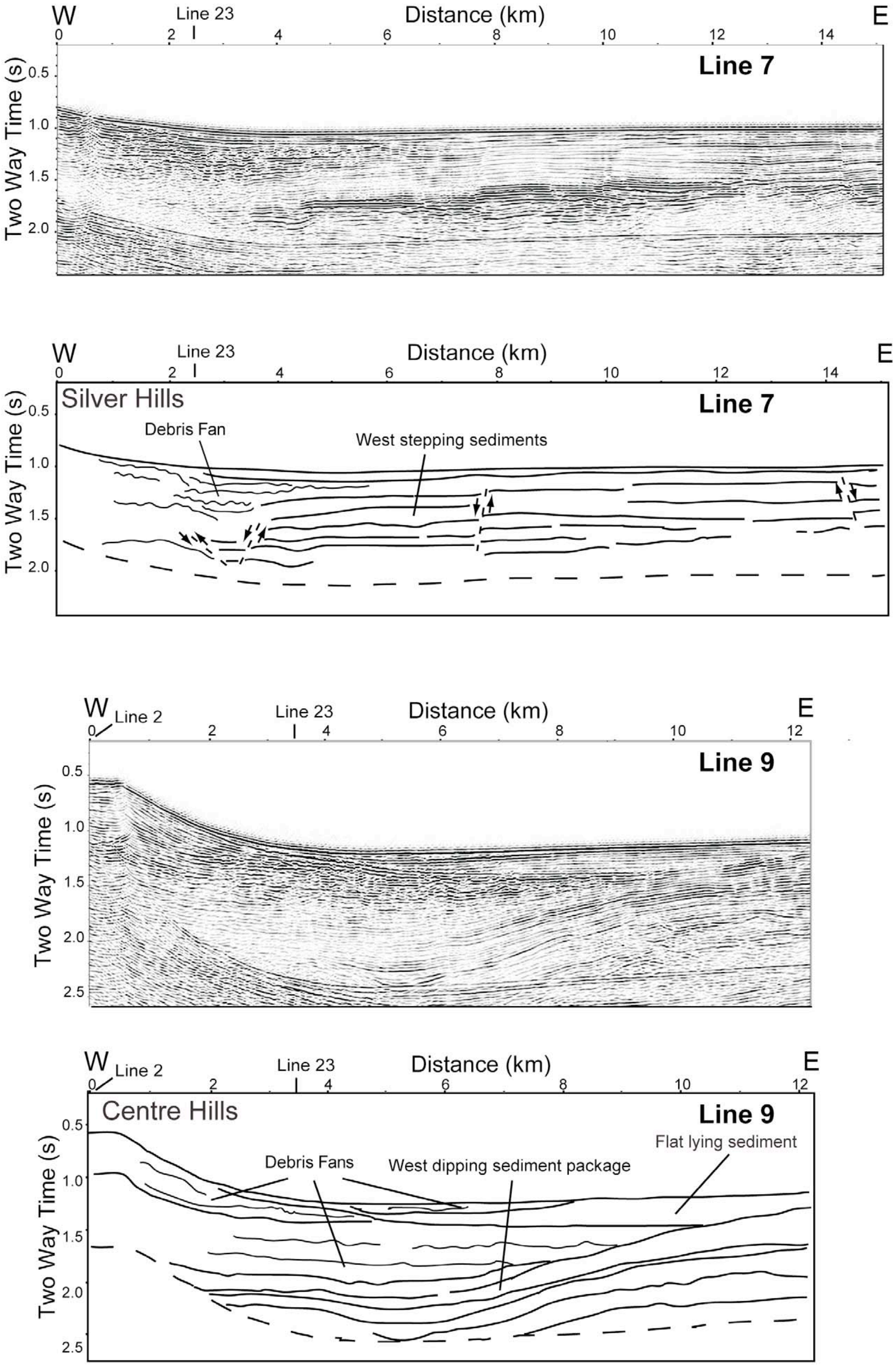

W
Line 23
Distance (km)
E
Line 7
Two Way Time (s)
W
Line 23
Distance (km)
E
Silver Hills
Line 7
Debris Fan
West stepping sediments
Two Way Time (s)
W
Line 2
Line 23
Distance (km)
E
Line 9
Two Way Time (s)
W
Line 2
Line 23
Distance (km)
E
Centre Hills
Line 9
Flat lying sediment
Debris Fans
West dipping sediment package
Two Way Time (s)

Fig. 41. Seismic reflection profiles and annotated interpretations of radial Lines 7 and 9. Solid lines: strong reflectors and sediment packages. Short dashed lines: faults. Thin dashed line: bottom multiple. Intersection with Lines 2 and 23 indicated at top. After Kenedi *et al*. (2010).

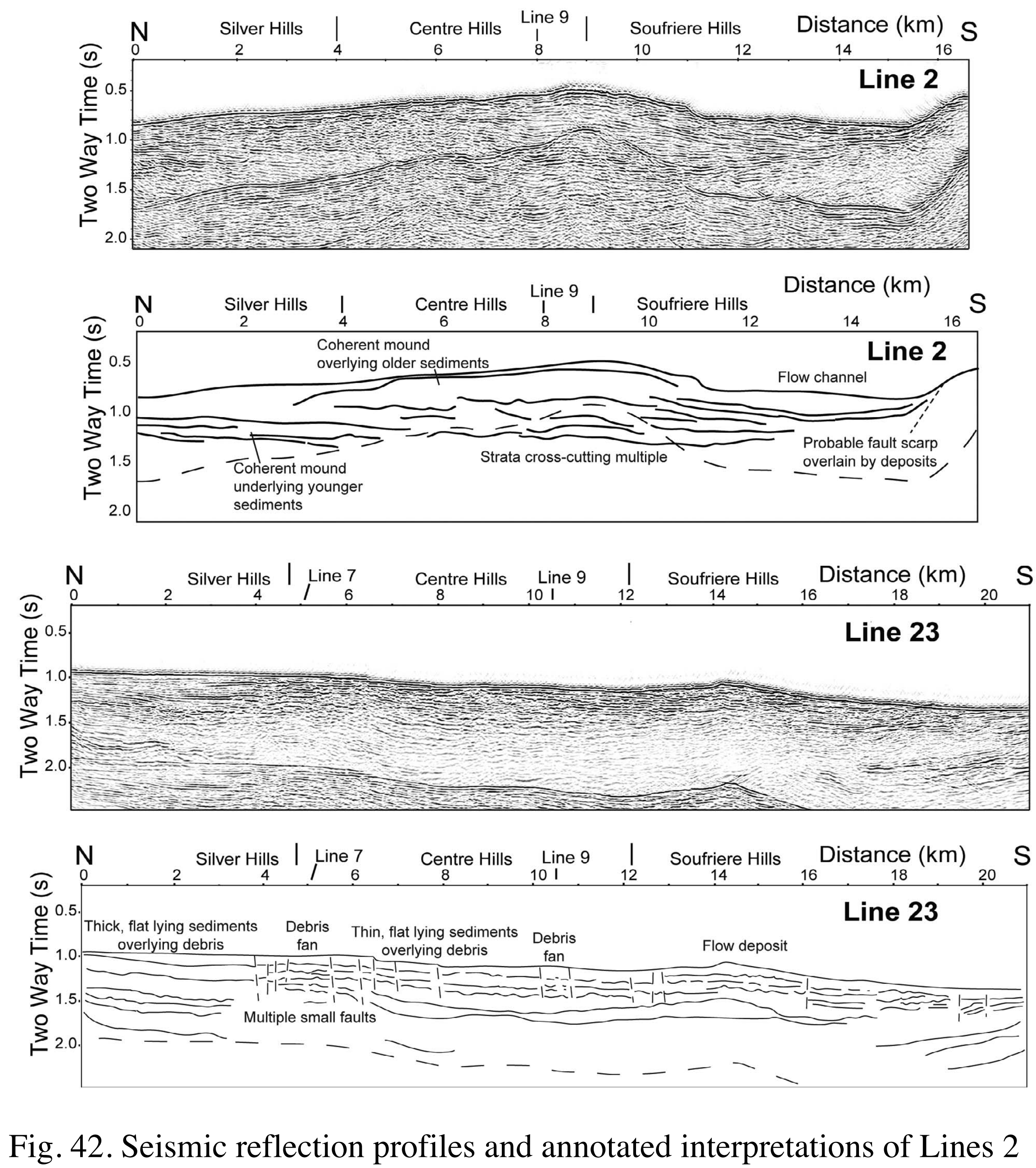

Fig. 42. Seismic reflection profiles and annotated interpretations of Lines 2 and 23, parallel to the east coast. Description as in Fig. 41. Intersection with Lines 7 and 9 indicated at top. Vertical lines at the top: boundaries between the major volcanic centres. After Kenedi *et al*. (2010).

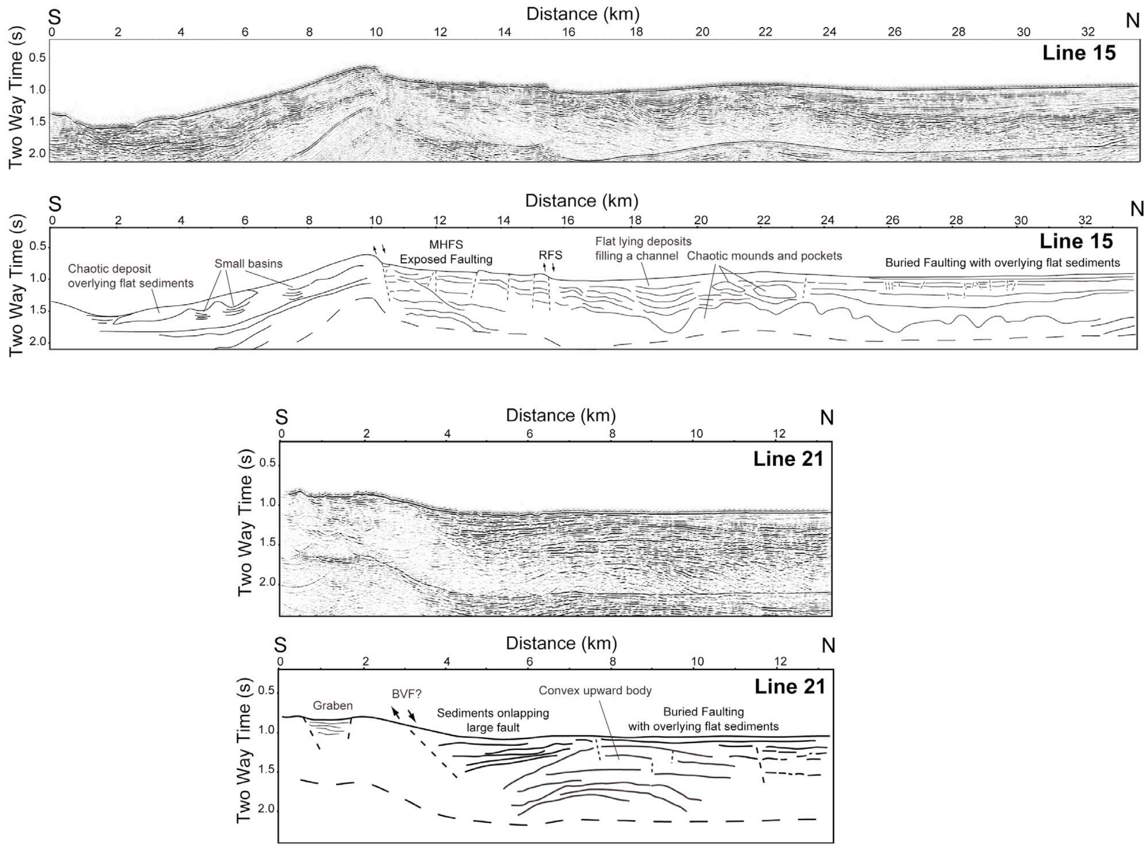

Fig. 43. Seismic reflection profiles and annotated interpretations of Lines 15 and 21, off the west coast. Description as in Fig. 41. After Kenedi *et al*. (2010).

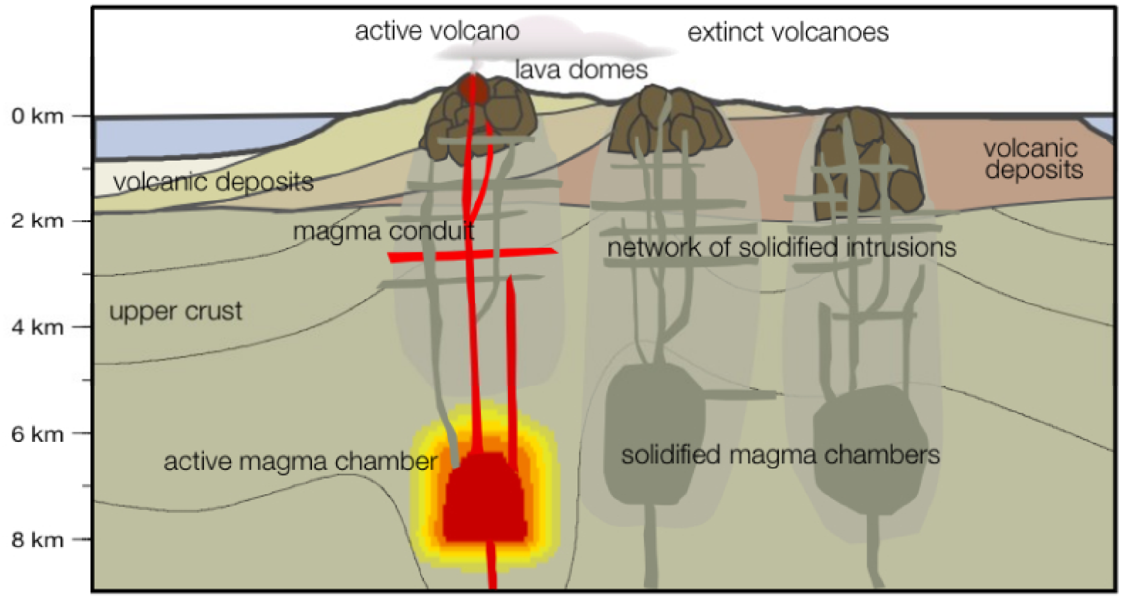

Fig. 44. Schematic N-S (from right to left) cross-section through Montserrat, illustrating insights from the SEA-CALIPSO experiment. The volcanic centres shown are, right to left, the extinct Silver Hills and Centre Hills complexes, underlain by solidified intrusions and magma chambers, and the Soufriere Hills Volcano, underlain by some solidified intrusions at shallow level, but with a partly molten magma chamber below 5 km depth. Contours of P-wave velocity are shown schematically and can be compared with Fig. 36.